UC Berkeley
UC Berkeley Electronic Theses and Dissertations

Title

Understanding Cellular Choices in Energy Production

Permalink

https://escholarship.org/uc/item/7dh9v771

Author

Kukurugya, Matthew Alexander

Publication Date

2024

Peer reviewed|Thesis/dissertation

eScholarship.org Powered by the California Digital Library
University of California

Understanding Cellular Choices in Energy Production

By

Matthew Kukurugya

A dissertation submitted in partial satisfaction of the

requirements for the degree of

Doctor of Philosophy

in

Molecular and Cell Biology

in the

Graduate Division

of the

University of California, Berkeley

Committee in charge:
Professor Denis V. Titov, Co-Chair
Professor Rebecca Heald, Co-Chair
Professor Hernan G. Garcia
Professor Adam P. Arkin

Fall 2024

Abstract

Understanding Cellular Choices in Energy Production

By
Matthew Kukurugya

Doctor of Philosophy in Molecular and Cell Biology
University of California, Berkeley

Professor Denis V. Titov & Rebecca Heald, Co-Chairs

Many prokaryotic and eukaryotic cells metabolize glucose to organism-specific byproducts instead of fully oxidizing it to carbon dioxide and water–a phenomenon referred to as the Warburg Effect. The benefit to a cell is not fully understood, given that partial metabolism of glucose yields an order of magnitude less ATP per molecule of glucose than complete oxidation. Here, we test a previously formulated hypothesis that the benefit of the Warburg Effect is to increase ATP production rate by switching from high-yielding respiration to faster glycolysis when excess glucose is available and respiration rate becomes limited by proteome occupancy. We show that glycolysis produces ATP faster per gram of pathway protein than respiration in *E. coli*, *S. cerevisiae*, and mammalian cells. We then develop a simple mathematical model of energy metabolism that uses five experimentally estimated parameters and show that this model can accurately predict absolute rates of glycolysis and respiration in all three organisms under diverse conditions, providing strong support for the validity of the ATP production rate maximization hypothesis. In addition, our measurements show that mammalian respiration produces ATP up to 10-fold slower than respiration in *E. coli* or *S. cerevisiae*, suggesting that the ATP production rate per gram of pathway protein is a highly evolvable trait that is heavily optimized in microbes. We also find that *E. coli* respiration is faster than fermentation, explaining the observation that *E. coli*, unlike *S. cerevisiae* or mammalian cells, never switch to pure fermentation in the presence of oxygen.

Glycolytic ATP production is critical for meeting the high energy demands of rapidly proliferating cells. We establish a strong linear correlation between ATP production rates and cellular growth across diverse organisms, including *E. coli*, *S. cerevisiae*, and mammalian cells. We found that glycolysis can fully compensate for the inhibition of respiration, whereas the respiratory pathway is insufficient to meet ATP demands when glycolysis is inhibited. When glycolytic ATP production is lost, cell growth slows, demonstrating the necessity of glycolysis in sustaining fast growth. Furthermore, we investigate how cells dynamically adjust their metabolic preferences in response to altered ATP demands by using cycloheximide to inhibit protein synthesis. This treatment uncovers a remarkable flexibility in energy metabolism, with cells shifting between glycolysis and respiration to optimize ATP production under varying conditions. Our findings uncover the indispensable role of glycolysis in facilitating rapid proliferation. This work provides novel insights into the mechanisms the metabolic flexibility of ATP production.

To my parents, Kevin and Nancy Kukurugya, whose support and belief in me instilled the confidence that anything is possible, and to Rebecca Wang, for being the guiding light that continues to make it so.

AKNOWLEDGEMENTS

Throughout my graduate school journey, I was carried by the guidance, care, collaboration, and enthusiasm of many. My work is in gratitude of the support from the people mentioned here.

I would like to express my deepest gratitude to my advisor, Professor Denis Titov, for his guidance, patience, and unwavering support throughout my doctoral journey. Denis, your genuine care for both my personal and professional growth has profoundly shaped my development. Your creativity and enthusiasm for science have continually inspired me to strive for excellence as a researcher. Your selfless approach to mentorship provided me the freedom to explore and discover my scientific voice. For all of this, thank you.

Thank you to Saharon Rosset for our fruitful collaboration. Thank you for genuinely listening to the Titov lab presentations. Your mastery of statistics and excitement for biology brought new mathematical insight to our study.

To my committee members, Rebecca Heald, Hernan Garcia, and Adam Arkin – thank you for your guidance, support, and insight in both my research and career direction. Your encouragement to persevere and your feedback on exploring new directions have strengthened both my thesis work and the depth of my scientific thinking. Hernan, your Physical Biology of Cell course changed the trajectory of my scientific career. Thank you all!

To the members of the Titov lab, Mangyu, Priyanka, Alex, Megan, Bowen, James, Xinyi, Catherin, and Lynn. I could not have picked a more eclectic set of lab mates over the past five years. Thank you for being an inspiring set of scientists to be around, keeping things weird, and indulging in trips to Yali's. I have a lifetime of memories of sharing nonsensical laughs, wallowing in experimental failure, and celebrating the rare scientific wins. Thank you for your continued friendship. To Lynn, thank you for working with me over the past year. You all will achieve great things!

To all my family and friends that supported me through the many phases of my PhD, thank you for always cheering me on along the journey. To my parents, Nancy and Kevin, thank you for always be in my corner – for raising a kid that liked to catch and collect insects and play with plastic sea creatures to always supporting each step of my scientific career - for letting me dream big and always being there to support me. To my siblings, Michael and Hannah, thanks for putting up with your crazy scientist brother and thinking my research is cool.

To my partner, Rebecca Wang, Thank you for your immeasurable support and care throughout my PhD rollercoaster. Thank you for celebrating the highs and being there for me at the lows. I could not have picked anyone better to be by my side during this adventure!

TABLES OF CONTENTS

Abstract 1

Dedication i

Acknowledgments ii

Table of Contents iii

List of Figures v

Chapter 1: The Warburg Effect is the result of faster ATP production by glycolysis

Introduction 2

Results 5

- The Warburg Effect emerges from a simple model of energy metabolism that maximizes ATP production rate 5
- Glycolysis produces ATP at a faster rate than respiration 7
- Model with no adjustable parameters quantitatively predicts the onset of Warburg Effect 10
- Model predicts the onset of Warburg Effect independent of growth rate 11

Discussion 13

Materials and Methods 16

Chapter 2: Glycolytic ATP production enables rapid cell proliferation

Introduction 27

Results 28

ATP production rate increases linearly with faster growth 28

Glycolytic ATP production can support higher growth rates compared to respiration 30

Glycolysis utilization, not respiration, is necessary for meeting the demand of the ATP demand of fast growth 32

Lower ATP Demand through reduced protein synthesis preferentially decreases the ATP production rate from glycolysis 35

Discussion 35

Materials and Methods 36

References 38

Chapter 1 Appendix

Overview of Linear Program and Derivation of Analytical Solution 46

Theoretical Model of Respiratory Substrate Utilization and Co-utilization with Glucose 52

Derivation of Analytical Solution for *E.coli*, including the Pta-AckA Pathway 56

Model Predictions of ATP production with cycloheximide treatment 59

Supplementary Figures 60

Chapter 2 Appendix

Supplementary Figures 72

LIST OF FIGURES

Chapter 1: The Warburg Effect is the result of faster ATP production by glycolysis

Fig. 1. The Warburg Effect emerges from a simple model of energy metabolism that maximizes ATP production rate 4

Fig. 2. Specific activities of ATP production of relevant pathways for E. coli, S. cerevisiae, and mammalian cells 8

Fig. 3. The model with no adjustable parameters that maximizes ATP production rate accurately predicts glycolysis and respiration rates and onset of the Warburg Effect 10

Fig. 4. The Warburg Effect is driven by glucose availability and not growth rate 12

Chapter 2: Glycolytic ATP production enables rapid cell proliferation

Fig. 1. Energy production and growth are highly correlated across organisms 29

Fig. 2. Glycolysis supports higher ATP production rates in fast-growing cells 31

Fig. 3. Glycolysis, not respiration, enables higher ATP production rates in fast-growing cells 33

Fig. 4. Inhibition of protein synthesis reduces growth and ATP demand 35

Chapter 1 Appendix

Fig. S1. Model predictions under varying glucose uptake rates 60

Fig. S2. Model predictions under varying glucose and respiratory substrate uptake rates 61

Fig. S3. Glycolysis and respiration pathway sizes in *E. coli*, *S. cerevisiae* and mammals 62

Fig. S4. Parameter estimates for *E. coli*, *S. cerevisiae*, and mammalian cells 63

Fig. S5. Cell line-specific maximal ATP production rate capacities of glycolysis and respiration in mammalian cells 64

Fig. S6. Parameter differences in the current study and Shen et al. 2024 65

Fig. S7. Pathway-specific ATP production rates for *S. cerevisiae* and mammalian cells with additional mitochondrial proteins 66

Fig. S8. Organism-specific model predictions of ATP production using different contributions towards biomass production 67

Fig. S9. Organism-specific model predictions of ATP production using different inclusion criteria for mitochondrial proteins 68

Fig. S10. Conservation of ATP-producing proteome allocation and variation in translational proteome allocation 69

Fig. S11. Model predictions of ATP production under nitrogen limitation 70

Fig. S12. Model predictions of ATP production with cycloheximide treatment 71

Chapter 2 Appendix

Fig. S1. Cellular measurements of ten mammalian cells 72

Fig. S2. Lactate production rate and oxygen consumption rate correlation with growth 73

Fig. S3. Maintenance ATP production rates compared to surface area to volume ratio 74

Fig. S4. ATP production rate (ATP molecules per amino acid per hr^{-1}) 75

Fig. S5. Lactate production rate (μmol mg protein^{-1} min^{-1}), oxygen consumption rate (μmol mg protein^{-1} min^{-1}), and growth rate (hr^{-1}) with increasing treatment with GSK-2837808A (GSK). 76

Fig. S6. Lactate production rate (μmol mg protein^{-1} min^{-1}), oxygen consumption rate (μmol mg protein^{-1} min^{-1}), and growth rate (hr^{-1}) with 10 mM glucose or 10 mM galactose 77

Fig. S7. Lactate production rate (μmol mg protein^{-1} min^{-1}), oxygen consumption rate (μmol mg protein^{-1} min^{-1}), and growth rate (hr^{-1}) with 1 uM antimycin treatment. 78

Chapter 1

The Warburg Effect is the result of faster ATP production by glycolysis than respiration

The work presented in this chapter has been published previously as part of the following paper: Kukurugya, M. A., Rosset, S., & Titov, D. V. The Warburg Effect is the result of faster ATP production by glycolysis than respiration. *Proc. Natl. Acad. Sci. USA* **121**, e2409509121 (2024). https://doi.org/10.1073/pnas.2409509121

Introduction

The Warburg Effect remains one of the most well-documented, yet incompletely understood phenomena in metabolism and cancer biology. In 1924, Otto Warburg made the observation that *in vivo* tumors preferred converting glucose to lactic acid via fermentation in the presence of oxygen instead of complete oxidation to carbon dioxide and water[1,2]. Mammalian respiration yields more than ten times more ATP per molecule of glucose than fermentation. The rationale for why cells prefer lower ATP-yielding fermentation for ATP production in the presence of oxygen is not fully understood.

Although the initial discovery was made in tumor cells, Warburg Effect-like metabolism has since been observed for numerous proliferating cells, including acetate production through the Pta-AckA pathway in *E. coli,* ethanol fermentation in *S. cerevisiae,* and lactic acid fermentation in non-transformed mammalian cells. This phenomenon is also referred to as the Crabtree Effect in *S. cerevisiae* and "overflow metabolism" in *E. coli*. To simplify nomenclature, we will collectively refer to various organism-specific pathways for partial metabolism of glucose (i.e., fermentation in *E. coli*, *S. cerevisiae*, and mammalian cells and respiro-fermentative Pta-AckA acetate pathway in *E. coli*) as *glycolysis*, to organism-specific pathways for complete oxidation of glucose to carbon dioxide and water as *respiration*, and to the preference for incomplete oxidation of glucose in the presence of oxygen as *the Warburg Effect*.

No unifying hypothesis is widely accepted to explain the occurrence of the Warburg Effect[3–6] in a variety of organisms. Otto Warburg himself proposed that high glycolysis rates in cancer cells were due to an impairment in respiration[2]. However, numerous studies have since demonstrated a prominent role of respiration in ATP production during cell proliferation[7,8]. Other proposed mechanisms for why the Warburg Effect occurs include satisfying biosynthetic demand[9,10], regulating redox balance[11], limiting reactive oxygen species[12,13], allowing for faster growth in hypoxic conditions[14], increasing the ATP production rate[15,16], out-competing other microorganisms for resources[17–19], and optimizing metabolism under the constraints of the proteome space[20–23], mitochondrial respiratory capacity[24–26] or bacterial plasma membrane area[18,19].

We focus on testing the previously formulated hypothesis that the Warburg Effect allows cells to maximize ATP production rate[15,16]. There is strong evolutionary pressure for cells and organisms to be able to generate ATP at a maximal rate under given conditions[15,16]. For example, unicellular organisms can grow faster than competition, cells in multicellular organisms can divide faster to speed up the immune response and wound healing, and multicellular organisms can move faster to evade predators or catch prey if they can generate ATP at a higher rate. To produce ATP at a faster rate, cells can either use a high-yield biochemical pathway that produces more ATP per molecule of glucose or a high-rate pathway that consumes more molecules of glucose per unit of time[15,16]. The switch to a high-rate pathway can only be beneficial when there is some constraint that prevents cells from simply increasing the activity of a high-yield pathway. Such a constraint can come from a finite proteome space that can be allocated to ATP-producing pathways while allowing for the expression of other pathways such as translation, biosynthesis,

protein folding machinery, cytoskeleton components, etc. Here, our work builds on the resource allocation models of microbial growth[20–24]. Several groups have proposed that microbes maximize their growth rate under different conditions by optimally allocating their proteome to translation, biosynthesis, energy production, and other processes. Resource allocation models are based on the observation that intracellular protein concentration is relatively stable[27,28] and, thus, to increase the expression of one pathway, another pathway's expression must be decreased. Within the resource allocation framework, glycolysis has been proposed to be more proteome efficient than respiration and, therefore, switching from respiration to glycolysis allows microbial cells to either increase their allocation to ATP-producing enzymes or allocate more of their proteome to ribosomes and other biosynthetic enzymes[20,22] to grow faster.

Here, we extend the resource allocation models to mammalian cells and provide a simple unifying explanation for the occurrence of Warburg Effect-like metabolism in *E. coli*, *S. cerevisiae*, and mammalian cells. Specifically, we test the hypothesis that the Warburg Effect allows cells to produce ATP at a maximal rate depending on glucose availability and irrespective of cell growth. At low glucose availability, respiration produces ATP faster due to its higher yield, while at high glucose availability, glycolysis produces ATP faster due to its higher rate. To test this hypothesis, we developed a coarse-grained mathematical model that predicts the occurrence of the Warburg effect at specific values of five biochemical parameters, including yield and specific activity of respiration and glycolysis, and maximal proteome fraction that can be occupied by ATP-producing enzymes. Our model has a unique analytical solution and no adjustable parameters, allowing for the direct prediction of experimental results. We experimentally estimated the values of the five biochemical parameters for each organism. Using these biochemical parameters, we show that our model quantitatively predicts the onset of the Warburg Effect, as well as glycolytic and respiration rates under various conditions in *E. coli*, *S. cerevisiae*, and mammalian cells, irrespective of growth rate. The ability of our model to predict the results of experiments in diverse organisms and conditions and without adjustable parameters provides strong evidence for the validity of this hypothesis.

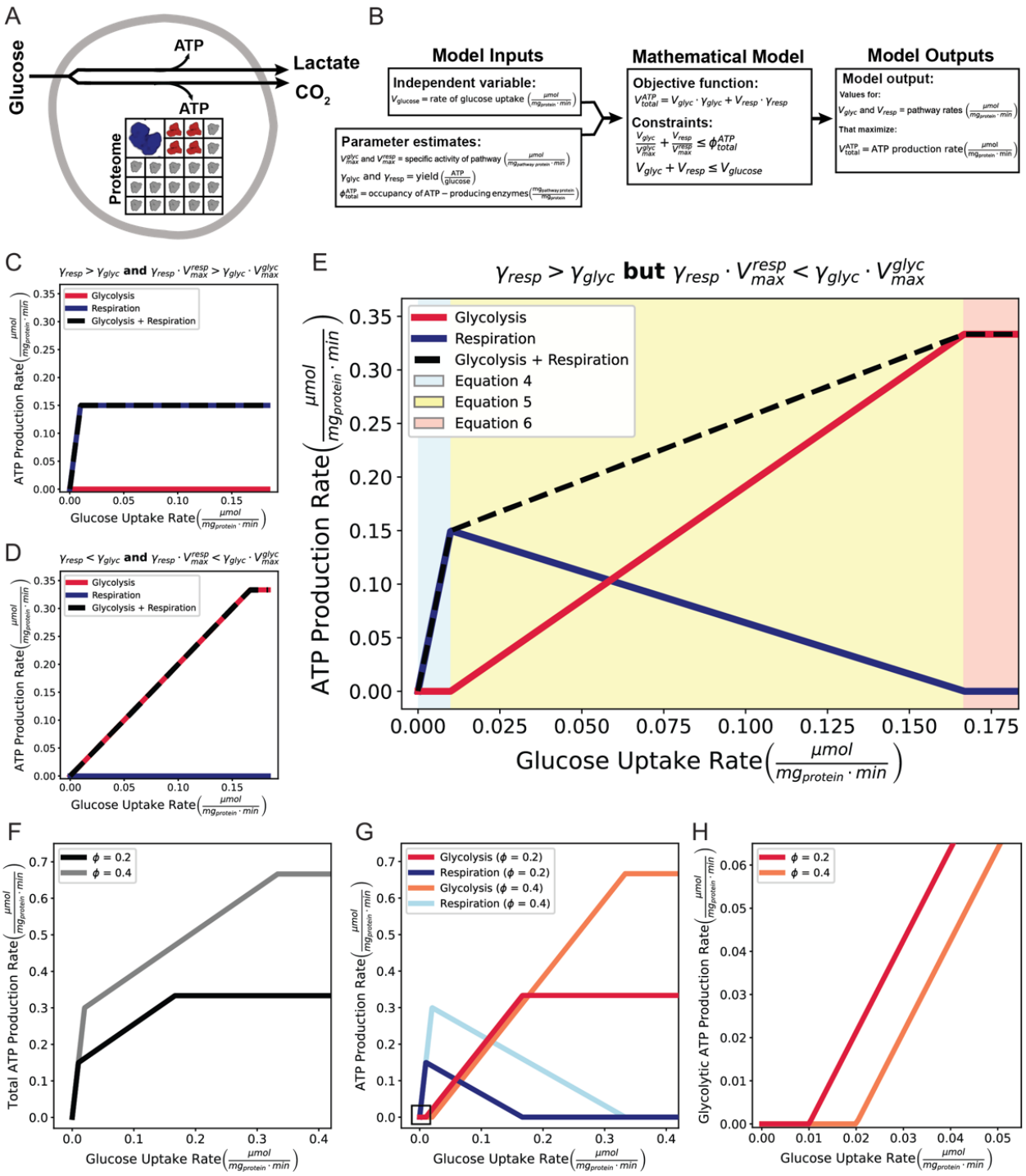


Fig. 1. The Warburg Effect emerges from a simple model of energy metabolism that maximizes ATP production rate. (*A*) Illustration of model. (*B*) Overview of mathematical model. (*C*) Preferred ATP-producing pathways if parameters of yield of ATP per molecule of glucose (γ) and the specific activity of ATP production ($\gamma \cdot V$) are both higher for respiration, (*D*) both higher for glycolysis, or (*E*) if the yield is higher for respiration ($\gamma_{resp} > \gamma_{glyc}$), but the specific activity of ATP production is higher for glycolysis ($\gamma_{resp} \cdot V_{max}^{resp} < \gamma_{glyc} \cdot V_{max}^{glyc}$). In each case, the total ATP production rate is represented by the dashed line. (*F*) Increasing the proteome space dedicated to ATP-producing enzymes increases ATP production rate across glucose uptake rates and (*G*) delays the switch from respiration to glycolysis. The box in Fig. 1*G* is shown in (*H*) to highlight the delayed onset of glycolysis.

Results

The Warburg Effect emerges from a simple model of energy metabolism that maximizes ATP production rate

We test a hypothesis that the Warburg Effect results from cells switching between glycolysis and respiration to achieve maximal ATP production rates at different environmental conditions. The ATP production rate is controlled to meet cellular ATP demand. In proliferating-cells, ATP demand correlates with growth as it supports biosynthesis. In differentiated cells, ATP demand can increase from non-growth activities, such as muscle contraction or biosynthesis of macromolecules for secretion. We assume cells obey three biochemical constraints while optimizing ATP production (Fig. 1*A*): i) Glucose consumption is limited by either its availability in the surrounding media or by glucose uptake capacity of the cell. We assume that oxygen is present at saturating levels, but this assumption is not required, as we describe at the end of this section. ii) A limited fraction of the proteome can be allocated to ATP-producing enzymes. We assume that cells are free to shift the relative rates of glycolysis and respiration through a combination of changes in the expression of enzymes and transporters, post-translational modifications, and allosteric regulation as long as the sum of glycolysis and respiration enzymes stays within the proteome fraction allocated to ATP-producing enzymes. iii) The maximal ATP production rate by either glycolysis or respiration pathways is limited by the maximal activity of respective enzymes. To describe the maximal ATP production rate by glycolysis or respiration, we utilize a metric that we call the specific activity of the pathway. The specific activity of the pathway (V_{max}) is defined as the μmol of substrate per minute per milligram of pathway protein. This metric is analogous to the widely used specific activity of enzymes and has also been referred to as proteome efficiency in previous studies[14,22]. We will use specific activities of glucose consumption and ATP production, where the latter is obtained by multiplying the former by the ATP yield per glucose of the relevant pathway.

To test the feasibility of our hypothesis, we constructed a mathematical model (Fig. 1*B*). Our aim was to keep the mathematical model as simple as possible to keep the interpretation of results straightforward. Our model calculates the cellular rates of glycolysis (V_{glyc}) and respiration (V_{resp}) that yield maximal ATP production rate (V_{ATP}) at a given glucose uptake rate ($V_{glucose}$), which are all in units of μmol per minute per milligram of cellular protein. The model uses five biochemical parameters, including the ATP yield (γ_{glyc} and γ_{resp}) and specific activity of glycolysis and respiration (V_{max}^{glyc} and V_{max}^{resp}) and fraction of the proteome that is occupied by ATP-producing enzymes (ϕ_{total}^{ATP}). The model must also satisfy two simple constraints that i) the rate of glycolysis and respiration cannot proceed faster than what is allowed by the proteome allocation for ATP-producing enzymes (ϕ_{total}^{ATP}) and ii) glucose uptake rate cannot be larger than the combined rates of glycolysis and respiration.

The model can be written as an optimization problem:

$$Maximize: \quad V_{ATP} = V_{glyc} \cdot \gamma_{glyc} + V_{resp} \cdot \gamma_{resp} \quad [1]$$

$$Subject\ to: \quad \frac{V_{glyc}}{V_{max}^{glyc}} + \frac{V_{resp}}{V_{max}^{resp}} \leq \phi_{total}^{ATP} \quad [2]$$

$$V_{glyc} + V_{resp} \leq V_{glucose} \quad [3]$$

The model can either be solved numerically using linear programming, which guarantees identification of a global maximum, or analytically using Lagrange multipliers with Karush-Kuhn-Tucker conditions[29] (see *SI Appendix* for details). The solution predicts that if one pathway has both a greater yield of ATP per molecule of glucose (γ) and a higher specific activity of ATP production ($V \cdot \gamma$), that pathway allows for maximal ATP production rate, independent of the glucose uptake rate (Fig. 1 *C* and *D*). However, if the yield is greater for one pathway (e.g., respiration such that $\gamma_{glyc} < \gamma_{resp}$), but the specific activity of ATP production is higher for the other pathway (e.g., glycolysis such that $V_{max}^{glyc} \cdot \gamma_{glyc} > V_{max}^{resp} \cdot \gamma_{resp}$), each pathway allows for maximal ATP production rate depending on glucose availability (Fig. 1*E*). The analytical solution of the model with respect to the glucose availability assuming that $\gamma_{glyc} < \gamma_{resp}$ and $V_{max}^{glyc} \cdot \gamma_{glyc} > V_{max}^{resp} \cdot \gamma_{resp}$ is given by the following equations:

If $V_{max}^{resp} \cdot \phi_{total}^{ATP} > V_{glucose}$ then $V_{glyc} = 0, V_{resp} = V_{glucose}$ [4]

If $\phi_{total}^{ATP} \cdot V_{max}^{glyc} > V_{glucose} > \phi_{total}^{ATP} \cdot V_{max}^{resp}$ then $V_{glyc} = \frac{\phi_{total}^{ATP} \cdot V_{max}^{glyc} \cdot V_{max}^{resp} - V_{glucose} \cdot V_{max}^{glyc}}{V_{max}^{resp} - V_{max}^{glyc}}$, $V_{resp} = \frac{V_{max}^{resp} (\phi_{total}^{ATP} \cdot V_{max}^{glyc} \cdot V_{max}^{resp} - V_{glucose})}{V_{max}^{glyc} - V_{max}^{resp}}$ [5]

If $V_{max}^{glyc} \cdot \phi_{total}^{ATP} < V_{glucose}$ then $V_{glyc} = V_{max}^{glyc} \cdot \phi_{total}^{ATP}, V_{resp} = 0$ [6]

Equations 4-6 predict that only respiration is used at low glucose uptake rates when $V_{max}^{resp} \cdot \phi_{total}^{ATP} > V_{glucose}$ (Equation 4); respiration proves beneficial when glucose is limited as it maximizes ATP production per glucose molecule (Fig. 1*E*, blue shaded region). As the glucose uptake rate increases, the limiting factor shifts from substrate availability to the capacity of the proteome (ϕ_{total}^{ATP}) (Fig. 1*E*). When the proteome allocation to ATP-producing enzymes is filled by respiratory enzymes, glycolysis can be substituted for respiration to further increase the ATP production rate since it generates ATP more rapidly per unit of protein (Fig. 1*E*, yellow shaded region). The rate of this trade-off is defined by Equation 5. The shift from respiration to glycolysis occurs as a gradual substitution until only glycolysis is utilized; glycolysis is favored at high glucose uptake rates when $\boldsymbol{V_{max}^{glyc} \cdot \phi_{total}^{ATP} < V_{glucose}}$(Equation 6) (Fig. 1*E*, red shaded region). In other words, a cell can produce ATP at the fastest rate using high yielding respiration at low glucose availability (Fig. 1*E* and *SI Appendix*, Fig. S1 *A* and *E*), a mixture of high yielding respiration and high rate glycolysis at intermediate glucose availability (Fig. 1*E* and *SI Appendix*, Fig. S1 *B*, *C*, *F*, and *G*), and with glycolysis alone at high glucose availability to achieve the maximal ATP production rate (Fig. 1*E* and *SI Appendix*, Fig. S1 *D* and *H*).

While the specific values of the yield and specific activity predict the benefit of switching from respiration to glycolysis, the glucose uptake rate when the switch occurs is determined by the total proteome space dedicated to ATP-producing enzymes (ϕ_{total}^{ATP}) (Equation 2). Without the proteome constraint, cells would always be able to express more respiratory proteins to increase ATP production without compromising on ATP yield. Increasing the proteome fraction dedicated to ATP-producing enzymes (ϕ_{total}^{ATP}) increases the capacity for ATP production across glucose uptake rates (Fig. 1*F*) and delays the switch from respiration to glycolysis (Fig. 1 *G*-*H*).

Our simple model assumes that glucose is used as the substrate for both glycolysis and respiration; however, the conclusions stay the same if a respiratory substrate other than glucose is used for respiration, such as acetate, glycerol, fatty acids, or amino acids (*SI Appendix*, Fig. S2 and see *SI Appendix* for details). The latter can be intuitively understood by considering that the majority of respiratory ATP is produced by the tricarboxylic acid (TCA) cycle and electron transport chain (ETC) enzymes for physiologically relevant respiratory substrates, and thus, the specific activity of respiratory ATP production is similar for different substrates.

All data used for parameter estimation and prediction validation in the following sections were collected under oxygen-rich conditions, therefore we assume oxygen saturation in our model. However, our model can also be extended to include an oxygen consumption constraint to simulate anaerobic or hypoxic environments (see *SI Appendix* for model formulation). In these oxygen limiting conditions, our model predicts that glycolysis will be utilized for ATP production at a lower glucose uptake rate as compared to oxygen-rich environments (*SI Appendix*, Fig S3). Furthermore, our model predicts the Pasteur Effect, where glycolysis is inhibited as oxygen becomes more available (*SI Appendix*, Fig S3)[30] and is well known to be driven by the maximization of the ATP production rate[31–34].
In summary, our model predicts a transition from respiration to glycolysis as glucose availability increases (i.e., the Warburg Effect) under certain combinations of yield and specific activity of glycolysis and respiration.

Glycolysis produces ATP at a faster rate than respiration

We next estimated the yields (γ_{glyc} and γ_{resp}) and specific activities of ATP production of glycolysis and respiration ($V_{max}^{glyc} \cdot \gamma_{glyc}$ and $V_{max}^{resp} \cdot \gamma_{resp}$) to determine if their values fall into the range where our model predicts the occurrence of the Warburg Effect: $\gamma_{glyc} < \gamma_{resp}$ and $V_{max}^{glyc} \cdot \gamma_{glyc} > V_{max}^{resp} \cdot \gamma_{resp}$. To test the general applicability of our hypothesis, we chose to focus on three organisms, *E. coli*, *S. cerevisiae*, and mammalian cells, since they span multiple kingdoms of life, exhibit a Warburg Effect-like metabolic switch, have unique bioenergetic pathways (*SI Appendix*, Fig. S4), and have been extensively studied. We first compiled the ATP yields of each pathway per molecule of glucose (*SI Appendix*, Fig. S5 *A*-*C*, Datasets S1-S3). We found that respiration yields 10-, 8-, and 12-fold more ATP per glucose than fermentative glycolysis in *E. coli*, *S. cerevisiae*, and mammalian cells, respectively (*SI Appendix*, Fig. S5 *A*-*C*). In *E. coli*, we considered the respiro-fermentative Pta-AckA pathway as it is one of the main ATP producing pathways in *E. coli* in the presence of both oxygen and glucose[35–37]. This pathway, involving

phosphotransacetylase (Pta) and acetate kinase (AckA), is a distinct form of glycolysis because it is not strictly fermentative. Unlike fermentative pathways, the Pta-AckA pathway uses ETC to oxidize NADH produced by glycolysis, but unlike respiration, it does not use the TCA cycle to produce more NADH. Consequently, it requires both glycolysis and the ETC to function. This integration leads to obligate oxygen consumption and results in a higher ATP yield per glucose molecule as compared to fermentation. However, respiration in *E. coli* still yields 2-fold more ATP per glucose than the Pta-AckA pathway.
We used experimental data to estimate the specific activities of ATP production for each pathway ($V \cdot \gamma$). To that end, we compiled an extensive dataset of physiological measurements to estimate the maximal rate of glycolysis and respiration per mg of cellular protein and divided those values by the fraction of the proteome occupied by glycolysis and respiration, respectively, determined from proteomics data (*SI Appendix*, Fig. S5 *D-I*, Datasets S1-S3). Our estimates showed that glycolysis has 0.54- (2.1- for Pta-AckA pathway), 2.1- and 3.1-fold faster rates per mg of pathway protein than respiration for *E. coli*, *S. cerevisiae*, and mammalian cells, respectively (Fig. 2). Our estimates allowed us to calculate the maximal ATP production rates of fermentative glycolysis and respiration in eleven transformed mammalian cell lines (*SI Appendix*, Fig. S6).

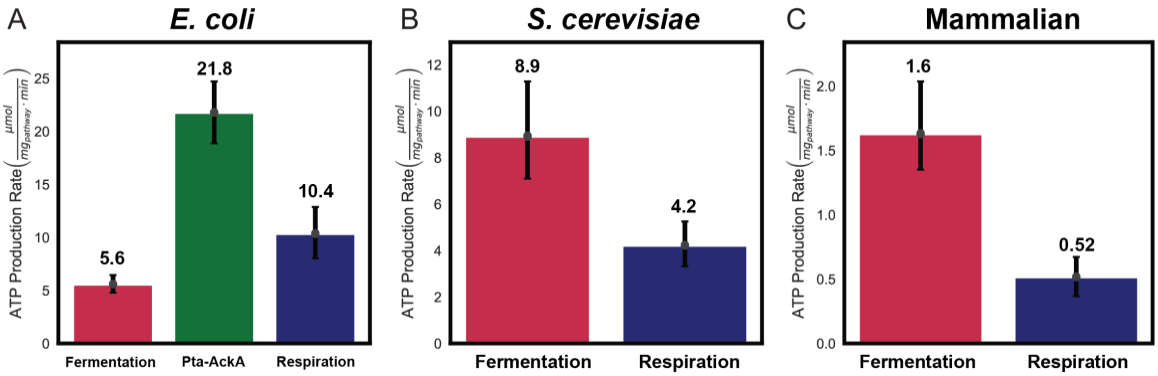


Fig. 2. Specific activities of ATP production of relevant pathways for *E. coli*, *S. cerevisiae*, and mammalian cells. (*A*) Specific activity of ATP production (μmol $mg_{pathway}^{-1}$ min^{-1}) for fermentation (red), the Pta-AckA pathway (green), and respiration (blue) for *E. coli*. (*B* and *C*) Specific activity of ATP production (μmol $mg_{pathway}^{-1}$ min^{-1}) for fermentation (red) and respiration (blue) for *S. cerevisiae* and mammalian cells, respectively. Specific activity of ATP production rate is given by $V_{max} \cdot \gamma$. Error bars are the 95 percent confidence interval calculated from 10,000 bootstrap iterations.

Previous studies have used different methodology to estimate the ratios of specific activities of ATP production (referred to as proteome efficiencies) of Pta-AckA pathway and respiration in *E. coli* to be 1.92[22] and 2.31[23] and for fermentation and respiration in *S. cerevisiae* to be 1.66[23] and 1.63[38], which are all within the 95% confidence interval of our estimates (Fig. 2 *A* and *B*). Absolute values for *E. coli* were reported[22] to be 65 and 34 μmol $mg_{pathway}^{-1}$ min^{-1} for Pta-AckA and respiration, respectively (converted from 750 and 390 mM per OD600 per hour using OD600 = 192.5 mg protein / L), which are same ratio but approximately three-fold higher absolute values compared to our estimates. The values of acetate secretion and percent proteome allocation of Pta-AckA pathway appear to be similar between the latter study and our estimates. However, the difference in absolute values remains unclear and might be attributed to minor discrepancies in unit

conversion. Absolute values for *S. cerevisiae* were previously estimated[38] using a genome-scale flux balance model and molecular weights of enzymes to be 4.6 and 7.5 μmol $mg_{pathway}^{-1}$ min^{-1} for respiration and glycolysis, respectively, which are within the 95% confidence interval of our estimates. Finally, one study[14] found that respiration is more proteome efficient than glycolysis in *S. cerevisiae* and $CD8^+$ T cells. The study reported experimental values that differ from those observed in several previous studies, including a 10-fold higher oxygen consumption in activated T cells and ~4-fold higher ratio of glycolysis to respiration proteome occupancy in *S. cerevisiae*, which likely contributed to a different conclusion (*SI Appendix*, Fig. S7).

In addition to direct experimental measurements, we estimated the molecular weight of glycolysis and respiration by summing up the molecular weights of the individual components multiplied by their stoichiometry in the relevant pathway (*SI Appendix*, Fig. S5 *J-L*, Datasets S1-S3). Respiration pathways were dramatically larger than glycolysis pathways in all three organisms (*SI Appendix*, Fig. S5 *J-L*, Datasets S1-S3). Strikingly, the increase in the size of respiration in relation to glycolysis is larger than the increase in yield afforded by respiration for all pathways except for fermentation in *E. coli* (*SI Appendix*, Fig. S5 *M-O*). Furthermore, 1.2-2.5-fold differences between the ratios of ATP yield to pathway size of glycolysis and respiration are similar to the respective differences in specific activity of ATP production (Fig. 2). These calculations further support our conclusion that the ATP production rate per mg of protein is higher for glycolysis than for respiration.

Our estimates for ATP yield ($\gamma_{glyc} < \gamma_{resp}$) and specific activity of ATP production ($V_{max}^{glyc} \cdot \gamma_{glyc} > V_{max}^{resp} \cdot \gamma_{resp}$) satisfied the parameter requirements in which our model predicts the switch from respiration to glycolysis at high glucose availability for respiro-fermentative Pta-AckA pathway in *E. coli*, and redox-neutral fermentative glycolysis in *S. cerevisiae* and mammalian cells. If additional mitochondrial proteins are included in ϕ_{resp}, the specific activity of respiration would be even lower for *S. cerevisiae* and mammalian cells, reinforcing the robustness of our conclusion that glycolysis is faster than respiration per mg protein (*SI Appendix*, Fig. S8). Importantly, our results do not predict a benefit for switching from respiration to fermentative glycolysis in *E. coli*. Thus, in addition to explaining why *E. coli*, *S. cerevisiae* and mammalian cells exhibit the Warburg Effect, our model provides an explanation for why *E. coli* exclusively use the respiro-fermentative Pta-AckA pathway in the presence of glucose and oxygen and not redox-neutral fermentative glycolysis as is the case for *S. cerevisiae*, and mammalian cells. Finally, we note that the specific activities of ATP production increase from mammalian cells to *E. coli* by over an order of magnitude for respiration and over 5-fold for glycolysis, suggesting that these parameters can evolve and that there might be evolutionary pressure for microbes to increase the specific activity of ATP production.

Model with no adjustable parameters quantitatively predicts the onset of Warburg Effect

Having demonstrated that our hypothesis predicts the benefit of the Warburg Effect, we next tested whether our model can quantitatively predict the onset of the Warburg Effect as well as rates of glycolysis and respiration measured under different experimental conditions in *E. coli*, *S. cerevisiae*, and mammalian cells. The additional biochemical parameter that we needed for this test was the total fraction of the proteome allocated to ATP-producing enzymes (ϕ_{total}^{ATP}) that we estimated from proteomics data (*SI Appendix*, Fig. S5 *D-F*, Datasets S1-S3). We used glucose uptake rate as the only model input. For each given glucose uptake rate, the model used the four organism-specific biochemical parameters as described in the last section (γ_{glyc}, γ_{resp}, V_{max}^{glyc}, and V_{max}^{resp}) and the total fraction of the proteome allocated to ATP-producing enzymes (ϕ_{total}^{ATP}) to determine the onset of the Warburg Effect as well as the glycolysis and respiration rates that allow cells to achieve a maximal ATP production rate (Fig. 3).

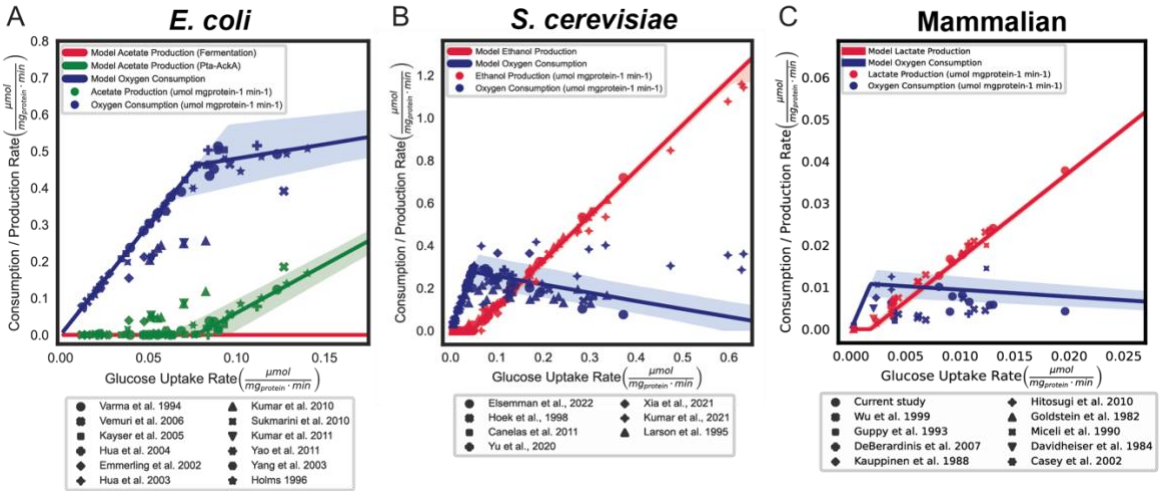


Fig. 3. The model with no adjustable parameters that maximizes ATP production rate accurately predicts glycolysis and respiration rates and onset of the Warburg Effect in *E. coli*, *S. cerevisiae*, and mammalian cells. (*A-C*) Comparison of model predictions (lines) and experimental observations (points) for glycolysis (red) and respiration (blue) rates of *E. coli*, *S. cerevisiae*, and mammalian cells, respectively. Note that each unique point shape represents data from a distinct publication. The glucose uptake rate for each point is calculated from the sum of oxygen consumption and glycolytic byproduct production.

The datasets used for parameter estimation and model validation are entirely independent and differ qualitatively in several ways. Here, we detail how the datasets differ and how these datasets enable us to make quantitative predictions. To estimate model parameters, we use data collected under conditions that maximize either glycolysis or respiration rates. Conditions used to estimate glycolysis parameters include saturating glucose concentrations, respiratory inhibitors, or anaerobic cultures, while respiration parameters are estimated using non-fermentable substrates at saturating concentrations or ETC uncouplers. These experimentally-derived parameter estimates enable our model to predict absolute rates of glycolysis and respiration rates depending on glucose uptake rate and proteome allocation to ATP-producing enzymes. We compared our predictions

to independent data collected under aerobic conditions with variable glucose availability and no inhibitors or ETC uncouplers. Under these conditions, such as in a chemostat at low growth rates, glycolysis and respiration rates are typically much lower than the maximal rate determined by our parameter estimation. Therefore, the model output is not simply a fit of the data, but a demonstration our model's ability to predict independently generated data.

Our model accurately predicted the absolute rates of acetate, ethanol, and lactate production, and oxygen consumption over two orders of magnitude of glucose consumption rates in *E. coli*, *S. cerevisiae,* and mammalian cells (Fig. 3). Importantly, the results in Figure 3 are not data fitting but predictions of the model using biochemical parameters estimated from independent experiments and no adjustable parameters. Most of the experimental data are within the 95% confidence interval of model predictions. Our predications for *E. coli* indicate that the Pta-AckA pathway (Fig 3*A*, green) is utilized for acetate production, while fermentation (Fig 3*A*, red) is never utilized in the presence of oxygen (Fig. 3*A*). These model predictions align with our expectations based on the relative ATP yield per glucose and the specific activities of each pathway (Fig. 2*A*). Our predictions were robust to different methods of accounting either contribution of each pathway to biomass formation (*SI Appendix*, Fig. S9) in all three organisms or for mitochondrial proteome size in the estimation of ϕ_{total}^{ATP} and V_{max}^{resp} for *S. cerevisiae* and mammalian cells (*SI Appendix*, Fig. S10). Finally, we note that we used average proteome allocation to ATP-producing enzymes across many conditions for each organism. This assumption is supported by our observation of the conservation of the proteome allocation to ATP-producing enzymes as compared to the protein translation space in response to changes in growth rate in glucose-limited chemostats in *E. coli* and *S. cerevisiae* or between mammalian cell lines (*SI Appendix*, Fig. S11). However, the size of ATP-producing space could change depending on cell type, nutrient availability, or disease state, so the accuracy of our model predictions could be further improved by measuring the proteome allocation to ATP-producing enzymes under relevant conditions.

Model predicts the onset of Warburg Effect independent of growth rate

Our model proposes that glucose availability and not the growth rate is driving the onset of the Warburg Effect. To tease apart the role of growth rate and glucose availability, we have used *E. coli* and *S. cerevisiae* datasets from nitrogen, and phosphorus-limited growth conditions where carbon uptake rate and growth rate diverge significantly (Datasets S1-S3). In these datasets, the correlation between growth rate and glycolysis is weak (ρ = 0.50 and ρ = 0.43 for *E. coli* and *S. cerevisiae*, respectively) (Fig. 4 *A* and *B*) as compared to the correlation between the carbon uptake rate and glycolysis (ρ = 0.68 and ρ = 0.99, respectively), which has been previously observed for *S. cerevisiae*[39] (Fig. 4 *C* and *D*). Our model accurately predicted the relationship between the carbon uptake and glycolytic rates in *S. cerevisiae* irrespective of growth rate and nutrient limitation (Fig. 4*D*). Furthermore, our model can predict the onset of glycolysis for various carbon substrates, including glucose, maltose, and galactose without any alterations to the model as were done in a previous study to fit the data[38]. For *E. coli*, our model overestimated the shift to acetate production under nitrogen-limited conditions (yellow points)[40].

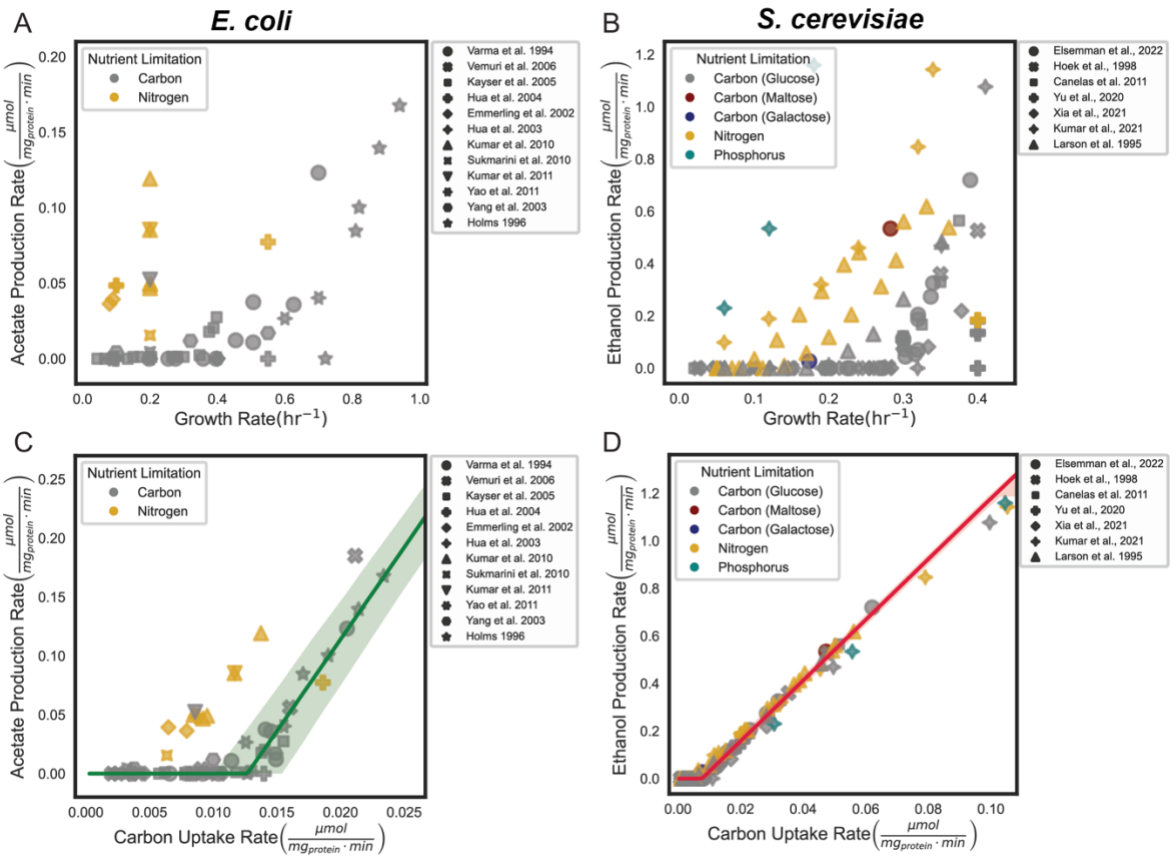


Fig. 4. The Warburg Effect is driven by glucose availability and not growth rate. (*A*) Growth rate (hr^{-1}) vs. the observed acetate production rate (μmol per mg cellular protein per min) for carbon- and nitrogen-limited cultures (grey and yellow, respectively) in *E. coli* or (*B*) the observed ethanol production rate (μmol per mg cellular protein per min) for carbon (glucose, maltose, galactose)-, nitrogen-, phosphorus-limited cultures (grey, burgundy, navy, yellow, green, respectively) in *S. cerevisiae.* (*C*) Carbon uptake rate (μmol per mg cellular protein per min) vs. the observed acetate production rate (μmol per mg cellular protein per min) for carbon- and nitrogen-limited cultures (grey and yellow, respectively) in *E. coli* or (*D*) the observed ethanol production rate (μmol per mg cellular protein per min) for carbon (glucose, maltose, galactose)-, nitrogen-, phosphorus-limited cultures (grey, burgundy, navy, yellow, green, respectively) in *S. cerevisiae*. The carbon uptake rate for each point is calculated from the sum of oxygen consumption and glycolytic byproduct production.

We speculate this is due to the known preference of *E. coli* to decrease the proteome fraction allocated to ATP-producing enzymes (ϕ_{total}^{ATP}) at high glucose availability[22,41]. The latter challenges the constant ϕ_{total}^{ATP} assumption of our simple model under these specific conditions in *E. coli,* but is entirely consistent with our overall hypothesis that *E. coli* switched to the Pta-AckA glycolysis pathway because of its higher specific activity of ATP production in relation to respiration. We estimate that the proteome allocation dedicated to ATP-producing enzymes must undergo an approximate two-fold decrease to account for the earlier onset of acetate production observed until nitrogen limitation (*SI Appendix*, Fig. S12). While the average proteome allocation to ATP-producing enzymes is 12%, we observed a range from as low as 6% to as high as 20% in our estimates of ϕ_{total}^{ATP} for *E. coli*. Therefore, two-fold decrease in ϕ_{total}^{ATP} is within the observed range of the proteome allocation to ATP-producing enzymes. Furthermore, in cases in which the rate of change

in the ATP-producing proteome space is known, our model is also able to predict resulting rates of glycolysis and respiration (see *SI Appendix* for details, *SI Appendix*, Fig. S13). These results suggest that, under nitrogen- and phosphorus-limited conditions in *E. coli* and *S. cerevisiae*, glycolysis is utilized as a major ATP production strategy as compared to the glucose-limited culture with the same growth rate due to the excess availability of glucose (Fig. 4 *C* and *D*).

Discussion

Our study tests a hypothesis that the Warburg Effect arises from the optimization of energy metabolism that allows cells to maximize the ATP production rate depending on glucose availability. We find that although cellular respiration generates more ATP per glucose molecule, the rate at which ATP is produced per the amount of enzyme protein involved is higher for the Pta-AckA pathway in *E. coli*, as well as for fermentative glycolysis in *S. cerevisiae*, and mammalian cells. Simply put, glycolysis is more compact than respiration, which allows glycolysis to produce ATP faster than respiration. Therefore, glycolysis is utilized when excess glucose is available and the ATP-producing space is limited. Our estimates show that in *E. coli*, only the Pta-AckA pathway and not redox-neutral fermentation is faster than respiration. Our observation explains a long-standing observation that *E. coli*, unlike mammalian cells or *S. cerevisiae*, do not use fermentation in the presence of oxygen[35].

We tested our hypothesis using a course-grained model of energy metabolism. Our model quantitatively predicts the onset of the Warburg Effect and glycolysis and respiration rates under diverse conditions in each of the three organisms using only the five biochemical parameters estimated with independent data, which provides strong support for our hypothesis. The ability of our model to make quantitative predictions provides a path for further validation of our hypothesis with additional experiments to improve estimates of the five model parameters and to generate more data connecting glucose uptake rate to glycolysis and respiration rates under different experimental conditions. Our model builds on the work of multiple groups that have utilized resource allocation models to explain the occurrence of the Warburg Effect in microbes[20–24]. Our two novel contributions in terms of modeling are the use of measured biochemical parameters from independent experiments to quantitatively predict the occurrence of the Warburg Effect in each of the three organisms and the use of a resource allocation model to explain the occurrence of the Warburg Effect in mammalian cells.

To test our model, we have measured the specific activities of ATP production for both glycolysis and respiration. Our measurements for *E. coli* and *S. cerevisiae* complement previous estimates of these parameters[22,23,38]. We note that the specific activity of the pathway has been referred to as “proteome efficiency” in several publications. Improved estimates of the specific activity of ATP production and measurement of specific activities of other pathways should allow the community to develop resource allocation models that predict cellular behavior beyond ATP production from independently measured biochemical parameters. Interestingly, we observed that the specific activities of ATP production for both glycolysis and respiration increase from mammalian cells through *S.*

cerevisiae to *E. coli*, suggesting an evolutionary adaptation that may reflect selective pressure favoring more compact ATP synthetic pathways in microbes. An example of a molecular mechanism of such an adaptation is Complex I of the ETC. Mammalian proton-pumping Complex I has 45 subunits and weighs 1 MDa, while *E. coli* proton-pumping Complex I has only 13 subunits and weighs 0.5 MDa despite being homologous to the mammalian enzyme[42]. In addition, both *E. coli* and *S. cerevisiae* have non-proton pumping versions of Complex I (*S. cerevisiae* does not have a proton pumping Complex I at all) called NDH-II[43] and Ndi1[44], respectively, that are not homologous to proton-pumping Complex I and have only one ~50 kDa subunit. Thus, the same or similar reactions are catalyzed by much smaller enzyme complexes in microbes than in mammalian cells, leading to higher specific activity of respiration in microbes. High specific activities may be selected for in microbial environments, such as soils, in which carbon substrates are typically scarce, but competition for them with other organisms is high. The lower rate of specific activities in mammalian cells may reflect the adaptation to multicellular cooperation, which represents investment in traits that are beneficial to the organism as a whole, but may come at the cost of vigor in an individual cell in the form of cellular function or metabolic activity[45,46]. Further investigation is necessary to determine the additional molecular mechanisms that drive the differences in the specific activity of ATP-producing pathways between species.

Our model could explain phenomena beyond the Warburg Effect or preference for the Pta-AckA pathway in rapidly growing cells. We show that the Warburg Effect depends on glucose availability rather than growth rate. Therefore, our model can be used to investigate the preference for glycolysis vs. respiration in differentiated cells. For example, fast-twitch muscle fibers are well known to prefer to use fermentation to produce energy used for short bursts of intensive physical activity[47]. Fast-twitch muscle uses glycogen instead of glucose, which raises the yield of glycolysis from 2 to 3 ATP per glucose equivalent. Our estimates from Figure 2C, in combination with the yield of 3 vs. 2 ATP per glucose, suggest that fast twitch muscle cells can produce ATP up to five times as fast if they dedicate the same fraction of their proteome to glycolysis than respiration– a large advantage in energy production rate that likely drove the evolution of fast-twitch muscle to rely on glycolytic fermentation. Moreover, our approach may clarify why microbes choose between expression of proton-pumping and non-proton-pumping versions of the same ETC complexes as mentioned above. Specifically, our model suggests that microbes could modulate the specific activity of their ATP-producing pathways by switching between high-yield (proton-pumping) and fast-rate (non-proton-pumping) respiratory chain components. This idea is supported by proteomics data showing that in *E. coli*, the expression of the faster, but lower-yielding non-proton pumping NADH dehydrogenase II increases with growth rate, while expression of the high-yielding proton-pumping NADH dehydrogenase I decreases[48].

While our model provides a unified explanation for the Warburg Effect by focusing on ATP production rates, several limitations should be considered. First, our model only accounts for the occurrence of the Warburg Effect in three organisms, where our parameter estimates demonstrate that $\gamma_{glyc} < \gamma_{resp}$ and $V_{max}^{glyc} \cdot \gamma_{glyc} > V_{max}^{resp} \cdot \gamma_{resp}$. To robustly test our hypothesis, it would be especially valuable to measure our model parameters in

organisms that do not exhibit the Warburg Effect, such as Crabtree-negative yeast. Specifically, we would aim to assess if $\gamma_{glyc} < \gamma_{resp}$ and $V_{max}^{glyc} \cdot \gamma_{glyc} < V_{max}^{resp} \cdot \gamma_{resp}$ as would be predicted by our model. Second, the mathematical formulation of our model is intentionally simple, which inherently limits its ability to fully account for the complex and dynamic regulatory mechanisms that control respiratory and glycolytic rates. This limitation is evident by our observation that model parameters, such as fraction of the proteome occupied by ATP-producing enzymes, can vary under specific conditions like nitrogen limitation in *E. coli*. Our current model lacks the complexity to account for such dynamic changes. Additionally, our hypothetical model estimates for the regulation of glycolytic rates in response to oxygen limitation, have not experimentally tested where both may contribute to the high glycolytic rates observed in tumors with limited vasculature[49]. Finally, we highlight that while our study provides an explanation for why it is beneficial for diverse organisms to switch between fast glycolysis and high-yielding respiration, more work needs to be done to investigate the molecular mechanisms of how cells optimize their energy metabolism, given the fundamental trade-offs of yield and rate.

Materials and Methods

Analysis code and figure generation

All data and code used in the figure generation are available as a GitHub repository via https://github.com/DenisTitovLab/WarburgEffectModel

Estimation of proteome occupancy by metabolic pathways (ϕ_{glyc}, ϕ_{resp} and ϕ_{total}^{ATP})

We utilized a total protein approach and previously published measurements of the absolute quantification of proteins using mass spectrometry to estimate the fraction of the proteome occupied by glycolysis ϕ_{glyc}, respiration ϕ_{resp}, or all ATP-producing pathways ϕ_{total}^{ATP} (Datasets S1-S3). We only included studies that used 8M urea or sodium dodecyl sulfate in the lysis buffer to improve the estimation of membrane proteins, which are not extracted using milder lysis buffers. Total protein approach assumes that a protein's abundance within a cell's proteome is proportional to that protein's mass spectrometry (MS) signal over the total MS signal (Equation 7).

$$\frac{Protein\ mass}{Total\ protein\ mass} \propto \frac{Protein\ MS\ Signal}{Total\ MS\ Signal} \quad [7]$$

This approach was previously validated[50] by showing that it can accurately quantify proteins within their expected physiological range spanning five orders of magnitude.

ETC complexes are imbedded in the mitochondrial membrane and, therefore, are often extracted with less efficiency. The level of ETC complex subunits with greater than 20 percent missing values were imputed using the average levels of subunits of the same complex that where not missing on a per sample basis. Both subunit mass and stoichiometry were accounted for in the correction.

The specific enzymes included in the calculation of ϕ_{glyc} and ϕ_{resp} for *E. coli*, *S. cerevisiae*, and mammalian cells are included in Datasets S1-S3. To match the respective physiological measurements for *E. coli* and *S. cerevisiae*, ϕ_{glyc} was only calculated for fermentable carbon substrates (i.e. sugars) and ϕ_{resp} is only calculated for non-fermentable carbon substrates (i.e. acetate, pyruvate, succinate, glycerol, fumarate) both in batch culture. For the respiro-fermentative Pta-AckA pathway in *E. coli*, ETC components were included to account for redox balance and additional ATP production. For the translational proteome space, the enzymes included in the Gene Ontology for translation (GO:0006412) were used for each organism.

All the estimates of respiration proteome occupancy reported in the main text included only core respiration and TCA cycle enzyme. To determine the effect of additional mitochondrial proteins on our predictions, we included two further predictions for *S. cerevisiae* and mammalian cells. First, in addition to core respiratory enzymes, we included mitochondrial proteins that positively correlated with the expression of the sum of the core respiration proteins ($\rho > 0$) and was statistically significant after Benjamini-Hochberg correction ($p < 0.05$). The statistical significance represents a two-tailed p-value, which is the probability of a correlation coefficient at least as big to be observed if

the null hypothesis is true. All proteins included in the ϕ_{resp} for *S. cerevisiae* and mammalian cells are listed in Datasets S2 and S3. Second, all MitoCarta mitochondrial proteins were included in the estimate ϕ_{resp}. The model estimations using these two additional estimates are reported in Fig. S10.

For mammalian cells, eleven cell lines from distinct origins were utilized including: A549, GAMG, HeLa, HepG2, Jurkat, K562, LnCap, MCF7, RKO, U2OS, and HEK293.

We did not correct proteome allocations for biosynthesis because the magnitude of the required correction is small (<30%, see discussion below) and accurate correction would require extensive metabolomics flux measurements that will complicate the model and discussion considerably. The magnitude of the correction is <30% for the following reasons. First, for respiration the correction for biosynthesis flux will be small because a large fraction of the proteome allocated to respiration is occupied by respiratory chain which only carries energy production flux and not biosynthesis flux (e.g., see Fig. S3). Furthermore, *E. coli* and *S. cerevisiae* grown on respiratory substrates divert a max of only ~45-55% of glucose to biosynthesis based on the biomass yield of ~0.45-0.55 g dry weight per g glucose. Second, the correction for glycolysis is small because cells grown in glucose in batch culture divert most of their glucose flux to glycolytic ATP production. For example, *E. coli* grown on glucose divert ~70% of glucose mass for acetate secretion[51] and the Pta-AckA pathway used under these conditions uses respiration so the correction is even smaller due to latter point. For *S. cerevisiae* grown on glucose ~80% of glucose mass is secreted as ethanol[52], and mammalian cells often use >90% of glucose mass for glycolytic fermentation as they are grown in rich media with amino acids and do not have to use as much glucose for biosynthesis. The correction of glycolysis for biosynthesis would have increased the specific activity of glycolysis making it even faster compared to respiration. We have now included the above description in the methods section.

Estimation of maximal cellular activity of glycolysis and respiration

Absolute specific activities of glycolysis and respiration per weight of cellular proteins were estimated from experiments in which the maximal activity of each pathway was measured. These values are then combined with proteomic fractions of respective pathways to estimate specific activity per weight of pathway as describe in another section below. For *E. coli, S. cerevisiae*, and mammalian cells, the maximal acetate, ethanol, and lactate production rates, respectively, were used for glycolysis (Datasets S1-S3). For *E. coli and S. cerevisiae*, these values were taken from measurements grown in batch culture on a fermentable substrate. For mammalian cells, lactate production values were taken from measurements where cells were treated with oligomycin to maximize lactate production. For respiration, the maximal oxygen consumption rates were utilized for *E. coli, S. cerevisiae*, and human cells (Datasets S1-S3). For *E. coli* and *S. cerevisiae*, these values were taken from measurements grown in batch culture or accelerostat on a nonfermentable substrate. For human cells, all oxygen consumption data is from Agilent Seahorse Bioanalyzer assays, and maximal respiration rate is estimated as the difference

between oxygen consumption in the presence of uncoupler FCCP and respiration inhibitor Antimycin A (or Rotenone) to account for non-mitochondrial respiration. FCCP uncouples mitochondrial ETC activity from ATP production by dissipating the proton gradient, forcing the ETC to operate at a maximum rate, which allows the measurement of maximal OCR that is not limited by the ATP demand[53,54]. Each value was converted to units of μmol per mg cellular protein per min from oxygen consumption or glycolytic byproduct formation to account only for glucose consumption towards ATP production and not biomass.

For studies that reported values in units consisting of gram cell dry weight (gCDW), it was calculated that 55% and 44% of dry cell mass consisted of protein in *E. coli* and *S. cerevisiae,* respectively (Datasets S1 and S2). The estimates of gCDW per g protein are based on the studies for *E. coli* and *S. cerevisiae* compiled in Datasets S1 and S2. For mammalian cells studies that reported values in units of cell number, representing 9 of 14 studies, it was assumed that each cell contained 300 pg of protein[55,56,50]. The following mammalian cell lines were utilized for these estimates: C2C12, H1299, HeLa, 4T1, K562, $CD4^+$ T cell, primary isolated cardiomyocytes, Ehrlich ascites tumor cells, and primary rat cerebellar neurons.

Estimation of the molecular weight of glycolysis and respiration pathways

Molecular weights of the pathways were calculated by summing the molecular weights of all proteins in each of the pathways corrected for pathway stoichiometry (Datasets S1-S3). For each enzyme that has isoforms, the average molecular weight of isoforms was used. For each enzyme that is a multi-subunit protein complex, the sum of the subunits was used with subunit stoichiometry accounted.

Estimation of ATP yield per glucose of glycolysis and respiration

The ATP yield for (γ_{resp} and γ_{glyc}) was estimated for *E. coli*, *S. cerevisiae*, and mammalian cells. Fermentative glycolysis yield of 2 ATP per glucose is well-defined for all three organisms (*SI Appendix*, Fig. S4 *A*-*C* and Datasets S1-S3).

To define the ATP yield of respiration for each organism, experimentally derived measurements[57–59], in combination with the following calculations, were used to account for ATP produced from glycolysis, the TCA cycle, and the ETC (Datasets S1-S3). In fermentative glycolysis, glucose is converted to a glycolytic byproduct, producing a net gain of 2 ATP per glucose for each organism.

Fermentative glycolysis:

E. coli $C_6H_{12}O_6 + 2\ ADP + 2\ P_i \rightarrow Various\ Products + 2\ ATP$ [8]

S. cerevisiae $C_6H_{12}O_6 + 2\ ADP + 2\ P_i \rightarrow 2\ C_2H_6O + 2\ CO_2 + 2\ ATP$ [9]

Mammalian cells $C_6H_{12}O_6 + 2\ ADP + 2\ P_i \rightarrow 2\ C_3H_6O_3 + 2\ ATP$ [10]

In respiration, glucose is converted to a pyruvate, generating ATP and NADH. Pyruvate is further oxidized through the TCA cycle, generating additional NADH, $CoQH_2$, and ATP per glucose in all three organisms.

$$C_6H_{12}O_6 + 6\ O_2 + 4\ ADP + 4\ P_i + 2\ CoQ + 10\ NAD^+ + 14\ H^+ \rightarrow 6\ CO_2 + 6\ H_2O + 4\ ATP + 2\ CoQH_2 + 10\ NADH \quad [11]$$

In the ETC, NADH and $FADH_2$ are oxidized to generate a proton gradient in the inner mitochondrial membrane (or plasma membrane in *E. coli*). In *S. cerevisiae* and mammalian cells, the NADH produced from glycolysis is shuttled into the mitochondria to enter the ETC at a cost of 1 H^+ per NADH. The proton gradient is then used to drive the production of ATP synthase. Each organism has a unique number of H^+ translocated per NADH and $FADH_2$ based on the translocated H+ per electron ratio of the utilized ETC components. For *E. coli*, the ratio of translocated H^+ per electron is 2 for NADH-ubiquinone reductase (NDH-I) and 2 for quinol oxidase (cytochrome bo_3 oxidase). For *S. cerevisiae*, the ratio of translocated H^+ per electron is 0 for NADH-ubiquinone reductase (Ndi1), 1 for quinol-cytochrome c reductase (Complex III), and 2 for cytochrome c oxidase (Complex IV). For mammalian cells, the ratio of translocated H^+ per electron is 2 NADH-ubiquinone reductase (Complex I), 1 for quinol-cytochrome c reductase (Complex III), and 2 for cytochrome c oxidase (Complex IV). Note that each NADH or $FADH_2$ donates two electrons. Therefore, the total number of translocated H^+ is calculated by the following equation where mammalian cells are used as an example:

$$H^+_{maximum} = 2 \cdot H^+_{CI} \cdot NADH_{total} + 2 \cdot H^+_{CIII} \cdot (NADH_{total} + FADH2_{total}) + 2 \cdot H^+_{CVI} \cdot (NADH + \mathrm{FADH2}) - NADH_{glycolysis} \cdot H^+_{Transport} \quad [12]$$

However, it is well-known that proton leak occurs in the membrane. For mammalian cells, the proton leak was calculated from the difference in the oxygen consumption rate in the presence of oligomycin and antimycin A (or rotenone) (Dataset S3). We determined that the proton leak was ~25%. For *E. coli* and *S. cerevisiae*, we also assumed ~75% of theoretical maximal yield to account for proton leak. Furthermore, the ratio of H^+/ATP was measured to be 4, 3, and 3 for *E. coli*, *S. cerevisiae*, and mammalian cells, respectively [57–59]. Note that in mammalian cells and *S. cerevisiae*, we assume the adenine nucleotide translocator (ANT) is active, and therefore, the cost of transporting each ATP from the mitochondria is 1 H^+. Therefore, the total number of ATP produced through respiration is calculated by:

$$\gamma_{resp} = \frac{(H^+_{maximum} - H^+_{Leak})}{(H^+/ATP + H^+/ATP\ transport)} \quad [13]$$

The ATP yield of respiration was determined to be 20, 16, and 24 ATP per molecule of glucose for *E. coli*, *S. cerevisiae*, and mammalian cells, respectively.

E. coli $C_6H_{12}O_6 + 6\ O_2 + 20\ ADP + 20\ P_i \rightarrow 6\ CO_2 + 6\ H_2O + 20\ ATP$ [14]

S. cerevisiae $C_6H_{12}O_6 + 6\ O_2 + 16\ ADP + 20\ P_i \rightarrow 6\ CO_2 + 6\ H_2O + 16\ ATP$ [15]

Mammalian cells $C_6H_{12}O_6 + 6\ O_2 + 24\ ADP + 20\ P_i \rightarrow 6\ CO_2 + 6\ H_2O + 24\ ATP$ [16]

The Pta-AckA pathway in *E. coli* utilizes the ETC for oxidation of the 4 NADH produced per molecule of glucose in the *E. coli* Pta-AckA pathway that converts glucose to acetate, yielding 10 ATP per molecule of glucose. The Pta-AckA pathway in *E. coli* utilizes the ETC for oxidation of the 4 NADH produced per molecule of glucose in the *E. coli* Pta-AckA pathway that converts glucose to acetate.

$$C_6H_{12}O_6 + 2\ O_2 + 4\ ADP + 4\ P_i + 4\ NAD^+ + 4H^+ \rightarrow 2\ C_2H_4O_2 + 2\ CO_2 + 2\ H_2 + 2\ H_2O + 4\ ATP + 4\ NADH \quad [17]$$

Estimation of the specific activity of ATP production of glycolysis and respiration

We used experimental data to estimate the specific activities of ATP production of glycolysis and respiration (*SI Appendix*, Fig. S4 *G-I*, Datasets S1-S3). The specific activity of glucose consumption was calculated by taking the maximal cellular glucose consumption rate by a given pathway (μmol glucose per mg of cellular protein per min) and dividing it by the fraction of the proteome occupied by the pathway (ϕ_{glyc} or ϕ_{resp}).

$$V_{max}^{glyc/resp} = \frac{Max\ cellular\ glyc/resp\ rate}{\phi_{glyc/resp}} \quad [18]$$

As described above in *Estimation of maximal cellular activity of glycolysis and respiration*, we determined the maximal glycolysis and respiration rates for *E. coli, S. cerevisiae*, and mammalian cells by compiling an extensive dataset from 38 independent publications containing 57 measurements of production rate of glycolysis products (i.e, acetate, ethanol, lactate) and oxygen consumption rates, which were converted to glucose consumption rate using known stoichiometry of the pathways (Datasets S1-S3). For each organism, we calculated ϕ_{glyc}, and ϕ_{resp} from proteomics data as described above in *Estimation of proteome occupancy by metabolic pathways (ϕ_{glyc}, ϕ_{resp} and ϕ_{total}^{ATP})*.

We made two additional predictions for *S. cerevisiae*, and mammalian cells that were only used for data reported in Fig. S6 and S7. In the first, corrections to ϕ_{resp} to account for mitochondrial proteins that are required for mitochondrial biogenesis and function but are not core respiration components by including into ϕ_{resp} mitochondrial proteins whose expression was significantly ($p < 0.05$) and positively correlated ($\rho > 0$) with the sum of the TCA and ETC proteins. In the second, we included all mitochondrial proteins.

Mathematical Model

To describe the Warburg Effect, we use a constrained optimization model. The objective function of the model is to maximize the ATP production rate given the constraints as described in Equation 1, Equation 2, and Equation 3 reproduced here for convenience:

$$Maximize: \qquad V_{ATP} = V_{glyc} \cdot \gamma_{glyc} + V_{resp} \cdot \gamma_{resp} \quad [1]$$

$$Subject\ to: \quad \frac{V_{glyc}}{V_{max}^{glyc}} + \frac{V_{resp}}{V_{max}^{resp}} \leq \phi_{total}^{ATP} \quad [2]$$

$$V_{glyc} + V_{resp} \leq V_{glucose} \quad [3]$$

We can use the V_{glyc} and V_{resp}values to calculate the absolute rates of glycolytic by-product (i.e. acetate, ethanol, or lactate) or oxygen consumption from the predicted rates of glycolysis and respiration (equation 19 and 20, respectively):

$$V_{glyc}^{byproduct} = \gamma_{gluc}^{byproduct} \cdot V_{glyc} \quad [19]$$

$$V_{resp}^{O2} = \gamma_{resp}^{O2,consumed} \cdot V_{resp} \quad [20]$$

We used the method of Lagrange multipliers with Karush-Kuhn-Tucker conditions to solve this optimization problem with inequality constraints. We report an analytical solution here. We note that the global optimum can also be found using the linear programming software PuLP[60]. The full derivation is presented in Supplemental Discussion 1. Here we present the full set of cases, unlike in the main text where we have just provided those which have biological relevance. With $V_{max}^{glyc}, \gamma_{glyc}, V_{max}^{resp}, \gamma_{resp}, \phi_{total}^{ATP}, V_{glucose} > 0$, the solution is explicitly written by cases:

If $\boldsymbol{\gamma_{glyc} < \gamma_{resp}}$ $\boldsymbol{V_{max}^{resp} \cdot \phi_{total}^{ATP} > V_{glucose}}$ then $\boldsymbol{V_{glyc} = 0, V_{resp} = V_{glucose}}$ [4]

If $\gamma_{glyc} < \gamma_{resp}$ $V_{max}^{glyc} \cdot \gamma_{glyc} > V_{max}^{resp} \cdot \gamma_{resp}$ $\phi_{total}^{ATP} \cdot V_{max}^{glyc} > V_{glucose} > \phi_{total}^{ATP} \cdot V_{max}^{resp}$ then

$$V_{glyc} = \frac{\phi_{total}^{ATP} \cdot V_{max}^{glyc} \cdot V_{max}^{resp} - V_{glucose} \cdot V_{max}^{glyc}}{V_{max}^{resp} - V_{max}^{glyc}}$$

$$V_{resp} = \frac{V_{max}^{resp}(\phi_{total}^{ATP} \cdot V_{max}^{glyc} \cdot V_{max}^{resp} - V_{glucose}}{V_{max}^{glyc} - V_{max}^{resp}}$$ [5]

If $V_{max}^{glyc} \cdot \gamma_{glyc} > V_{max}^{resp} \cdot \gamma_{resp}$ $V_{max}^{glyc} \cdot \phi_{total}^{ATP} < V_{glucose}$ then $V_{glyc} = V_{max}^{glyc} \cdot \phi_{total}^{ATP}, V_{resp} = 0$ [6]

If $\gamma_{glyc} > \gamma_{resp}$ $V_{max}^{glyc} \cdot \phi_{total}^{ATP} > V_{glucose}$ then $V_{glyc} = V_{glucose}, V_{resp} = 0$ [21]

$$\text{If } \begin{array}{l} \gamma_{glyc} > \gamma_{resp} \\ V_{max}^{glyc} \cdot \gamma_{glyc} < V_{max}^{resp} \cdot \gamma_{resp} \\ \phi_{total}^{ATP} \cdot V_{max}^{glyc} < V_{glucose} < \\ \phi_{total}^{ATP} \cdot V_{max}^{resp} \end{array} \quad \text{then} \quad \begin{array}{l} V_{glyc} \\ = \dfrac{\phi_{total}^{ATP} \cdot V_{max}^{glyc} \cdot V_{max}^{resp} - V_{glucose} \cdot V_{max}^{glyc}}{V_{max}^{resp} - V_{max}^{glyc}} \\ V_{resp} \\ = \dfrac{V_{max}^{resp}(\phi_{total}^{ATP} \cdot V_{max}^{glyc} \cdot V_{max}^{resp} - V_{glucose}}{V_{max}^{glyc} - V_{max}^{resp}} \end{array} \quad [22]$$

$$\text{If } \begin{array}{l} V_{glyc} \cdot \gamma_{glyc} < V_{resp} \cdot \gamma_{resp} \\ V_{max}^{resp} \cdot \phi_{total}^{ATP} \leq V_{glucose} \end{array} \quad \text{then} \quad V_{glyc} = 0, V_{resp} = V_{max}^{resp} \cdot \phi_{total}^{ATP} \quad [23]$$

To predict the absolute rates of three pathways in *E. coli* – fermentation, Pta-AckA, and respiration, we extended model to include the Pta-AckA pathway as follows:

$$Maximize: \quad V_{ATP} = V_{ferm} \cdot \gamma_{ferm} + V_{pta} \cdot \gamma_{pta} + V_{resp} \cdot \gamma_{resp} \quad [24]$$

$$Subject\ to: \quad \frac{V_{ferm}}{V_{max}^{ferm}} + \frac{V_{pta}}{V_{max}^{pta}} + \frac{V_{resp}}{V_{max}^{resp}} \leq \phi_{total}^{ATP} \quad [25]$$

$$V_{ferm} + V_{pta} + V_{resp} \leq V_{glucose} \quad [26]$$

We used the method of Lagrange multipliers with Karush-Kuhn-Tucker conditions to solve this optimization problem with inequality constraints for the additional Pta-AckA pathway. Since adding a third pathway increases the number of cases for the analytical solution, we also present the three relevant cases to demonstrate that given the relationship between the yield (i.e. $\gamma_{ferm} < \gamma_{pta} < \gamma_{resp}$) and the specific activity (i.e. $\gamma_{ferm} < \gamma_{resp} < \gamma_{pta}$) of the three pathways (*SI Appendix*, Fig. S4 *A* and Fig 2*A*, respectively). We limited our analysis to demonstrate that fermentation would never be under the estimated parameter relationships (*SI Appendix*, Supplementary Discussion 1). The following three cases describe that fermentation is not an energetically favorable option with oxygen is available:

$$\text{If } \begin{array}{l} \boldsymbol{\gamma_{ferm} < \gamma_{resp}} \\ \boldsymbol{\gamma_{pta} < \gamma_{resp}} \\ \boldsymbol{V_{max}^{resp} \cdot \phi_{total}^{ATP} > V_{glucose}} \end{array} \quad \text{then} \quad \boldsymbol{V_{ferm} = 0, V_{pta} = 0, V_{resp} = V_{glucose}} \quad [27]$$

$$\text{If } \begin{array}{l} \gamma_{ferm} < \gamma_{resp} \\ \gamma_{pta} < \gamma_{resp} \\ V_{max}^{ferm} \cdot \gamma_{ferm} < V_{max}^{pta} \cdot \gamma_{pta} \\ V_{max}^{pta} \cdot \gamma_{pta} > V_{max}^{resp} \cdot \gamma_{resp} \\ \phi_{total}^{ATP} \cdot V_{max}^{glyc} > V_{glucose} > \phi_{total}^{ATP} \cdot V_{max}^{resp} \end{array} \text{ then } \begin{array}{l} V_{ferm} = 0 \\ V_{pta} \\ = \dfrac{\phi_{total}^{ATP} \cdot V_{max}^{pta} \cdot V_{max}^{resp} - V_{glucose} \cdot V_{max}^{pta}}{V_{max}^{resp} - V_{max}^{pta}} \\ V_{resp} \\ = \dfrac{V_{max}^{resp}(\phi_{total}^{ATP} \cdot V_{max}^{pta} \cdot V_{max}^{resp} - V_{glucose}}{V_{max}^{pta} - V_{max}^{resp}} \end{array} \quad [28]$$

$$\text{If } \begin{array}{l} V_{max}^{ferm} \cdot \gamma_{ferm} < V_{max}^{pta} \cdot \gamma_{pta} \\ V_{max}^{pta} \cdot \gamma_{pta} > V_{max}^{resp} \cdot \gamma_{resp} \\ V_{max}^{pta} \cdot \phi_{total}^{ATP} < V_{glucose} \end{array} \text{ then } \begin{array}{l} V_{ferm} = 0, V_{pta} = V_{max}^{glyc} \cdot \phi_{total}^{ATP}, V_{resp} \\ = 0 \end{array} \quad [29]$$

To estimate the confidence intervals of model prediction, we performed bootstrapping to resample the five parameter estimates (i.e., fraction of the proteome occupied by pathway, specific activity, and ATP yield) with replacement (N=10,000). After each round of sampling, the specific activity of each pathway and total proteome occupancy of ATP-production enzymes is calculated as described previously. The sampled parameter values for proteome occupied by pathway, specific activity, and ATP yield from each round of bootstrapping were then used for either the linear program or analytical solution described above. All 10,000 results were stored then the mean was plotted with the 95% confidence intervals, signifying the confidence levels. For *S. cerevisiae* and mammalian cells, two additional estimates were conducted: (1) with correlated additional mitochondrial proteins and (2) with all mitochondrial proteins (*SI Appendix*, Fig. S8, Datasets S2 and S3).

To ensure we accurately model only the metabolic fluxes involved in energy production and not biomass production, we calculated the glucose uptake rate by applying the stoichiometric ratios derived from oxygen consumption and glycolytic byproduct formation. The glucose uptake rate used for energy production was then determined by the following:

$$Glucose\ Uptake\ Rate = \frac{V_{resp}^{O2consumption}}{6} + \frac{V_{glyc}^{production}}{2} \quad [30]$$

Cell lines and cell culture

All cell lines were culture in Dulbecco's modified eagle's medium [DMEM (Gibco™ 12800082), 3.7 g/L $NaHCO_3$, 10% FBS (Gibco™ 10437028), and 100 U / mL Penicillin-Streptomycin (Gibco™ 15140122)]. All experiments were performed in the absence of

Penicillin-Streptomycin. The following cell lines were used: C2C12, Huh7, HeLa, U2OS, A549, BR3, H1703, PC3, and MCF7. In addition, published data from following cell lines were used to compare our model estimates: SiHa, Bcap37, 4T1, H1299, HepG2, SW620, HeLa, SKBR3, A549, SF188, primary thymocytes from Wistar rat, primary astrocytes from Wistar rat, H1299, human fibroblast, human retinal pigment epithelium, Anococcygeus muscle from Wistar rat, primary cardiomyocytes from Sprague-Dawley rats.

Measurement of cell volume

During each cell passage, the Coulter Z2 Counter Cell Particle Analyzer (Beckman) was used to determine the concentration and volume of cells. The average volume (fL) and standard deviation of each cell line are reported in Dataset S3.

Cell Protein Concentration Measurement

Protein concentration was determined using bicinchoninic acid (BCA) assay. One million cells were collected in a 2-mL centrifuge tube. Cells were pelleted at 600 g. Media was aspirated. Cells were washed with phosphate-buffered saline, spun, and aspirated twice to remove protein contained in the media. Cells were resuspending in 500 µL of lysis buffer containing 1% sodium dodecyl sulfate and incubated at 90°C for 10 min. Samples were prepared for analysis in triplicate as instructed in the Pierce™ BCA Protein Assay Reagent Kit (Thermo Fisher Scientific 23225). Samples intensity was measured at 562 nm using BioTek Cytation1. Protein concentrations per cell volume for each analyzed mammalian cell line as compared to a bovine serum albumin standard (Dataset S3).

Measurement of lactate production rate

Lactate production rates (LPR) of cell lines were measured using the L-Lactate Assay Kit-I (Colorimetric) (Eton Bioscience 120001400A). Cells were seeded at the volumetric equivalent of 0.5 million HeLa cells, where the average HeLa cell volume was measured to be 2300 fL, per well of a 6-well plate in 3 mL of DMEM and were incubated at 37°C in 5% CO2 incubator. The medium was replaced 24 hours later with 3 mL of the assay medium [DMEM (Gibco™ 12100061), 10 % dialyzed FBS (Gibco™ 26400044) and 3.7 g/L $NaHCO_3$]. Two hundred µL of media was collected every hour for 4 hours and immediately frozen on dry ice. Samples were stored at -80°C until analyzed. At the end of the 4 hour sampling period, cells were trypsinized and counted using the coulter counter. To analyze the samples, 50 µL of sample was combined with 50 µL L-Lactate assay solution. The absorbance at 490 nm was measured for 45 min at 37°C on the BioTek Cytation1. The slope of each well was determined. A standard curve was made by plotting the slope of OD490 nm values for each L-Lactate standards as a function of L-Lactate concentration. The L-Lactate concentration of each biological sample was determined using the equation obtained from the linear regression of the standard curve. L-Lactate in each sample was converted from concentration to moles per g protein using obtained cell counts and protein concentrations per cell volume for each mammalian cell line. Linear regression was performed across the four-hour time course to determine the lactate production rate for each cell line.

Measurement of oxygen consumption rate

Oxygen consumption rates (OCR) of cell lines were measured with the Agilent Seahorse XFe24 Analyzer. Cells were seeded at the volumetric equivalent of 100,000 HeLa cells, where the average HeLa cell volume was measured to be 2300 fL, per well of XFe24 cell culture microplates in 150 µL of DMEM and were incubated at 37°C in 5% CO2 incubator. The medium was replaced 24 hours later with 500 µL of the assay medium [DMEM (Gibco™ 12100061), 10 % dialyzed FBS (Gibco™ 10437028) and 5 mM HEPES-KOH, pH 7.4] and the plates were placed in the Agilent Seahorse XFe24 Analyzer for OCR measurements. Each measurement was performed over 4 min after a 2 min mix and 2 min wait period. Basal measurements were collected 3 times, 3 measurements were collected after injection of oligomycin (final concentration of 1 µM), 3 measurements were collected addition of an initial injection FCCP (final concentration of 3 µM), 3 measurements were collected after a subsequent addition of FCCP (final concentration of 6 µM), 3 measurements were collected after addition of antimycin A and rotenone (final concentration of 1 µM each). Each drug was injected as a concentrated 50 µL solution of the assay medium. At the end of the measurements, cells were trypsinized and counted using the Coulter Z2 Counter Cell Particle Analyzer (Beckman). Oxygen consumption rates were converted to µmol per mg protein per min using obtained cell counts and protein concentrations per cell volume for each mammalian cell line.

Data availability

All data are available in the main text or the supplementary materials of the peer reviewed and published manuscript[61].

Code availability

All data and code used in the figure generation are available as a GitHub repository via https://github.com/DenisTitovLab/WarburgEffectModel

Acknowledgments

Research reported in this publication was supported by the National Institute Of General Medical Sciences of the National Institutes of Health under Award Numbers DP2 GM132933 (D.V.T.) and R35 GM152114 (D.V.T.), by the the Koret-UC Berkeley-Tel Aviv University Initiative in Computational Biology and Bioinformatics (D.V.T. and S.R), and by UC Cancer Research Coordinating Committee of the University of California under Faculty Seed Award Grant Number C24CR7706 (D.V.T) and Predoctoral Fellowship (M.A.K.). We thank A. Arkin, B. Bennett, D. Botstein, A. Flamholtz, H. Garcia, R. Heald, J. Thorner, R. Wang, X. Yang and members of the Titov Lab for valuable comments on the manuscript.

Chapter 2

Glycolytic ATP production enables rapid cell proliferation

Introduction

Adenosine triphosphate (ATP) serves as the universal energy currency of the cell, mediating the coupling of catabolic and anabolic reactions essential for cellular function. Proliferating cells require more ATP than non-proliferating cells to synthesize the biomass necessary for division and the production of two daughter cells. While respiration generates a majority of cellular ATP due to its high efficiency, rapidly proliferating cells often rely on glycolysis to meet the elevated ATP demands associated with cell division. This reliance on glycolysis, despite its lower ATP yield per glucose molecule, is thought to stem from its higher maximal rate, enabling it to produce ATP faster[15]. However, whether glycolysis is strictly necessary for meeting the ATP demands of rapid proliferation or if respiration alone can compensate remains unknown. Here, we quantify the ATP demands associated with increasing growth rates and determine the extent to which glycolysis and respiration are necessary to meeting the elevated ATP requirements of rapid proliferation.

The relationship between ATP production and cell growth has been extensively studied, yet it remains unclear whether ATP production directly limits proliferation. While the limits of ATP production in mammalian cells are not well-quantified, studies in *E. coli* have demonstrated that an elevated ATP demand reduces growth rate, despite the upregulation of glycolysis to increase ATP synthesis[62]. This suggests that ATP may be a limiting factor for growth, as the compensatory increase in glycolytic ATP production is insufficient to fully meet heightened energy demands. In mammalian cells, the role of ATP production rate continues to be debated, with studies suggesting that cancer cells possess a spare capacity for both respiration and glycolysis, allowing compensation when one pathway is inhibited[63,64]. Similar to *E. coli*, elevated ATP demand in mammalian cells induces compensatory glycolysis; however, its effect on growth rate remains unclear[65]. Furthermore, some evidence indicates that cancer cells may have excess ATP[66,67] and increased ATP consumption could potentially drive faster proliferation[11,66]. Furthermore, ATP production rates in solid tumor have been shown to be lower than those in native tissues; however, metastasizing tumors appear to exhibit higher ATP production rates than their tumors of origin[68]. Therefore, it remains unknown how necessary glycolytic ATP production is in rapidly proliferating cells.

Here we demonstrate that glycolysis is necessary for meeting the high ATP demands of rapidly proliferating cells. Specifically, we hypothesize that glycolysis, with its higher specific activity of the pathway, plays a necessary role in supporting rapid growth when respiration alone is insufficient for meeting the ATP demands of the cell. To test this, we showed a strong linear relationship between ATP production rate and growth across three organisms: *E. coli*, *S. cerevisiae*, and mammalian cells. Our predictions indicate that respiration alone cannot sustain the ATP demands observed in faster-growing cells of all three species. Additionally, we demonstrate a causal relationship between ATP production and growth rate by inhibiting each metabolic pathway and quantifying the resulting growth. Notably, we discovered that glycolysis, but not respiration, can compensate for the loss of the other pathway. Finally, we quantified the impact of changes in ATP demand

and revealed how cells preferentially adjust their pathway utilization in response to these changes.

Results

ATP production rate increases linearly with faster growth

In proliferating-cells, ATP production rate must increase with growth as it supports biosynthesis. Increasing ATP production rates with faster growth have been well-appreciated in microbes[69–72]. However, only one study has investigated the relationship between ATP production rate and cell growth in a single mammalian cell type, highlighting the need for more comprehensive studies[73]. Previous results in microbes have demonstrated that the ATP production rate increases with faster growth rates. We were able to corroborate these findings by demonstrating a linearly increase in the ATP production rate (μmol mg protein^{-1} min^{-1}) with growth rate through analyzing curated data from *E. coli* (R^2 = 0.87, p = 3.71e-18) and *S. cerevisiae* (R^2 = 0.91, p = 1.54e-33) (Fig. 1 *A* and *B*). In addition, we tested the correlation between ATP production rate and proliferation rate in ten mammalian cell culture lines by measuring lactate production, oxygen consumption, and growth rates of ten mammalian cells lines (*SI Appendix*, Fig S1). We selected mammalian cells with varying size, growth rates, and tissue of origin to demonstrate that this is a conserved relationship across cell types. Using the summed ATP production rate from oxygen consumption and lactate production, we found a strong correlation between ATP production rate and faster growth for mammalian cells (R^2 = 0.85, p = 0.0017) (Fig. 1*C*). The strong correlation between lactate production and growth rate (R^2 = 0.769, p = 0.0009) supports the hypothesis that glycolysis plays a critical role in meeting the elevated ATP demands of rapidly proliferating cells (*SI Appendix*, Fig S2B). This is further reinforced by the lack of a significant relationship between oxygen consumption and growth rate (R^2 = 0.046, p = 0.5112), indicating that respiration may not be needed to sustain the energy requirements of fast-growing cells (*SI Appendix*, Fig S2A). Our findings underscore the conserved relationship between ATP production rate and growth across diverse cell types, including mammalian cells.

A previous study from Kilburn et al. 1969 determined a linear relationship between ATP production and growth rate for a single mouse cell line, in which variable growth rates were obtained by adjusting pO_2. Though the study concluded that a linear relationship between the ATP production rate and growth, we saw one major issue with their calculations in that the study assumes a yield of 38 ATP per molecule of glucose through respiration. In our analysis, we have revisited recent studies examining the H+/ATP ratio of ATP synthase and proton leak in mammalian cells[74]. Based on these assessments, we propose a revised ATP yield from respiration, suggesting a yield of 24 ATP molecules per glucose molecule. Therefore, we both find a linear relationship between ATP production and growth through different approaches, we out forth a different slope based on a different ATP yield per molecule of glucose from respiration.

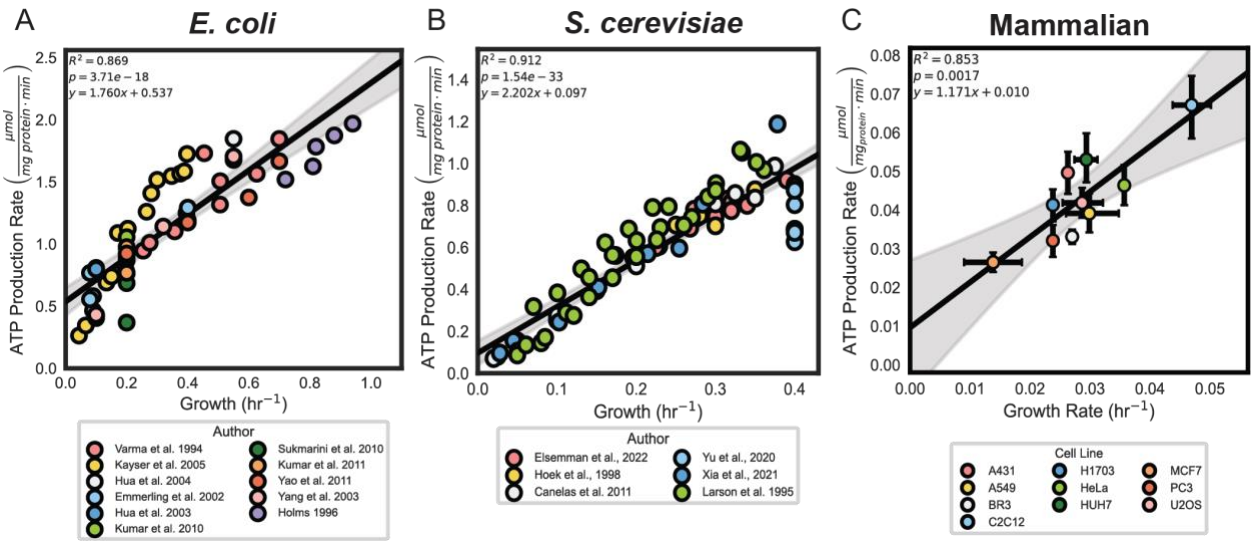


Fig. 1. Energy production and growth are highly correlated across organisms. (*A*-*C*) The correlation between ATP production rate (µmol mg protein^{-1} min^{-1}) and growth rate (hr^{-1}) in *E. coli*, *S. cerevisiae*, and ten mammalian cell lines. Point colors represent data sources or cell lines. Note that all mammalian cell data was generated in the current study. The grey shading in the plot represents the 95% confidence interval of the regression line. The error bars in represent the 95% confidence interval calculated from 10,000 bootstrap iterations**.**

For each organism, the slope of the line did not intersect the origin, indicating that a baseline level of ATP production is required for maintenance in non-growing cells. Maintenance energy supports essential processes such as ion homeostasis, protein turnover, pH regulation, and DNA repair[75]. Interestingly, we observed a log-fold decrease in the required ATP production rate from maintenance from *E. coli* to mammalian cells (*SI Appendix*, Fig S3A). A previous study observed a similar magnitude of change in the maintenance energy requirements of mouse LS cells compared to those of the fungus *P. chrysogenum* and the bacterium *A. aerogenes*[73] (*SI Appendix*, Fig S3B). We found the change in maintenance energy has strikingly resemblance to the surface area to volume (µM^{-1}) ratios between these organisms and may be a consequential cost of maintaining homeostasis with the surrounding media (*SI Appendix*, Fig S3C). Accordingly, we hypothesize that processes such as ion homeostasis, metabolite transport, and pH regulation, rather than protein turnover and DNA repair, account for the majority of ATP demand in non-growing cells.

We converted the ATP production rate from µmol mg$_{protein}$$^{-1}$ min^{-1} to ATP molecules per a mino acid per hr (*SI Appendix*, Fig S4). The slope here reflects the ATP molecules need per amino acid in cell. Mammalian cells require 7.74 ± 1.7 per amino acid, approximately reflecting the energy needed for peptide bond formation for protein synthesis. *E. coli* (11 .6 ± 0.90) and *S. cerevisiae* (14.5 ± 0.72) exhibited higher values potentially due to the a dditional biosynthetic cost of synthesizing amino acids from glucose[76] (*SI Appendix*, Fig S4). Together our results indicate the ATP production rate increases with faster growth, suggesting that it may be a limiting factor in supporting rapid proliferation.

Glycolytic ATP production can support higher growth rates compared to respiration

The ATP production rate adjusts to meet cellular ATP demand. In response to meet the ATP demand of faster growth, previous models predict a metabolic shift from sole reliance on respiration to the concurrent use of glycolysis. The metabolic switch enables rapidly proliferating cells to satisfy their increase ATP requirements efficiently by using a faster pathway per mg proliferation[20,77,22,23,71,61]. Using our previous estimates of the maximal rate ATP production for glycolysis and respiration (μmol $mg_{pathwayprotein}^{-1}$ min^{-1}), we estimated the maximal growth rate that could be supported by the proteome fraction that can be occupied by ATP-producing enzymes in each organism[74]. To theoretically determine the upper limits of cellular ATP production rates via glycolysis and respiration, we propose a calculation for a hypothetical scenario where either pathway exclusively occupies the entire proteome fraction available to ATP-producing enzymes (Equation 1). The maximum ATP production rates (V_{ATP}), expressed in μmol $mg_{protein}^{-1}$ min^{-1}, are calculated by:

$$V_{ATP} = V_{max}^{pathway} \cdot \gamma_{pathway} \cdot \phi_{total}^{ATP} \quad [1]$$

Here, $V_{max}^{pathway}$ denotes the maximum specific activity of the pathway, $\gamma_{pathway}$represents the yield of ATP per molecule of glucose, and ϕ_{total}^{ATP} is the fraction of the proteome allocated to ATP-producing enzymes. This theoretical framework does not reflect feasible physiological conditions since glycolysis nor respiration can occupy the entire fraction of the proteome allocated to ATP-producing enzymes; however, our calculation serves to illustrate potential maximal cellular rates. Utilizing our previous estimates for these variables[61], we initially determined the theoretical maximum ATP production rate and the corresponding growth rate that could be supported by the proteome fraction allocated to ATP-producing enzymes in each organism. We plotted these theoretical maximum rates for glycolysis (red box) and respiration (blue box) (Fig. 2 *A*-*C*).

The point at which each dotted black line intersects the regression line and the x-axis represents the maximum growth rate (dashed gold line) that can theoretically be supported if the respective pathway were solely responsible for ATP production. For each organism, we found that respiration is insufficient to meet ATP production demands required to support the observed high growth rates (Fig. 2 *A*-*C*). However, all growth rates could theoretically be supported by the maximal glycolytic ATP production rate (Fig 2 *A*-*C*).

To further support our findings, we calculated required proteome fraction would need to be occupied by ATP-producing enzymes for both glycolysis and respiration to achieve the observed ATP production rates (Fig 2 *D*-*F*). We compared this required proteome occupancy for each pathway to the upper bound of the 95 percent confidence interval for observed expression of glycolytic (red dashed) and respiratory (blue dashed) enzymes. Our analysis revealed that, while the required proteome occupancy for glycolysis was consistent with the observed values, respiration would require approximately twice the proteome occupancy observed in proteomics experiments to meet the ATP demand of growing cells. Our theoretical calculations align with the experimental demonstrations that

glycolysis alone can meet the ATP demands of cells[78–80]. However, respiration alone appears insufficient to support the ATP production rate requirements of rapidly proliferating cells.

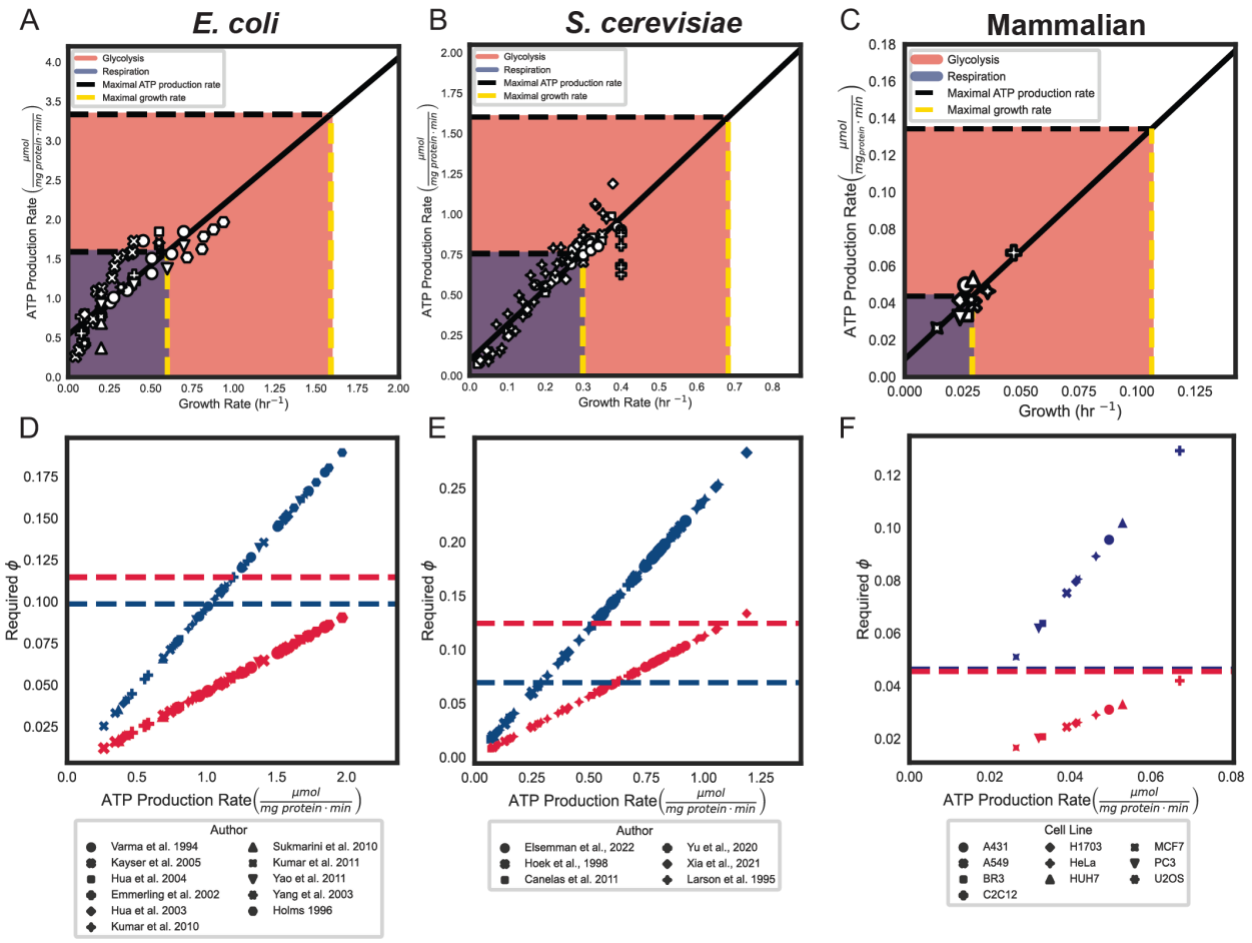


Fig. 2. Glycolysis supports higher ATP production rates in fast-growing cells. (*A-C*) Theoretical ATP production rates (μmol mg protein^{-1} min^{-1}) t achievable exclusively by respiration (blue) or glycolysis (red) in *E. coli*, *S. cerevisiae*, and ten mammalian cell lines, assuming the ATP-producing proteome is fully allocated to one pathway. (*D-F*) Fraction of the proteome (Φ) required to support the observed ATP production rates for growth. Dashed lines indicate the upper bounds of the 95% confidence interval calculated from 10,000 bootstrap iterations for proteome fractions allocated to glycolysis (red) or respiration (blue). Each point represents a distinct publication for *E. coli* and *S. cerevisiae* or a specific mammalian cell line for the mammalian dataset. Point shapes represent data sources or cell lines.

Our results underscore the limitations of respiration in fast-growing cells, where its lower specific activity of the pathway of ATP production becomes insufficient for meeting the ATP demand. Glycolysis, by contrast, can meet the energetic demands of rapid growth due to its higher specific activity, even if it is less efficient in terms of ATP yield per glucose. This observation aligns with the hypothesis that the ability of cells to achieve faster growth rates requires a shift toward pathways with higher ATP production capacity, given the

finite proteome space of the cell. By calculating the theoretical limits of each pathway, our analysis finds glycolysis as a critical metabolic strategy for overcoming the physical constraints imposed by proteome allocation to achieve fast growth.

Glycolysis utilization, not respiration, is necessary for meeting the demand of the ATP demand of fast growth

Previous studies have demonstrated that cells can enhance either glycolysis or oxidative phosphorylation to sustain ATP production when the alternative pathway is genetically or chemically inhibited[81–83]. However, quantifying the extent to which each energy production pathway can compensate for the another in sustaining ATP production to maintain a constant proliferation rate remains unclear. Based on our estimates from Figure 2, we hypothesized that glycolysis, but not oxidative phosphorylation, would compensate for the loss of the alternative pathway. To test this prediction, we evaluated the capacity of cells to adapt to the inhibition of each pathway by measuring ATP production and proliferation rates under pharmacological inhibition of glycolysis or oxidative phosphorylation, quantifying the extent of compensation by the remaining pathway. We selected three of the ten previously studied cell lines—MCF7, U2OS, and C2C12—because they originate from distinct tissues, rely on different ratios of glycolysis and respiration for ATP production, and exhibit varying proliferation rates. If a causal relationship exists between ATP production rate and growth rate, we expect cells to shift along the diagonal line, reflecting proportional changes in both parameters. If no such relationship exists, data points would shift vertically, indicating a reduction in ATP production without a corresponding change in growth rate.

To test the ability for respiration to compensate for glycolysis, we chose to inhibit the terminal step of glycolysis, lactate dehydrogenase (LDH) (Fig. 3*A*). Inhibition lactate dehydrogenase prevents the oxidation of NADH generated in glycolysis to NAD^+, thus disallowing the pathway to be redox neutral and able to generate ATP independently. We used a potent inhibitor LDH, GSK-2837808A (GSK), has demonstrated a high potency with an IC_{50} of 2.6 nM for human LDHA and 43 nM for human LDHB[84] and shown to reduce lactate production in mammalian cells[85,86]. We treated MCF7, U2OS, and C2C12 cells with increasing concentrations of GSK (0, 12.5, 25, 50, 75, and 100 μM). In all cell lines, we observed a dose-dependent decrease in both proliferation rate (hr^{-1}) and lactate production rate (μmol μg^{-1} protein min^{-1}) (*SI Appendix*, Fig S5). While the oxygen consumption rate displayed a modest upward trend, this change was not statistically significant. (*SI Appendix*, Fig S5) Additionally, we found that the growth rate and total ATP production rate (μmol μg^{-1} pathway protein min^{-1}) declined in parallel, exhibiting a similar slope to previously reported data (Fig. 3*D*). Our findings suggest a potential causal relationship between growth rate and ATP production rate. Notably, the oxygen consumption rate did not appear to fully compensate for the loss of lactate production, supporting our hypothesis. Our findings align with a previous study in which double knockout of LDHA and LDHB in human colon adenocarcinoma (LS174T) and murine melanoma (B16-F10) cells led to a two-fold reduction in growth rates compared to wild-type cells[83].

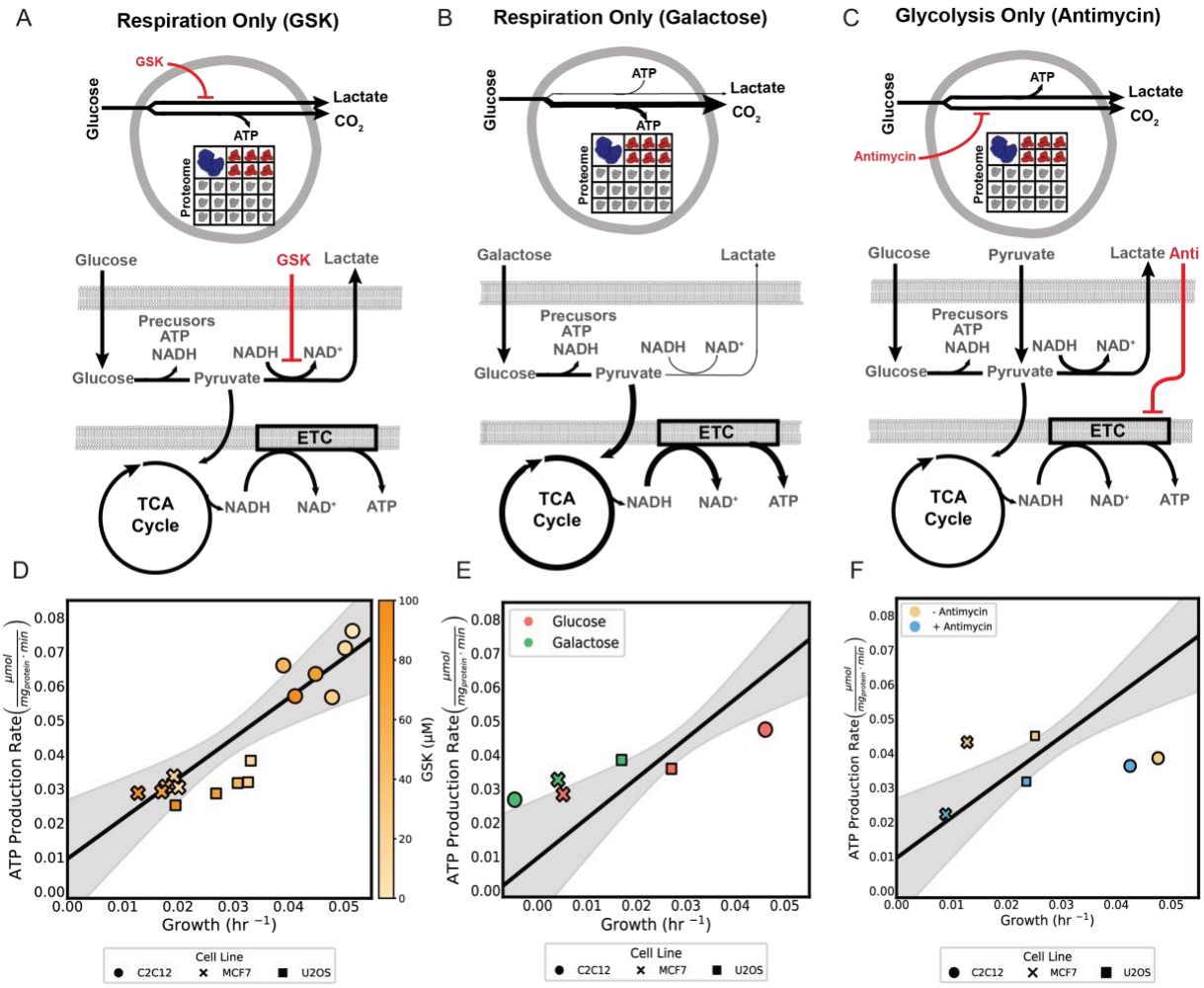


Fig. 3. Glycolysis, not respiration, supports higher ATP production rates in fast-growing cells. (*A*) Increasing concentrations of GSK-2837808A (GSK), an inhibitor of lactate dehydrogenase (LDH), or (*B*) 10 mM Galactose (in the absence of glucose) were used to inhibit lactate production. (*C*) Antimycin was used to inhibit the electron transport chain (ETC). (*D-F*) The relationship between ATP production and growth highlights the ability of one metabolic pathway to compensate for the inhibition of the other. Each point shape represents a distinct cell line. The grey shading represents the 95% confidence interval of the regression line from Figure 1C. Error bars represent the 95% confidence interval calculated from 10,000 bootstrap iterations.

As an additional approach to investigate the effects of reducing lactate production, we cultured cells in media containing equimolar concentrations of glucose or galactose. Galactose, an isomer of glucose, is known to shift cellular metabolism from glycolysis to oxidative phosphorylation, thereby reducing lactate production while increasing oxygen consumption[87,88] (Fig. 3*B*). We observed a significant reduction in lactate production by 7.5-fold, 4.1-fold, and 13.2-fold in MCF7, U2OS, and C2C12 cells, respectively, when grown in galactose compared to glucose (*SI Appendix*, Fig S6). Conversely, oxygen consumption increased by 1.43-fold, 1.79-fold, and 1.54-fold in MCF7, U2OS, and C2C12 cells, respectively, under the same conditions (*SI Appendix*, Fig S6). Notably, the reduction in growth rate depended on the extent to which the cell lines relied on glycolysis

versus oxidative phosphorylation when grown in glucose (Fig. 3*E*). In C2C12 cells, growth rate is tightly coupled to glycolytic ATP production. The transition to galactose impairs growth due to reduced glycolysis, despite increased oxidative phosphorylation. U2OS cells exhibit a balance between glycolysis and oxidative phosphorylation. While growth rate is reduced in galactose, the increase in ATP production and oxygen consumption compensates partially. MCF7 cells maintain similar growth rates in both glucose and galactose, reflecting a greater reliance on oxidative phosphorylation even in glucose. Consistent with the results from pharmacological inhibition of lactate dehydrogenase, culturing cells in glucose or galactose highlights the limited ability of oxidative phosphorylation to fully compensate for reduced glycolysis in faster-growing, highly glycolytic cells such as C2C12. Together, these findings further support a causal relationship between ATP production and growth rate, demonstrating that the ability of cells to meet the ATP demands of growth depends on both the growth rate itself and their relative reliance on glycolysis versus oxidative phosphorylation.

To test the ability for glycolysis to compensate for respiration, we chose to inhibit cytochrome c reductase of the electron transport chain using antimycin (Fig. 3*C*). This inhibition blocks ATP production via oxidative phosphorylation, allowing us to assess the extent to which glycolysis can upregulate to maintain ATP production in the absence of a functional electron transport chain. Antimycin treatment resulted in a 6.5-, 16.4-, and 5.6-fold decrease in oxygen consumption in MCF7, U2OS, and C2C12 cells (*SI Appendix*, Fig S7). To compensate, the lactate production rate increased 1.2-, 1.2-, and 1.7-fold in MCF7, U2OS, and C2C12 cells (*SI Appendix*, Fig S7). We observed minimal growth decrease in each cell line with antimycin treatment (*SI Appendix*, Fig S7). Minimal effect on growth has been reported with other ETC inhibitors, including antimycin for various mammalian cell lines[79,89,90]. Despite significant reductions in oxygen consumption, the minimal changes in growth rate observed in these cell lines suggest that glycolytic upregulation can effectively meet ATP demands, but only to a limited extent, as indicated by the lower overall ATP production rates (Fig. 3*F*).

Our results provide quantification of how glycolysis and oxidative phosphorylation compensate for one another to sustain ATP production and maintain proliferation rates under pathway-specific inhibition. We demonstrate that glycolysis plays a predominant compensatory role in supporting ATP production and growth in highly glycolytic cells, such as C2C12, when oxidative phosphorylation is impaired. Oxidative phosphorylation partially compensates for reduced glycolysis, but its capacity is insufficient to fully sustain growth in faster-growing cells reliant on glycolysis. These findings establish a causal relationship between ATP production and growth rate, where metabolic flexibility varies depending on the inherent reliance on glycolysis or oxidative phosphorylation, which themselves reflect the proliferation rate of the cell.

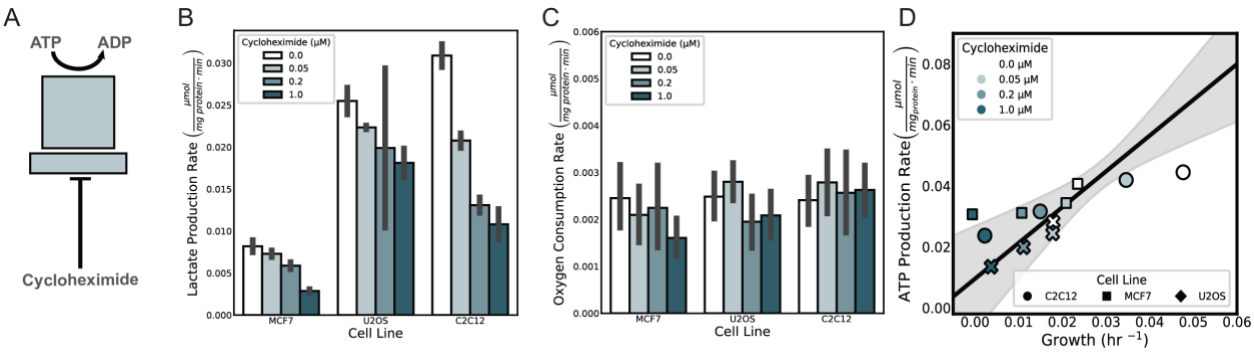


Fig 4. Inhibition of protein synthesis reduces growth and ATP demand. (*A*) Cycloheximide inhibits reduces synthesis by inhibiting the 60S ribosome. (*B*) Effect of increased cycloheximide treatment on lactate production or (*B*) oxygen consumption. Error bars represent the 95% confidence interval. (*D*) The relationship between ATP production and growth with reduce protein synthesis. The grey shading represents the 95% confidence interval of the regression line from Figure 1C. Error bars represent the 95% confidence interval calculated from 10,000 bootstrap iterations.

Lower ATP Demand through reduced protein synthesis preferentially decreases the ATP production rate from glycolysis

We next sought to uncover the effects of manipulating the ATP demand on the preference of glycolysis and respiration. Protein synthesis is one of the most energetically expensive cellular processes. In *E. coli*, proteins constitute over half of the cellular biomass and the process of protein synthesis consumes more than two-thirds of the cell's ATP during periods of rapid growth[91]. Cycloheximide is a potent inhibitor of eukaryotic protein synthesis that functions by binding to the 60S ribosomal subunit, thereby blocking the elongation step during translation[92] (Fig 4*A*). This inhibition reduces the ATP demand of the cell, leading to a potential decrease in ATP production and energy utilization pathways. We observed a concentration dependent decrease in the lactate production rate with increasing cycloheximide treatment, while little change in the oxygen consumption rate (Fig 4 *B*-*D*). The preferential decreased in glycolytic activity was also observed in *S. cerevisiae* treated with cycloheximide[71].

Discussion

Our study demonstrates that glycolysis supports rapid cell proliferation due to its ability to produce ATP at a faster rate per unit of pathway protein as compared to respiration. Using experimental data from *E. coli*, *S. cerevisiae*, and mammalian cells, we established a strong linear correlation between ATP production and growth rate and provide evidence for the causal role of glycolytic flux in supporting increased proliferation rates. Cycloheximide treatment revealed that cells adjust their metabolic preferences between glycolysis and respiration in response to changes in ATP demand, highlighting the hierarchy of choice in meeting the demands of energy metabolism. Together, these results confirm that glycolysis is not merely a supplementary pathway but a necessary for maintaining energy homeostasis and supporting the high biosynthetic demands of proliferating cells.

Materials and Methods

Cell lines and cell culture

All cell lines were culture in Dulbecco's modified eagle's medium [DMEM (Gibco™ 12800082), 3.7 g/L $NaHCO_3$, 10% FBS (Gibco™ 10437028), and 100 U / mL Penicillin-Streptomycin (Gibco™ 15140122)]. All experiments were performed in the absence of Penicillin-Streptomycin. The following cell lines were used: C2C12, Huh7, HeLa, U2OS, A549, BR3, H1703, PC3, A413, and MCF7.

Measurement of cell volume

During each cell passage, the Coulter Z2 Counter Cell Particle Analyzer (Beckman) was used to determine the concentration and volume of cells (fL).

Cell Protein Concentration Measurement

Protein concentration was determined using bicinchoninic acid (BCA) assay. One million cells were collected in a 2-mL centrifuge tube. Cells were pelleted at 600 g. Media was aspirated. Cells were washed with phosphate-buffered saline, spun, and aspirated twice to remove protein contained in the media. Cells were resuspending in 500 µL of lysis buffer containing 1% sodium dodecyl sulfate and incubated at 90°C for 10 min. Samples were prepared for analysis in triplicate as instructed in the Pierce™ BCA Protein Assay Reagent Kit (Thermo Fisher Scientific 23225). Samples intensity was measured at 562 nm using BioTek Cytation1. Protein concentrations per cell volume for each analyzed mammalian cell line as compared to a bovine serum albumin standard.

Measurement of lactate production rate

Lactate production rates (LPR) of cell lines were measured using the L-Lactate Assay Kit-I (Colorimetric) (Eton Bioscience 120001400A). Cells were seeded at the volumetric equivalent of 0.5 million HeLa cells, where the average HeLa cell volume was measured to be 2300 fL, per well of a 6-well plate in 3 mL of DMEM and were incubated at 37°C in 5% CO2 incubator. The medium was replaced 24 hours later with 3 mL of the assay medium [DMEM (Gibco™ 12100061), 10 % dialyzed FBS (Gibco™ 26400044) and 3.7 g/L $NaHCO_3$]. Two hundred µL of media was collected every hour for 4 hours and immediately frozen on dry ice. Samples were stored at -80°C until analyzed. At the end of the 4 hour sampling period, cells were trypsinized and counted using the coulter counter. To analyze the samples, 50 µL of sample was combined with 50 µL L-Lactate assay solution. The absorbance at 490 nm was measured for 45 min at 37°C on the BioTek Cytation1. The slope of each well was determined. A standard curve was made by plotting the slope of OD490 nm values for each L-Lactate standards as a function of L-Lactate concentration. The L-Lactate concentration of each biological sample was determined using the equation obtained from the linear regression of the standard curve. L-Lactate in each sample was converted from concentration to moles per g protein using obtained cell counts and protein concentrations per cell volume for each mammalian cell line. Linear regression was performed across the four-hour time course to determine the lactate production rate for each cell line.

Measurement of oxygen consumption rate

Oxygen consumption rates (OCR) of cell lines were measured with the Agilent Seahorse XFe24 Analyzer. Cells were seeded at the volumetric equivalent of 100,000 HeLa cells, where the average HeLa cell volume was measured to be 2300 fL, per well of XFe24 cell culture microplates in 150 µL of DMEM and were incubated at 37°C in 5% CO2 incubator. The medium was replaced 24 hours later with 500 µL of the assay medium [DMEM (Gibco™ 12100061), 10 % dialyzed FBS (Gibco™ 10437028) and 5 mM HEPES-KOH, pH 7.4] and the plates were placed in the Agilent Seahorse XFe24 Analyzer for OCR measurements. Each measurement was performed over 4 min after a 2 min mix and 2 min wait period. Basal measurements were collected 3 times, 3 measurements were collected after injection of oligomycin (final concentration of 1 µM), 3 measurements were collected addition of an initial injection FCCP (final concentration of 3 µM), 3 measurements were collected after a subsequent addition of FCCP (final concentration of 6 µM), 3 measurements were collected after addition of antimycin A and rotenone (final concentration of 1 µM each). Each drug was injected as a concentrated 50 µL solution of the assay medium. At the end of the measurements, cells were trypsinized and counted using the Coulter Z2 Counter Cell Particle Analyzer (Beckman). Oxygen consumption rates were converted to µmol per mg protein per min using obtained cell counts and protein concentrations per cell volume for each mammalian cell line.

Data availability

All data are available in the main text or the supplementary materials.

Code availability

All data and code used in the figure generation are available as a GitHub repository via https://github.com/DenisTitovLab/ATPGrowth

References

1. Warburg, O., Wind, F. & Negelein, E. The metabolism of tumors in the body. *J Gen Physiol* **8**, 519–530 (1927).
2. Warburg, O. On the origin of cancer cells. *Science* **123**, 309–314 (1956).
3. Potter, M., Newport, E. & Morten, K. J. The Warburg effect: 80 years on. *Biochem Soc Trans* **44**, 1499–1505 (2016).
4. Liberti, M. V. & Locasale, J. W. The Warburg Effect: How Does it Benefit Cancer Cells? *Trends Biochem Sci* **41**, 211–218 (2016).
5. DeBerardinis, R. J. & Chandel, N. S. We need to talk about the Warburg effect. *Nature Metabolism* **2**, 127–129 (2020).
6. Vaupel, P. & Multhoff, G. Revisiting the Warburg effect: historical dogma versus current understanding. *The Journal of Physiology* **599**, 1745–1757 (2021).
7. Fan, J. *et al.* Glutamine-driven oxidative phosphorylation is a major ATP source in transformed mammalian cells in both normoxia and hypoxia. *Molecular Systems Biology* **9**, 712 (2013).
8. Yao, C.-H. *et al.* Mitochondrial fusion supports increased oxidative phosphorylation during cell proliferation. *eLife* **8**, e41351 (2019).
9. Newsholme, E. A., Crabtree, B. & Ardawi, M. S. The role of high rates of glycolysis and glutamine utilization in rapidly dividing cells. *Biosci. Rep.* **5**, 393–400 (1985).
10. Vander Heiden, M. G., Cantley, L. C. & Thompson, C. B. Understanding the Warburg Effect: The Metabolic Requirements of Cell Proliferation. *Science* **324**, 1029–1033 (2009).
11. Luengo, A. *et al.* Increased demand for NAD+ relative to ATP drives aerobic glycolysis. *Molecular Cell* **81**, 691-707.e6 (2021).
12. Brand, K. Aerobic Glycolysis by Proliferating Cells: Protection against Oxidative Stress at the Expense of Energy Yield. 10.

13. Brand, K. A. & Hermfisse, U. Aerobic glycolysis by proliferating cells: a protective strategy against reactive oxygen species1. *The FASEB Journal* **11**, 388–395 (1997).
14. Shen, Y. *et al.* Mitochondrial ATP generation is more proteome efficient than glycolysis. *Nat Chem Biol* 1–10 (2024) doi:10.1038/s41589-024-01571-y.
15. Pfeiffer, T., Schuster, S. & Bonhoeffer, S. Cooperation and Competition in the Evolution of ATP-Producing Pathways. *Science* **292**, 504–507 (2001).
16. Schuster, S., Pfeiffer, T. & Fell, D. A. Is maximization of molar yield in metabolic networks favoured by evolution? *Journal of Theoretical Biology* **252**, 497–504 (2008).
17. Rozpędowska, E. *et al.* Parallel evolution of the make–accumulate–consume strategy in Saccharomyces and Dekkera yeasts. *Nat Commun* **2**, 302 (2011).
18. Zhuang, K., Vemuri, G. N. & Mahadevan, R. Economics of membrane occupancy and respiro-fermentation. *Molecular Systems Biology* **7**, 500 (2011).
19. Szenk, M., Dill, K. A. & de Graff, A. M. R. Why Do Fast-Growing Bacteria Enter Overflow Metabolism? Testing the Membrane Real Estate Hypothesis. *Cell Systems* **5**, 95–104 (2017).
20. Molenaar, D., van Berlo, R., de Ridder, D. & Teusink, B. Shifts in growth strategies reflect tradeoffs in cellular economics. *Molecular Systems Biology* **5**, 323 (2009).
21. Flamholz, A., Noor, E., Bar-Even, A., Liebermeister, W. & Milo, R. Glycolytic strategy as a tradeoff between energy yield and protein cost. *Proc Natl Acad Sci U S A* **110**, 10039–10044 (2013).
22. Basan, M. *et al.* Overflow metabolism in E. coli results from efficient proteome allocation. *Nature* **528**, 99–104 (2015).
23. Chen, Y. & Nielsen, J. Energy metabolism controls phenotypes by protein efficiency and allocation. *Proc Natl Acad Sci U S A* **116**, 17592–17597 (2019).
24. Majewski, R. A. & Domach, M. M. Simple constrained-optimization view of acetate overflow in E. coli. *Biotechnol Bioeng* **35**, 732–738 (1990).

25. Dai, Z., Shestov, A. A., Lai, L. & Locasale, J. W. A Flux Balance of Glucose Metabolism Clarifies the Requirements of the Warburg Effect. *Biophysical Journal* **111**, 1088–1100 (2016).
26. Wang, Y. *et al.* Saturation of the mitochondrial NADH shuttles drives aerobic glycolysis in proliferating cells. *Molecular Cell* **82**, 3270-3283.e9 (2022).
27. Mori, M., Schink, S., Erickson, D. W., Gerland, U. & Hwa, T. Quantifying the benefit of a proteome reserve in fluctuating environments. *Nat Commun* **8**, 1225 (2017).
28. Xia, J. *et al.* Proteome allocations change linearly with the specific growth rate of Saccharomyces cerevisiae under glucose limitation. *Nat Commun* **13**, 2819 (2022).
29. Kuhn, H. W. & Tucker, A. W. Nonlinear programming. in *Proceedings of the Second Berkeley Symposium on Mathematical Statistics and Probability, 1950* 481–492 (Univ. California Press, Berkeley-Los Angeles, Calif., 1951).
30. Pasteur, L. Mémoire sur la fermentation alcoolique. *Comptes rendus des séances de l'Académie des Sciences* **45**, 1032–1036 (1857).
31. Krebs, H. A. The Pasteur effect and the relations between respiration and fermentation. *Essays Biochem* **8**, 1–34 (1972).
32. Racker, E. History of the Pasteur effect and its pathobiology. *Mol Cell Biochem* **5**, 17–23 (1974).
33. Sols, A. The Paster Effect in the allosteric era. in *Reflections on Biochemistry* (eds. Kornberg, A., Horecker, B. L., Cornudella, L. & Oro, J.) 199–206 (Pergamon, 1976). doi:10.1016/B978-0-08-021010-0.50027-2.
34. Lagunas, R., Dominguez, C., Busturia, A. & Sáez, M. J. Mechanisms of appearance of the Pasteur effect in Saccharomyces cerevisiae: inactivation of sugar transport systems. *J Bacteriol* **152**, 19–25 (1982).
35. Clark, D. P. The fermentation pathways of Escherichia coli. *FEMS Microbiology Letters* **63**, 223–234 (1989).

36. Dittrich, C. R., Vadali, R. V., Bennett, G. N. & San, K.-Y. Redistribution of Metabolic Fluxes in the Central Aerobic Metabolic Pathway of E. coli Mutant Strains with Deletion of the ackA-pta and poxB Pathways for the Synthesis of Isoamyl Acetate. *Biotechnology Progress* **21**, 627–631 (2005).
37. Enjalbert, B., Millard, P., Dinclaux, M., Portais, J.-C. & Létisse, F. Acetate fluxes in Escherichia coli are determined by the thermodynamic control of the Pta-AckA pathway. *Sci Rep* **7**, 42135 (2017).
38. Elsemman, I. E. *et al.* Whole-cell modeling in yeast predicts compartment-specific proteome constraints that drive metabolic strategies. *Nat Commun* **13**, 801 (2022).
39. Huberts, D. H. E. W., Niebel, B. & Heinemann, M. A flux-sensing mechanism could regulate the switch between respiration and fermentation. *FEMS Yeast Research* **12**, 118–128 (2012).
40. You, C. *et al.* Coordination of bacterial proteome with metabolism by cyclic AMP signalling. *Nature* **500**, 301–306 (2013).
41. Erickson, D. W. *et al.* A global resource allocation strategy governs growth transition kinetics of Escherichia coli. *Nature* **551**, 119–123 (2017).
42. Sazanov, L. A. A giant molecular proton pump: structure and mechanism of respiratory complex I. *Nat Rev Mol Cell Biol* **16**, 375–388 (2015).
43. Heikal, A. *et al.* Structure of the bacterial type II NADH dehydrogenase: a monotopic membrane protein with an essential role in energy generation. *Mol Microbiol* **91**, 950–964 (2014).
44. Iwata, M. *et al.* The structure of the yeast NADH dehydrogenase (Ndi1) reveals overlapping binding sites for water- and lipid-soluble substrates. *Proc Natl Acad Sci U S A* **109**, 15247–15252 (2012).
45. Nelson, P. & Masel, J. Intercellular competition and the inevitability of multicellular aging. *Proc Natl Acad Sci U S A* **114**, 12982–12987 (2017).

46. Michaels, T. C. T. & Mahadevan, L. Optimal intercellular competition in senescence and cancer. *Proc. R. Soc. A.* **479**, 20230204 (2023).
47. Crow, M. T. & Kushmerick, M. J. Chemical energetics of slow- and fast-twitch muscles of the mouse. *Journal of General Physiology* **79**, 147–166 (1982).
48. Peebo, K. *et al.* Proteome reallocation in Escherichia coli with increasing specific growth rate. *Mol. BioSyst.* **11**, 1184–1193 (2015).
49. Brahimi-Horn, M. C., Chiche, J. & Pouysségur, J. Hypoxia signalling controls metabolic demand. *Current Opinion in Cell Biology* **19**, 223–229 (2007).
50. Wiśniewski, J. R., Hein, M. Y., Cox, J. & Mann, M. A "Proteomic Ruler" for Protein Copy Number and Concentration Estimation without Spike-in Standards *. *Molecular & Cellular Proteomics* **13**, 3497–3506 (2014).
51. Varma, A. & Palsson, B. O. Stoichiometric flux balance models quantitatively predict growth and metabolic by-product secretion in wild-type Escherichia coli W3110. *Appl Environ Microbiol* **60**, 3724–3731 (1994).
52. Van Hoek, P., Van Dijken, J. P. & Pronk, J. T. Effect of Specific Growth Rate on Fermentative Capacity of Baker's Yeast. *Appl Environ Microbiol* **64**, 4226–4233 (1998).
53. Plitzko, B. & Loesgen, S. Measurement of Oxygen Consumption Rate (OCR) and Extracellular Acidification Rate (ECAR) in Culture Cells for Assessment of the Energy Metabolism. *Bio Protoc* **8**, e2850 (2018).
54. Desousa, B. R. *et al.* Calculation of ATP production rates using the Seahorse XF Analyzer. *EMBO Reports* **24**, e56380 (2023).
55. Carroll, K. M. *et al.* Absolute Quantification of the Glycolytic Pathway in Yeast: *Mol Cell Proteomics* **10**, M111.007633 (2011).
56. Finka, A. & Goloubinoff, P. Proteomic data from human cell cultures refine mechanisms of chaperone-mediated protein homeostasis. *Cell Stress and Chaperones* **18**, 591–605 (2013).

57. Hinkle, P. C. P/O ratios of mitochondrial oxidative phosphorylation. *Biochim Biophys Acta* **1706**, 1–11 (2005).
58. Steigmiller, S., Turina, P. & Gräber, P. The thermodynamic H+/ATP ratios of the H+-ATPsynthases from chloroplasts and Escherichia coli. *Proceedings of the National Academy of Sciences* **105**, 3745–3750 (2008).
59. Petersen, J., Förster, K., Turina, P. & Gräber, P. Comparison of the H+/ATP ratios of the H+-ATP synthases from yeast and from chloroplast. *Proceedings of the National Academy of Sciences* **109**, 11150–11155 (2012).
60. Dunning, I., Mitchell, S. & O'Sullivan, M. PuLP: A Linear Programming Toolkit for Python. Preprint at https://optimization-online.org/?p=11731 (2011).
61. Kukurugya, M. A., Rosset, S. & Titov, D. V. The Warburg Effect is the result of faster ATP production by glycolysis than respiration. *Proceedings of the National Academy of Sciences* **121**, e2409509121 (2024).
62. Boecker, S. *et al.* Deciphering the physiological response of Escherichia coli under high ATP demand. *Molecular Systems Biology* **17**, e10504 (2021).
63. Birsoy, K. *et al.* Metabolic determinants of cancer cell sensitivity to glucose limitation and biguanides. *Nature* **508**, 108–112 (2014).
64. Andrzejewski, S., Gravel, S.-P., Pollak, M. & St-Pierre, J. Metformin directly acts on mitochondria to alter cellular bioenergetics. *Cancer Metab* **2**, 12 (2014).
65. Epstein, T., Xu, L., Gillies, R. J. & Gatenby, R. A. Separation of metabolic supply and demand: aerobic glycolysis as a normal physiological response to fluctuating energetic demands in the membrane. *Cancer & Metabolism* **2**, 7 (2014).
66. Fang, M. *et al.* The ER UDPase ENTPD5 promotes protein N-glycosylation, the Warburg effect, and proliferation in the PTEN pathway. *Cell* **143**, 711–724 (2010).
67. Vander Heiden, M. G. *et al.* Evidence for an alternative glycolytic pathway in rapidly proliferating cells. *Science* **329**, 1492–1499 (2010).

68. Bartman, C. R. *et al.* Slow TCA flux and ATP production in primary solid tumours but not metastases. *Nature* **614**, 349–357 (2023).
69. Nissen, T. L., Schulze, U., Nielsen, J. & Villadsen, J. Flux Distributions in Anaerobic, Glucose-Limited Continuous Cultures of Saccharomyces Cerevisiae. *Microbiology* **143**, 203–218 (1997).
70. Canelas, A. B., Ras, C., ten Pierick, A., van Gulik, W. M. & Heijnen, J. J. An in vivo data-driven framework for classification and quantification of enzyme kinetics and determination of apparent thermodynamic data. *Metab Eng* **13**, 294–306 (2011).
71. Elsemman, I. E. *et al.* Whole-cell modeling in yeast predicts compartment-specific proteome constraints that drive metabolic strategies. *Nat Commun* **13**, 801 (2022).
72. Kayser, A., Weber, J., Hecht, V. & Rinas, U. Metabolic flux analysis of Escherichia coli in glucose-limited continuous culture. I. Growth-rate-dependent metabolic efficiency at steady state. *Microbiology (Reading)* **151**, 693–706 (2005).
73. Kilburn, D. G., Lilly, M. D. & Webb, F. C. The energetics of mammalian cell growth. *Journal of Cell Science* **4**, 645–654 (1969).
74. Kukurugya, M. A. & Titov, D. V. The Warburg Effect is the result of faster ATP production by glycolysis than respiration. 2022.12.28.522160 Preprint at https://doi.org/10.1101/2022.12.28.522160 (2022).
75. Pirt, S. J. The Maintenance Energy of Bacteria in Growing Cultures. *Proceedings of the Royal Society of London. Series B, Biological Sciences* **163**, 224–231 (1965).
76. Akashi, H. & Gojobori, T. Metabolic efficiency and amino acid composition in the proteomes of Escherichia coli and Bacillus subtilis. *Proceedings of the National Academy of Sciences* **99**, 3695–3700 (2002).
77. Vazquez, A., Liu, J., Zhou, Y. & Oltvai, Z. N. Catabolic efficiency of aerobic glycolysis: The Warburg effect revisited. *BMC Systems Biology* **4**, 58 (2010).

78. King, M. P. & Attardi, G. Human cells lacking mtDNA: repopulation with exogenous mitochondria by complementation. *Science* **246**, 500–503 (1989).
79. Titov, D. V. *et al.* Complementation of mitochondrial electron transport chain by manipulation of the NAD+/NADH ratio. *Science* **352**, 231–235 (2016).
80. Choe, M. & Titov, D. V. Genetically encoded tool for manipulation of ΔΨm identifies the latter as the driver of integrative stress response induced by ATP Synthase dysfunction. *bioRxiv* 2023.12.27.573435 (2023) doi:10.1101/2023.12.27.573435.
81. Mookerjee, S. A., Nicholls, D. G. & Brand, M. D. Determining Maximum Glycolytic Capacity Using Extracellular Flux Measurements. *PLOS ONE* **11**, e0152016 (2016).
82. Mookerjee, S. A., Gerencser, A. A., Nicholls, D. G. & Brand, M. D. Quantifying intracellular rates of glycolytic and oxidative ATP production and consumption using extracellular flux measurements. *J Biol Chem* **292**, 7189–7207 (2017).
83. Ždralević, M. *et al.* Double genetic disruption of lactate dehydrogenases A and B is required to ablate the “Warburg effect” restricting tumor growth to oxidative metabolism. *Journal of Biological Chemistry* **293**, 15947–15961 (2018).
84. Billiard, J. *et al.* Quinoline 3-sulfonamides inhibit lactate dehydrogenase A and reverse aerobic glycolysis in cancer cells. *Cancer & Metabolism* **1**, 19 (2013).
85. Niu, X., Chen, Y.-J., Crawford, P. A. & Patti, G. J. Transport-exclusion pharmacology to localize lactate dehydrogenase activity within cells. *Cancer & Metabolism* **6**, 19 (2018).
86. Notarangelo, G. *et al.* Oncometabolite d-2HG alters T cell metabolism to impair CD8+ T cell function. *Science* (2022) doi:10.1126/science.abj5104.
87. Gohil, V. M. *et al.* Nutrient-sensitized screening for drugs that shift energy metabolism from mitochondrial respiration to glycolysis. *Nat Biotechnol* **28**, 249–255 (2010).
88. Aguer, C. *et al.* Galactose enhances oxidative metabolism and reveals mitochondrial dysfunction in human primary muscle cells. *PLoS One* **6**, e28536 (2011).

89. Birsoy, K. *et al.* An Essential Role of the Mitochondrial Electron Transport Chain in Cell Proliferation Is to Enable Aspartate Synthesis. *Cell* **162**, 540–551 (2015).
90. Jain, I. H. *et al.* Hypoxia as a therapy for mitochondrial disease. *Science* **352**, 54–61 (2016).
91. Russell, J. B. & Cook, G. M. Energetics of bacterial growth: balance of anabolic and catabolic reactions. *Microbiol Rev* **59**, 48–62 (1995).
92. Baliga, B. S., Pronczuk, A. W. & Munro, H. N. Mechanism of cycloheximide inhibition of protein synthesis in a cell-free system prepared from rat liver. *J Biol Chem* **244**, 4480–4489 (1969).

Appendix

Chapter 1

Supplementary Discussion 1

Overview of Linear Program and Derivation of Analytical Solution

Here we present our model of cellular ATP production. We aimed to maintain a simple mathematical model to allow for intuitive biological interpretation of both the underlying framework as well as the model outputs. Therefore, the model uses five biochemical parameters, including the ATP yield (γ_{glyc} and γ_{resp}) and specific activity (V_{glyc} and V_{resp}) of glycolysis and respiration and fraction of the proteome that can be occupied by ATP-producing enzymes (ϕ_{total}^{ATP}).

Model parameters:

- V_{total}^{ATP} represent the total ATP production rate (μmol mg protein^{-1} min^{-1})
- V_{max}^{glyc} and V_{max}^{resp} represent the specific activity of pathway (μmol mg pathway^{-1} min^{-1})
- γ_{glyc} and γ_{resp}represent the yield of ATP per glucose for the pathway (unitless)
- ϕ_{total}^{ATP} represent the fraction of the proteome dedicated to ATP-producing enzymes

The purpose of the model is to pointedly test our hypothesis that the Warburg Effect allows cells to produce ATP at a maximal rate. Accordingly, we chose to use linear programming, a mathematical method for optimizing a linear objective function subject to given constraints. The goal of the linear program is to find values of the free variable that maximize or minimize the objective function while satisfying the constraints. Our objective function is written to maximize the ATP production rate (V_{total}^{ATP}) (equation 1) by changing the rates V_{glyc} and V_{resp} within the allocated total proteome space for ATP-producing enzymes (ϕ_{total}^{ATP}) in response to the changes in glucose uptake rate ($V_{glucose}$).

Independent variable:

- $V_{glucose}$ represent the glucose uptake rate (μmol mg protein^{-1} min^{-1})

Decision variables (model output):

- V_{glyc} and V_{resp} represent the rates of glycolysis or respiration (μmol mg protein^{-1} min^{-1}) utilized to maximize the ATP production rate in response to the glucose uptake rate.

The objective function is given by:

$$Maximize: \quad V_{total}^{ATP} = V_{glyc} \cdot \gamma_{glyc} + V_{resp} \cdot \gamma_{resp} \quad [1]$$

The model must also satisfy three constraints that i) the rate of glycolysis and respiration cannot proceed faster than what is allowed by the proteome allocation for ATP-producing enzymes (ϕ_{total}^{ATP}) and ii) glucose uptake rate cannot be larger than the combined rates of glycolysis and respiration iii) the rate of the pathways cannot be negative (equation S1).

$$Subject\ to: \quad \frac{V_{glyc}}{V_{max}^{glyc}} + \frac{V_{resp}}{V_{max}^{resp}} \leq \phi_{total}^{ATP} \quad [2]$$

$$V_{glyc} + V_{resp} \leq V_{glucose} \quad [3]$$

$$V_{glyc} \geq 0, V_{resp} \geq 0 \quad [S1]$$

We can use the V_{glyc} and V_{resp}values to calculate the absolute rates of glycolytic by-product (i.e. acetate, ethanol, or lactate) or oxygen consumption from the predicted rates of glycolysis and respiration (equation S2 and S3, respectively):

$$V_{glyc}^{byproduct} = \gamma_{gluc}^{byproduct} \cdot V_{glyc} \quad [S2]$$

$$V_{resp}^{O2} = \gamma_{resp}^{O2,consumed} \cdot V_{resp} \quad [S3]$$

This optimization problem can either be solved using linear programming or analytically using the Lagrange Dual Function (LDF) with Karush-Kuhn-Tucker (KKT) conditions. The benefit of this approach is to reveal how the constraints are governing the optimum. Therefore, we gain additional insight from the analytical solution for the biologically relevant cases. The KKT conditions provide necessary conditions for optimality problems with inequality constraints. The four conditions are known as (1) primal feasibility, (2) dual feasibility, (3) stationary, (4) complementary slackness.

(1) The primal feasibility condition simply means that for a solution to be considered valid, it must not violate any of the original given constraints. The requirement ensures the solution lies within the feasible region drawn by the constraints.

(2) The dual feasibility conditions states that the Lagrange multipliers associated with inequality constraints are non-negative. The requirement ensures that the optimized solution of the objective function will wither stay the same or decrease in value if the constraints are relaxed.

(3) The stationary condition states that at the optimal point, the gradient of the Lagrangian with respect to decision variables (model output) must be zero. In other words, it is not possible to increase or decrease the value of the objective function by adjusting these variables while still satisfying the constraints.

(4) The complimentary slackness condition states that the product of the Lagrangian multiplier and the associated inequality constraint must be zero. The complimentary slackness KKT condition allows us to determine when each constraint is in effect for a given set of inputs. If the inequality is not constraining the optimal solution, the associated Lagrangian multiplier will be zero so that it does not influence the optimality for the solution.

It is standard practice to use minimization rather than maximation in the presentation of LDF. Therefore, we convert the maximization into the equivalent minimization problem by multiplying the objective function by -1. We must also multiply constraint S1 by -1 so V_{glyc} and V_{resp} remain non-negative. With $V_{max}^{glyc},\ \gamma_{glyc}, V_{max}^{resp}, \gamma_{resp} > 0,$ rewrite the program as:

$$Minimize: \quad V_{total}^{ATP} = -(V_{glyc} \cdot \gamma_{glyc}) - (V_{resp} \cdot \gamma_{resp}) \qquad [S4]$$

$$Subject\ to: \quad \frac{V_{glyc}}{V_{max}^{glyc}} + \frac{V_{resp}}{V_{max}^{resp}} \leq \phi_{total}^{ATP} \qquad [2]$$

$$V_{glyc} + V_{resp} \leq V_{glucose} \qquad [3]$$

$$-V_{glyc} \leq 0, -V_{resp} \leq 0 \qquad [S5]$$

Now, we form the Lagrangian function (L) by combing the objective function and constraints.
By combing the objective function and constraints, the Lagrangian function transforms a constrained optimization problem into an unconstrained one. The constraints here are weighted by the Lagrangian multipliers (λ), which gives us the change in value of objective function as the constraint changes, known as relaxing the constraint. Also, we assume $V_{max}^{glyc} \cdot \gamma_{glyc} \neq V_{max}^{resp} \cdot \gamma_{resp}, \quad V_{max}^{glyc} \neq V_{max}^{resp}, \quad V_{max}^{resp} \cdot \gamma_{resp} \cdot V_{max}^{glyc} \neq V_{glyc} \cdot \gamma_{glyc} \cdot V_{max}^{resp}, \quad \phi_{total}^{ATP} \cdot V_{max}^{glyc} \neq V_{glucose}, \quad \phi_{total}^{ATP} \cdot V_{max}^{resp} \neq V_{glucose}$ to avoid redundancies. The Lagrangian function for this:

$$L = -(V_{glyc} \cdot \gamma_{glyc}) - (V_{resp} \cdot \gamma_{resp}) + \lambda_1 \left(\frac{V_{glyc}}{V_{max}^{glyc}} + \frac{V_{resp}}{V_{max}^{resp}} - \phi_{total}^{ATP}\right) \qquad [S6]$$
$$+\lambda_2 \left(V_{glyc} + V_{resp} - V_{glucose}\right) - \lambda_{glyc} V_{glyc} - \lambda_{resp} V_{resp}$$

Next, we take the partial derivative of the Lagrangian function with respect to V_{glyc} and V_{resp}. The Lagrange multipliers associated with the inequality constraints must be non-negative. Therefore, derivatives are given by:

$$\frac{\partial L}{\partial V_{glyc}} = -\gamma_{glyc} + \lambda_1 \frac{1}{V_{max}^{glyc}} + \lambda_2 - \lambda_{glyc} = 0 \quad \text{[S7]}$$

$$\frac{\partial L}{\partial V_{resp}} = -\gamma_{resp} + \lambda_1 \frac{1}{V_{max}^{resp}} + \lambda_2 - \lambda_{resp} = 0 \quad \text{[S8]}$$

For the inequality constraints, the complementary slackness for non-negative Lagrange is given by:

$$\lambda_1 > 0 \Rightarrow \frac{V_{glyc}}{V_{max}^{glyc}} + \frac{V_{resp}}{V_{max}^{resp}} = \phi_{total}^{ATP} \quad \text{[S9]}$$

$$\lambda_2 > 0 \Rightarrow V_{glyc} + V_{resp} = V_{glucose} \quad \text{[S10]}$$

$$\lambda_{glyc} > 0 \Rightarrow V_{glyc} = 0 \quad \text{[S11]}$$

$$\lambda_{resp} > 0 \Rightarrow V_{resp} = 0 \quad \text{[S12]}$$

We also know that in the optimal solution either $\frac{V_{glyc}}{V_{max}^{glyc}} + \frac{V_{resp}}{V_{max}^{resp}} = \phi_{total}^{ATP}$ or $V_{glyc} + V_{resp} = V_{glucose}$ or both (otherwise can improve by increasing V_{glyc} or V_{resp}) and we can use that. We can consider different cases, solve them, and see when they are optimal:

- $V_{glyc} > 0$, $V_{resp} = 0$, $\frac{V_{glyc}}{V_{max}^{glyc}} + \frac{V_{resp}}{V_{max}^{resp}} = \phi_{total}^{ATP}$ and $V_{glyc} + V_{resp} < V_{glucose}$
  In this case, $V_{glyc} = V_{max}^{glyc} \cdot \phi_{total}^{ATP}$, $\lambda_{glyc} = 0$, $\lambda_2 = 0$. Thus from (S7) $\lambda_1 = \gamma_{glyc} \cdot V_{max}^{glyc}$, and from (S8) $\lambda_{resp} = \gamma_{glyc} \cdot V_{max}^{glyc} - \gamma_{resp} \cdot V_{max}^{resp} > 0$.
  So for this solution to be legal we require: $V_{glucose} > \phi_{total}^{ATP} \cdot V_{max}^{glyc}$ (for second constraint) and $\gamma_{glyc} \cdot V_{max}^{glyc} - \gamma_{resp} \cdot V_{max}^{resp} > 0$ (for $\lambda_{resp} > 0$).

- $V_{glyc} > 0$, $V_{resp} = 0$, $\frac{V_{glyc}}{V_{max}^{glyc}} + \frac{V_{resp}}{V_{max}^{resp}} < \phi_{total}^{ATP}$ and $V_{glyc} + V_{resp} = V_{glucose}$.
  This is similar, $V_{glyc} = V_{glucose}$, $\lambda_{glyc} = 0$, $\lambda_1 = 0$. Thus from (S7) $\lambda_2 = \gamma_{glyc}$, and from (S8) $\lambda_{resp} = \gamma_{glyc} - \gamma_{resp}$. So for this solution to be legal we require: $V_{max}^{glyc} \cdot \phi_{total}^{ATP} > V_{glucose}$ (for first constraint) and $\gamma_{glyc} > \gamma_{resp}$ (for $\lambda_{resp} > 0$).

- $V_{glyc} = 0$, $\phi_{resp} > 0$, $\frac{V_{glyc}}{V_{max}^{glyc}} + \frac{V_{resp}}{V_{max}^{resp}} = \phi_{total}^{ATP}$ and $V_{glyc} + V_{resp} < V_{glucose}$.
  $\phi_{resp} = V_{max}^{resp} \cdot \phi_{total}^{ATP}$, and the same calculations as the first case, give:
  $V_{glucose} > \phi_{total}^{ATP} \cdot V_{max}^{resp}$ (for second constraint) and $\gamma_{resp} \cdot V_{max}^{resp} - \gamma_{glyc} \cdot V_{max}^{glyc} > 0$ (for $\lambda_{glyc} > 0$).

- $V_{glyc} = 0$, $V_{resp} > 0$, $\frac{V_{glyc}}{V_{max}^{glyc}} + \frac{V_{resp}}{V_{max}^{resp}} < \phi_{total}^{ATP}$ and $V_{glyc} + V_{resp} = V_{glucose}$.
  $\phi_{resp} = V_{glucose}$ and the same calculations as second case, give:
  $V_{max}^{resp} \cdot \phi_{total}^{ATP} > V_{glucose}$(for first constraint) and $\gamma_{resp} > \gamma_{glyc}$ (for $\lambda_{glyc} > 0$).

- $\frac{V_{glyc}}{V_{max}^{glyc}} + \frac{V_{resp}}{V_{max}^{resp}} = \phi_{total}^{ATP}$ and $V_{glyc} + V_{resp} = V_{glucose}$. In this case, due to non-redundancy, we must have that both V_{glyc} and V_{resp} are non-zero. We can solve them:
  $$V_{glyc} = \frac{\phi_{total}^{ATP} \cdot V_{max}^{glyc} \cdot V_{max}^{resp} - V_{glucose} \cdot V_{max}^{glyc}}{V_{max}^{resp} - V_{max}^{glyc}},$$
  $$V_{resp} = \frac{V_{max}^{resp}(\phi_{total}^{ATP} \cdot V_{max}^{glyc} \cdot V_{max}^{resp} - V_{glucose})}{V_{max}^{glyc} - V_{max}^{resp}}$$

Note that neither can be zero by non-redundancy assumption, but they have to be positive, otherwise it's a violation of the non-negativity constraint. In this case, we have $\lambda_{glyc} = \lambda_{resp} = 0$ and λ_1, λ_2 can be positive. We can find them from (S9, S10):

$$\lambda_1 = \frac{V_{max}^{resp} \cdot V_{max}^{glyc}(\gamma_{resp} - \gamma_{glyc})}{V_{max}^{glyc} - V_{max}^{resp}}, \lambda_2 = \gamma_{glyc} - \frac{V_{max}^{resp}(\gamma_{resp} - \gamma_{glyc})}{V_{max}^{glyc} - V_{max}^{resp}}$$

Now to get the required positivity of ϕ_{resp}, ϕ_{glyc}, λ_1, λ_2, we have the following scenarios:

Either: $\phi_{total}^{ATP} \cdot V_{max}^{glyc} > V_{glucose} > \phi_{total}^{ATP} \cdot V_{max}^{resp}$ and $V_{max}^{glyc} \cdot \gamma_{glyc} > V_{max}^{resp} \cdot \gamma_{resp}$ and $V_{max}^{resp} \cdot \gamma_{resp} \cdot V_{max}^{glyc} > V_{max}^{glyc} \cdot \gamma_{glyc} \cdot V_{resp}$
OR: $\phi_{total}^{ATP} \cdot V_{max}^{glyc} < V_{glucose} < \phi_{total}^{ATP} \cdot V_{max}^{resp}$ and $\cdot V_{max}^{glyc} \cdot \gamma_{glyc} < V_{max}^{resp} \cdot \gamma_{resp}$ and $V_{max}^{resp} \cdot \gamma_{resp} \cdot V_{max}^{glyc} < \cdot V_{max}^{glyc} \cdot \gamma_{glyc} \cdot V_{max}^{resp}$

Finally, we would like to summarize the analytical solution below with the five cases. Our hope is that these equations as presented will be used in future efforts to study the resource allocation in energy metabolism.

If $\boldsymbol{\gamma_{glyc} < \gamma_{resp}}$ and $\boldsymbol{V_{max}^{resp} \cdot \phi_{total}^{ATP} > V_{glucose}}$ then $\boldsymbol{V_{glyc} = 0, V_{resp} = V_{glucose}}$ [4]

If $\gamma_{glyc} < \gamma_{resp}$ and $V_{max}^{glyc} \cdot \gamma_{glyc} > V_{max}^{resp} \cdot \gamma_{resp}$ and $\phi_{total}^{ATP} \cdot V_{max}^{glyc} > V_{glucose} > \phi_{total}^{ATP} \cdot V_{max}^{resp}$ then

$$V_{glyc} = \frac{\phi_{total}^{ATP} \cdot V_{max}^{glyc} \cdot V_{max}^{resp} - V_{glucose} \cdot V_{max}^{glyc}}{V_{max}^{resp} - V_{max}^{glyc}}$$

$$V_{resp} = \frac{V_{max}^{resp}(\phi_{total}^{ATP} \cdot V_{max}^{glyc} \cdot V_{max}^{resp} - V_{glucose}}{V_{max}^{glyc} - V_{max}^{resp}}$$

[5]

If $V_{max}^{glyc} \cdot \gamma_{glyc} > V_{max}^{resp} \cdot \gamma_{resp}$ and $V_{max}^{glyc} \cdot \phi_{total}^{ATP} < V_{glucose}$ then $V_{glyc} = V_{max}^{glyc} \cdot \phi_{total}^{ATP}, V_{resp} = 0$ [6]

If $\gamma_{glyc} > \gamma_{resp}$ and $V_{max}^{glyc} \cdot \phi_{total}^{ATP} > V_{glucose}$ then $V_{glyc} = V_{glucose}, V_{resp} = 0$ [11]

If $\gamma_{glyc} > \gamma_{resp}$ and $V_{max}^{glyc} \cdot \gamma_{glyc} < V_{max}^{resp} \cdot \gamma_{resp}$ and $\phi_{total}^{ATP} \cdot V_{max}^{glyc} < V_{glucose} < \phi_{total}^{ATP} \cdot V_{max}^{resp}$ then

$$V_{glyc} = \frac{\phi_{total}^{ATP} \cdot V_{max}^{glyc} \cdot V_{max}^{resp} - V_{glucose} \cdot V_{max}^{glyc}}{V_{max}^{resp} - V_{max}^{glyc}}$$

$$V_{resp} = \frac{V_{max}^{resp}(\phi_{total}^{ATP} \cdot V_{max}^{glyc} \cdot V_{max}^{resp} - V_{glucose}}{V_{max}^{glyc} - V_{max}^{resp}}$$

[12]

If $V_{glyc} \cdot \gamma_{glyc} < V_{resp} \cdot \gamma_{resp}$ and $V_{max}^{resp} \cdot \phi_{total}^{ATP} \leq V_{glucose}$ then $V_{glyc} = 0, V_{resp} = V_{max}^{resp} \cdot \phi_{total}^{ATP}$ [13]

Theoretical Model of Respiratory Substrate Utilization and Co-utilization with Glucose

We have extended our mathematical model to explore the effect of adding a respiratory substrate other than glucose. The only differences between the core model and extended model are that we decompose the original V_{resp} into a contribution from glucose V_{resp}^{gluc} and a contribution from alternative respiratory substrate V_{resp}^{sub}, and we add constraints to the core model to include these new terms to account for the maximal respiratory substrate uptake. We assumed that the specific activity of respiratory substrate utilization in units of μmol per mg cellular protein per min are the same for both glucose and the respiratory substrate as this value should be mostly set by the shared pathways of TCA cycle and ETC. Our simulations show that even in the presence of saturating respiratory substrate, there is no effect of additional respiratory substrate on the ratio of glycolysis and respiration used by the cell at all glucose uptake rates except for the very low glucose uptake rate when respiration is not saturated by glucose (*SI Appendix*, Fig. S2 *A* and *B*). Together, our results suggest that the excess of glucose that can be diverted to glycolysis, not the presence of a respiratory substrate, drive the Warburg Effect. We can use the same approach as Supplementary Discussion 1 to describe the additional uptake of a respiratory substrate. The linear program is given by:

$$Maximize: \quad V_{total}^{ATP} = \gamma_{glyc} \cdot V_{glyc} + \gamma_{resp} \cdot (V_{resp}^{gluc} + V_{resp}^{sub}) \quad \text{[S13]}$$

$$Subject\ to: \quad \frac{V_{glyc}}{V_{max}^{glyc}} + \frac{1}{V_{max}^{resp}}(V_{resp}^{gluc} + V_{resp}^{sub}) \leq \phi_{total}^{ATP} \quad \text{[S14]}$$

$$V_{glyc} + V_{resp}^{gluc} \leq V_{glucose} \quad \text{[S15]}$$

$$V_{resp}^{sub} \leq V_{sub} \quad \text{[S16]}$$

$$V_{glyc} \leq 0, V_{resp}^{gluc} \leq 0, V_{resp}^{sub} \leq 0 \quad \text{[S17]}$$

where, $V_{resp}^{sub}$is the substrate respiration, and we assume both the yield (γ_{resp}) and the specific activity of the pathway, V_{max}^{resp}, are equal for respiration from glucose or an additional respiratory substrate. We also assume: $\gamma_{glyc} < \gamma_{resp}$ and $\gamma_{glyc} \cdot V_{max}^{glyc} > \gamma_{resp} \cdot V_{max}^{resp}$, which we have shown are necessary for eliciting the Warburg Effect (Fig. 1 *C*-*E*). These assumptions reduce the number of cases which need to be solved, decreasing the complexity of the analytical solution so that it in more interpretable. For all considered cases, we assume that $V_{sub} > 0$. If $V_{sub} = 0$, the analytical solution yields identical cases as the original linear program as described in Supplementary Discussion 1.

The Lagrangian for this is given by:

$$L = -\left(\gamma_{glyc} \cdot V_{glyc}\right) - (\gamma_{resp} \cdot (V_{resp}^{gluc} + V_{resp}^{sub})) + \lambda_1 (V_{glyc} + V_{resp}^{gluc} - V_{glucose}) + \lambda_2 \left(\frac{V_{glyc}}{V_{max}^{glyc}} + \frac{V_{resp}^{gluc}}{V_{max}^{resp}} + \frac{V_{resp}^{sub}}{V_{max}^{resp}} - \phi_{total}^{ATP}\right) + \lambda_3 (V_{resp}^{sub} - V_{sub}) - \lambda_{glyc} V_{glyc} - \lambda_{resp}^{gluc} V_{resp}^{gluc} - \lambda_{resp}^{sub} V_{resp}^{sub} \quad [S18]$$

Lagrange multiplers are non-negative to account for the inequality constraints. Therefore, derivatives are given by:

$$\frac{\partial L}{\partial V_{glyc}} = -\gamma_{glyc} + \lambda_1 + \lambda_2 \frac{1}{V_{max}^{glyc}} - \lambda_{glyc} = 0 \quad [S19]$$

$$\frac{\partial L}{\partial V_{resp}^{gluc}} = -\gamma_{resp} + \lambda_1 + \lambda_2 \frac{1}{V_{max}^{resp}} - \lambda_{resp}^{gluc} = 0 \quad [S20]$$

$$\frac{\partial L}{\partial V_{resp}^{sub}} = -\gamma_{resp} + \lambda_2 \frac{1}{V_{max}^{resp}} + \lambda_3 - \lambda_{resp}^{sub} = 0 \quad [S21]$$

Complementary slackness for non-negative Lagrange multiplies:

$$\lambda_1 > 0 \Rightarrow V_{glyc} + V_{resp}^{gluc} = V_{glucose} \quad [S22]$$

$$\lambda_2 > 0 \Rightarrow \frac{V_{glyc}}{V_{max}^{glyc}} + \frac{V_{resp}^{gluc}}{V_{max}^{resp}} + \frac{V_{resp}^{sub}}{V_{max}^{resp}} = \phi_{total}^{ATP} \quad [S23]$$

$$\lambda_3 > 0 \Rightarrow V_{resp}^{sub} = V_{sub} \quad [S24]$$

$$\lambda_{glyc} > 0 \Rightarrow V_{glyc} = 0 \quad [S25]$$

$$\lambda_{resp}^{gluc} > 0 \Rightarrow V_{resp}^{gluc} = 0 \quad [S26]$$

$$\lambda_{resp}^{sub} > 0 \Rightarrow V_{resp}^{sub} = 0 \quad [S27]$$

The optimal solution needs to comply with all of these in addition to the original constraints. We know that in the optimal solution either $V_{glyc} + V_{resp}^{gluc} = V_{glucose}$ or $\frac{V_{glyc}}{V_{max}^{glyc}} + \frac{V_{resp}^{gluc}}{V_{max}^{resp}} + \frac{V_{resp}^{sub}}{V_{max}^{resp}} = \phi_{total}^{ATP}$ or both (otherwise can improve by increasing V_{glyc}, V_{resp}^{gluc}, or V_{resp}^{sub}). We consider the different cases in terms of glycolysis and respiration and see where they are optimal:

1. $V_{glyc} > 0, V_{resp}^{gluc} = 0$, or $V_{resp}^{sub} = 0$ (glycolysis only):
   First, we show that in this case we have that proteome allocation for ATP-producing enzymes is producing ATP at its maximum capacity. Thus, $V_{glyc} = \phi_{total}^{ATP} \cdot V_{max}^{glyc}$. And $\lambda_1 = \lambda_3 = \lambda_{glyc} = 0$, and consequently $\lambda_3 = \gamma_{glyc} \cdot V_{max}^{glyc}$,

$\lambda_{resp}^{gluc} = \lambda_{resp}^{sub} = \gamma_{resp} - \gamma_{glyc} \cdot V_{max}^{glyc} - \gamma_{resp} \cdot V_{max}^{resp} > 0.$

2. $V_{glyc} > 0, V_{resp}^{gluc} > 0$, or $V_{resp}^{sub} = 0$ (glycolysis and respiration with glucose, no use of substrate):
   This case is not possible when $V_{sub} = 0$. It requires $\lambda_{glyc} = \lambda_{resp}^{gluc} = \lambda_3 = 0$ and then from (S21, S22) we get $\lambda_{resp}^{sub} = -\lambda_1$, which is only possible if $\lambda_{resp}^{sub} = \lambda_1 = 0$. In that case, we get: $\lambda_2 = \gamma_{glyc} \cdot V_{max}^{glyc} = \gamma_{resp} \cdot V_{max}^{resp}$ from $(S20, S21)$, which we know is not possible

3. $V_{glyc} > 0, V_{resp}^{gluc} = 0$, or $V_{resp}^{sub} > 0$ (glycolysis and respiration with substrate, no use of respiration with glucose):
   In this case, we get that glucose uptake rate constraint and proteome allocation for ATP-producing enzymes and utilized. The proteome allocation for ATP-producing enzymes is at its maximum capacity ($\frac{V_{glyc}}{V_{max}^{glyc}} + \frac{V_{resp}^{sub}}{V_{max}^{resp}} = \phi_{total}^{ATP}$). Otherwise, $\lambda_{glyc} = \lambda_2 = 0$, and therefore from (S19) $\lambda_1 = \gamma_{glyc}$ and from (S20) $\lambda_1 - \lambda_{resp}^{gluc} = \gamma_{resp}$, which contradicts $\gamma_{glyc} < \gamma_{resp}$.
   Glucose is fully used ($V_{glyc} = V_{glucose}$), because otherwise $\lambda_{glyc} = \lambda_1 = 0$ and from (S19) $\lambda_2 = \gamma_{glyc} \cdot V_{max}^{glyc}$ and from (S21) $\lambda_3 = \gamma_{resp} - \frac{\gamma_{glyc} \cdot V_{max}^{glyc}}{V_{max}^{resp}} < 0,$ which is impossible.
   If glucose is not abundant, $V_{glucose} < \phi_{total}^{ATP} \cdot V_{max}^{glyc}$, but we can fill the space with glycolysis and substrate respiration $\frac{V_{glyc}}{V_{max}^{glyc}} + \frac{V_{resp}^{sub}}{V_{max}^{resp}} \geq \phi_{total}^{ATP}$, then we have full glycolysis ($V_{glyc} = V_{glucose}$) and add substrate respiration $V_{resp}^{sub} = V_{max}^{resp} \cdot \left(\phi_{total}^{ATP} - \frac{V_{glucose}}{V_{max}^{glyc}}\right)$.

4. $V_{glyc} > 0, V_{resp}^{gluc} > 0$, or $V_{resp}^{sub} > 0$ (all active):
   In this case too both Glucose and volume constraints must be full, and also the substrate must be fully used $V_{resp}^{sub} = V_{sub}$. This is because $\lambda_{glyc} = \lambda_{resp}^{gluc} = \lambda_{resp}^{sub} = 0$, the three equalities in (S19, S20, S21) can only hold simultaneously if $\lambda_1 > 0$, $\lambda_2 > 0$, $\lambda_3 > 0$. Note in this case we must also have that we cannot fill the proteome allocation for ATP-producing enzymes with just glycolysis and substrate, that is $\frac{1}{V_{max}^{glyc}} \cdot V_{glucose} + \frac{1}{V_{max}^{resp}} \cdot V_{sub} < \phi_{total}^{ATP}$, because $\frac{1}{V_{max}^{glyc}} \cdot V_{glyc} + \frac{1}{V_{max}^{resp}} \cdot V_{resp}^{gluc} > \frac{1}{V_{max}^{glyc}} \cdot V_{glucose}$ when $V_{glyc} + V_{resp}^{gluc} = V_{glucose}$. Summary: If we cannot fill the space as before $\frac{1}{V_{max}^{glyc}} \cdot V_{glucose} + \frac{1}{V_{max}^{resp}} \cdot V_{sub} < \phi_{total}^{ATP}$, but we can fill it with respiration $\frac{1}{V_{max}^{resp}}$

($V_{glucose}$ + V_{sub}) > ϕ_{total}^{ATP}, then we have all three modes, use all glucose, and fill the volume, and V_{resp}^{sub} = V_{sub} substrate is fully used.

5. $V_{glyc} = 0, V_{resp}^{gluc} > 0$, or $V_{resp}^{sub} > 0$ (no glycolysis):
   In this case, it is easy to see glucose uptake rate and substrate uptake rate are fully used, that is: V_{resp}^{gluc} = $V_{glucose}$, V_{resp}^{sub} = V_{sub}. This is because λ_{resp}^{gluc} = λ_{resp}^{sub} = 0 and from (S20,S21) we see λ_1 = λ_3. If they are both 0, then λ_2 = b/e and then in (S19) we get: λ_{glyc} = $\frac{\gamma_{resp} \cdot V_{max}^{resp}}{V_{max}^{glyc}}$ − γ_{glyc} < 0, and a contradiction. For the proteome allocation for ATP-producing enzymes constraint to hold this also requires that $\frac{1}{V_{max}^{resp}}$ ($V_{glucose}$ + V_{sub}) ≤ ϕ_{total}^{ATP} Summary: If we cannot fill the proteome allocation for ATP-producing enzymes $\frac{1}{V_{max}^{resp}}$ ($V_{glucose}$ + V_{sub}) ≤ ϕ_{total}^{ATP}, then we maximize respiration using both sources V_{resp}^{gluc} = $V_{glucose}$, V_{resp}^{sub} = V_{sub}.

Supplementary Discussion 3

Derivation of Analytical Solution for *E.coli*, including the Pta-AckA Pathway

We can use the same approach to solve the more complex linear program for E. coli, which includes the Pta-AckA pathway as a third option The linear program is given by:

$$Maximize: \quad V_{ATP} = V_{ferm} \cdot \gamma_{ferm} + V_{pta} \cdot \gamma_{pta} + V_{resp} \cdot \gamma_{resp} \quad [14]$$

$$Subject\ to: \quad \frac{V_{ferm}}{V_{max}^{ferm}} + \frac{V_{pta}}{V_{max}^{pta}} + \frac{V_{resp}}{V_{max}^{resp}} \leq \phi_{total}^{ATP} \quad [15]$$

$$V_{ferm} + V_{pta} + V_{resp} \leq V_{glucose} \quad [16]$$

$$V_{ferm} \geq 0, V_{pta} \geq 0, V_{resp} \geq 0 \quad [S13]$$

We write the minimization program as:

$$Minimize: \quad V_{total}^{ATP} = -(V_{ferm} \cdot \gamma_{ferm}) - (V_{pta} \cdot \gamma_{pta}) - (V_{resp} \cdot \gamma_{resp}) \quad [S14]$$

$$Subject\ to: \quad \frac{V_{ferm}}{V_{max}^{ferm}} + \frac{V_{pta}}{V_{max}^{pta}} + \frac{V_{resp}}{V_{max}^{resp}} \leq \phi_{total}^{ATP} \quad [15]$$

$$V_{ferm} + V_{pta} + V_{resp} \leq V_{glucose} \quad [16]$$

$$-V_{ferm} \leq 0, -V_{pta} \leq 0, -V_{resp} \leq 0 \quad [S15]$$

We assume $V_{max}^{ferm} \cdot \gamma_{ferm} \neq V_{max}^{pta} \cdot \gamma_{pta} \neq V_{max}^{resp} \cdot \gamma_{resp}$, $V_{max}^{ferm} \neq V_{max}^{pta} \neq V_{max}^{resp}$, $V_{max}^{resp} \cdot \gamma_{resp} \cdot V_{max}^{ferm} \neq V_{max}^{resp} \cdot \gamma_{resp} \cdot V_{max}^{pta} \neq V_{max}^{pta} \cdot \gamma_{pta} \cdot V_{max}^{ferm} \neq V_{max}^{pta} \cdot \gamma_{pta} \cdot V_{max}^{resp} \neq V_{ferm} \cdot \gamma_{ferm} \cdot V_{max}^{resp} \neq V_{max}^{ferm} \cdot \gamma_{ferm} \cdot V_{max}^{pta}$, $\phi_{total}^{ATP} \cdot V_{max}^{ferm} \neq V_{glucose}$, $\phi_{total}^{ATP} \cdot V_{max}^{pta} \neq V_{glucose,}$ $\phi_{total}^{ATP} \cdot V_{max}^{resp} \neq V_{glucose}$ to avoid redundancies. The Lagrangian function for this:

$$L = -(V_{ferm} \cdot \gamma_{ferm}) - (V_{pta} \cdot \gamma_{pta}) - (V_{resp} \cdot \gamma_{resp}) + \lambda_1 \left(\frac{V_{ferm}}{V_{max}^{ferm}} + \frac{V_{pta}}{V_{max}^{pta}} + \frac{V_{resp}}{V_{max}^{resp}} - \phi_{total}^{ATP}\right) + \lambda_2 \left(V_{ferm} + V_{resp} - V_{glucose}\right) - \lambda_{ferm} V_{ferm} - \lambda_{pta} V_{pta} - \lambda_{resp} V_{resp} \quad [S16]$$

We take the partial derivative of the Lagrangian function with respect to V_{ferm}, $V_{pta,}$ and V_{resp}. The Lagrange multipliers associated with the inequality constraints must be non-negative. Therefore, derivatives are given by:

$$\frac{\partial L}{\partial V_{ferm}} = -\gamma_{ferm} + \lambda_1 \frac{1}{V_{max}^{ferm}} + \lambda_2 - \lambda_{ferm} = 0 \quad [S17]$$

$$\frac{\partial L}{\partial V_{pta}} = -\gamma_{pta} + \lambda_1 \frac{1}{V_{max}^{pta}} + \lambda_2 - \lambda_{pta} = 0 \quad \text{[S18]}$$

$$\frac{\partial L}{\partial V_{resp}} = -\gamma_{resp} + \lambda_1 \frac{1}{V_{max}^{resp}} + \lambda_2 - \lambda_{resp} = 0 \quad \text{[S19]}$$

For the inequality constraints, the complementary slackness for non-negative Lagrange is given by:

$$\lambda_1 > 0 \Rightarrow \frac{V_{glyc}}{V_{max}^{glyc}} + \frac{V_{resp}}{V_{max}^{resp}} = \phi_{total}^{ATP} \quad \text{[S20]}$$

$$\lambda_2 > 0 \Rightarrow V_{glyc} + V_{resp} = V_{glucose} \quad \text{[S21]}$$

$$\lambda_{ferm} > 0 \Rightarrow V_{ferm} = 0 \quad \text{[S22]}$$

$$\lambda_{pta} > 0 \Rightarrow V_{pta} = 0 \quad \text{[S23]}$$

$$\lambda_{resp} > 0 \Rightarrow V_{resp} = 0 \quad \text{[S24]}$$

We also know that in the optimal solution either $\frac{V_{ferm}}{V_{max}^{ferm}} + \frac{V_{pta}}{V_{max}^{pta}} + \frac{V_{resp}}{V_{max}^{resp}} = \phi_{total}^{ATP}$ or $V_{ferm} + V_{pta} + V_{resp} = V_{glucose}$ or both (otherwise can improve by increasing V_{glyc} or V_{resp}) and we can use that. We can consider different cases, solve them, and see when they are optimal. Note we only present the three relevant cases to demonstrate that given the relationship between the yield (i.e. $\gamma_{ferm} < \gamma_{pta} < \gamma_{resp}$) and the specific activity (i.e. $\gamma_{ferm} < \gamma_{resp} < \gamma_{pta}$) of the three pathways:

- V_{ferm} = 0, $V_{pta} > 0$, V_{resp} = 0, $\frac{V_{ferm}}{V_{max}^{ferm}} + \frac{V_{pta}}{V_{max}^{pta}} + \frac{V_{resp}}{V_{max}^{resp}} = \phi_{total}^{ATP}$ and $V_{ferm} + V_{pta} + V_{resp} < V_{glucose}$
  In this case, $V_{pta} = V_{max}^{pta} \cdot \phi_{total}^{ATP}$, λ_{pta} = 0, λ_2 = 0. Thus from (S17) $\lambda_1 = \gamma_{pta} \cdot V_{max}^{pta}$, and from (S18) $\lambda_{resp} = \gamma_{ferm} \cdot V_{max}^{ferm} - \gamma_{resp} \cdot V_{max}^{resp} > 0$ and (S19) $\lambda_{pta} = \gamma_{ferm} \cdot V_{max}^{ferm} - \gamma_{pta} \cdot V_{max}^{pta} > 0$
  So for this solution to be legal we require: $V_{glucose} > \phi_{total}^{ATP} \cdot V_{max}^{ferm}$ (for second constraint), $\gamma_{ferm} \cdot V_{max}^{ferm} - \gamma_{resp} \cdot V_{max}^{resp} > 0$ (for $\lambda_{resp} > 0$), and $\gamma_{ferm} \cdot V_{max}^{ferm} - \gamma_{pta} \cdot V_{max}^{pta} > 0$ (for $\lambda_{pta} > 0$).

- V_{ferm} = 0, V_{pta} = 0, $V_{resp} > 0$, $\frac{V_{ferm}}{V_{max}^{ferm}} + \frac{V_{pta}}{V_{max}^{pta}} + \frac{V_{resp}}{V_{max}^{resp}} < \phi_{total}^{ATP}$ and $V_{ferm} + V_{pta} + V_{resp} = V_{glucose}$

In this case, $\phi_{resp} = V_{glucose}$, λ_{resp} = 0, λ_1 = 0. Thus from (S17) $\lambda_2 = \gamma_{resp}$, and from (S18) $\lambda_{ferm} = \gamma_{resp} - \gamma_{ferm}$ and from (S19) $\lambda_{pta} = \gamma_{resp} - \gamma_{pta}$. So for this solution to be legal we require:
$V_{max}^{resp} \cdot \phi_{total}^{resp} > V_{glucose}$ (for first constraint) and $\gamma_{resp} > \gamma_{ferm}$ (for $\lambda_{ferm} > 0$) and $\gamma_{resp} > \gamma_{pta}$ (for $\lambda_{pta} > 0$).

- V_{ferm} = 0, $V_{pta} > 0$, $V_{resp} > 0$, $\frac{V_{glyc}}{V_{max}^{glyc}} + \frac{V_{resp}}{V_{max}^{resp}} = \phi_{total}^{ATP}$ and $V_{glyc} + V_{resp} = V_{glucose}$.

$$V_{pta} = \frac{\phi_{total}^{ATP} \cdot V_{max}^{pta} \cdot V_{max}^{resp} - V_{glucose} \cdot V_{max}^{pta}}{V_{max}^{resp} - V_{max}^{pta}}, V_{resp} = \frac{V_{max}^{resp}(\phi_{total}^{ATP} \cdot V_{max}^{glyc} \cdot V_{max}^{resp} - V_{glucose})}{V_{max}^{glyc} - V_{max}^{resp}}$$

Finally, we would like to summarize the analytical solution below with the above three cases:

$$\text{If} \quad \gamma_{ferm} < \gamma_{resp},\ \gamma_{pta} < \gamma_{resp},\ V_{max}^{resp} \cdot \phi_{total}^{ATP} > V_{glucose} \quad \text{then} \quad V_{ferm} = 0, V_{pta} = 0, V_{resp} = V_{glucose} \qquad [4]$$

$$\text{If} \quad \gamma_{ferm} < \gamma_{resp},\ \gamma_{pta} < \gamma_{resp},\ V_{max}^{ferm} \cdot \gamma_{ferm} < V_{max}^{pta} \cdot \gamma_{pta},\ V_{max}^{pta} \cdot \gamma_{pta} > V_{max}^{resp} \cdot \gamma_{resp},\ \phi_{total}^{ATP} \cdot V_{max}^{glyc} > V_{glucose} > \phi_{total}^{ATP} \cdot V_{max}^{resp} \quad \text{then} \quad V_{ferm} = 0,\ V_{pta} = \frac{\phi_{total}^{ATP} \cdot V_{max}^{pta} \cdot V_{max}^{resp} - V_{glucose} \cdot V_{max}^{pta}}{V_{max}^{resp} - V_{max}^{pta}},\ V_{resp} = \frac{V_{max}^{resp}(\phi_{total}^{ATP} \cdot V_{max}^{pta} \cdot V_{max}^{resp} - V_{glucose}}{V_{max}^{pta} - V_{max}^{resp}} \qquad [5]$$

$$\text{If} \quad V_{max}^{ferm} \cdot \gamma_{ferm} < V_{max}^{pta} \cdot \gamma_{pta},\ V_{max}^{pta} \cdot \gamma_{pta} > V_{max}^{resp} \cdot \gamma_{resp},\ V_{max}^{pta} \cdot \phi_{total}^{ATP} < V_{glucose} \quad \text{then} \quad V_{ferm} = 0, V_{pta} = V_{max}^{glyc} \cdot \phi_{total}^{ATP}, V_{resp} = 0 \qquad [6]$$

Supplementary Discussion 4

Model Predictions of ATP production with cycloheximide treatment

Elsemann et al. 2022 treated *S. cerevisae* growing in glucose-excess batch culture with cycloheximide, a translation inhibitor. Our analysis of the proteomics data reveals changes in the ATP-producing proteome space (ϕ_{total}^{ATP}) with cycloheximide treatment (*SI Appendix*, Fig. S9*A*). More importantly, we found a strong linear correlation between the glucose uptake rate and ϕ_{total}^{ATP} (ρ = 0.94) during cycloheximide treatment (*SI Appendix*, Fig. S9*B*). We use the slope and intercept of this linear relationship to inform our model about how the ϕ_{total}^{ATP} expands with the glucose uptake rate. If this expansion in not accounted for (i.e. ϕ_{total}^{ATP} is held constant), our model predicts decrease in respiration as the glucose uptake rate increases (*SI Appendix*, Fig. S9*C*). However, by incorporating the empirically derived ϕ_{total}^{ATP} expansion rate, our model can predict glycolysis and respiration rates across the cycloheximide treatments (*SI Appendix*, Fig. S9*D*). Here, we observe a sustained utilization of respiration as an ATP-producing strategy due to the changing ATP-producing space (ϕ_{total}^{ATP}) as a result of cycloheximide treatment.

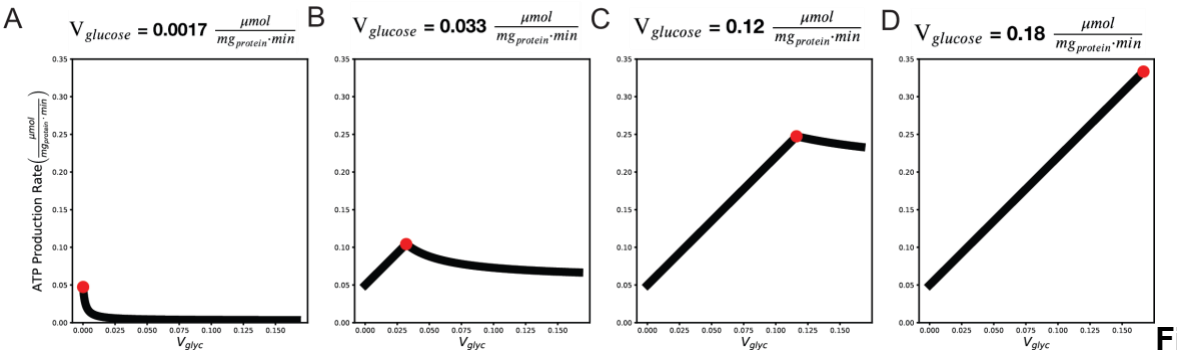


Fig. S1. Model predictions under varying glucose uptake rates. (*A*) Rate of glycolysis that yields the highest ATP production rate (highlighted with a red dot) for a glucose uptake rate $V_{glucose}$ = 0.0017 μmol per mg cellular protein per min. (*B*) $V_{glucose}$ = 0.033 μmol per mg cellular protein per min. (*C*) $V_{glucose}$ = 0.12 μmol per mg cellular protein per min. (*D*) $V_{glucose}$ = 0.18 μmol per mg cellular protein per min.

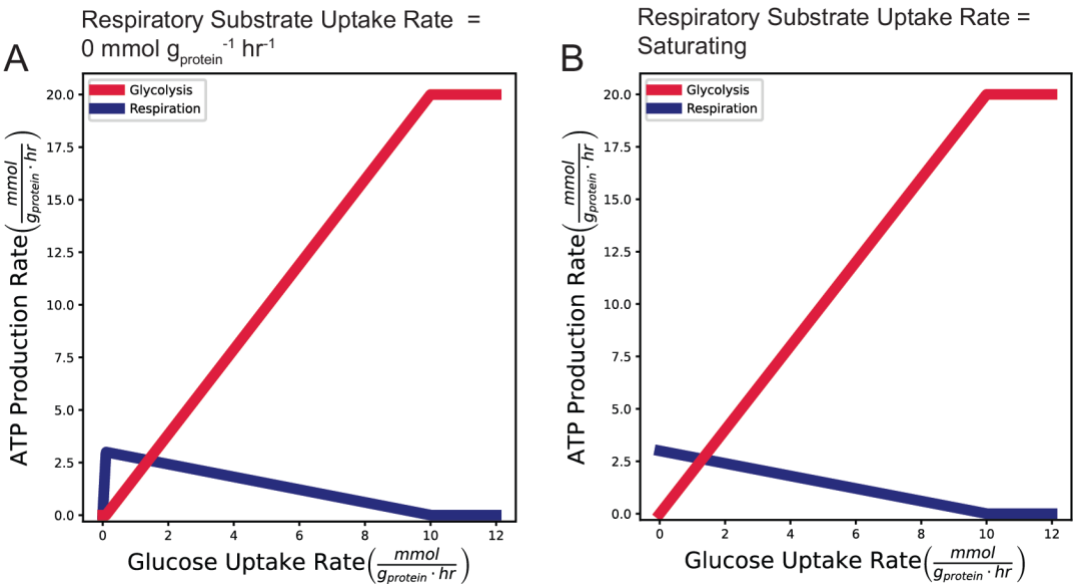


Fig. S2. Model predictions under varying glucose and respiratory substrate uptake rates. (*A*) ATP production rates of glycolysis (red) and respiration (blue) in the absence of respiratory substrate and (*B*) in the presence of saturating respiratory substrate.

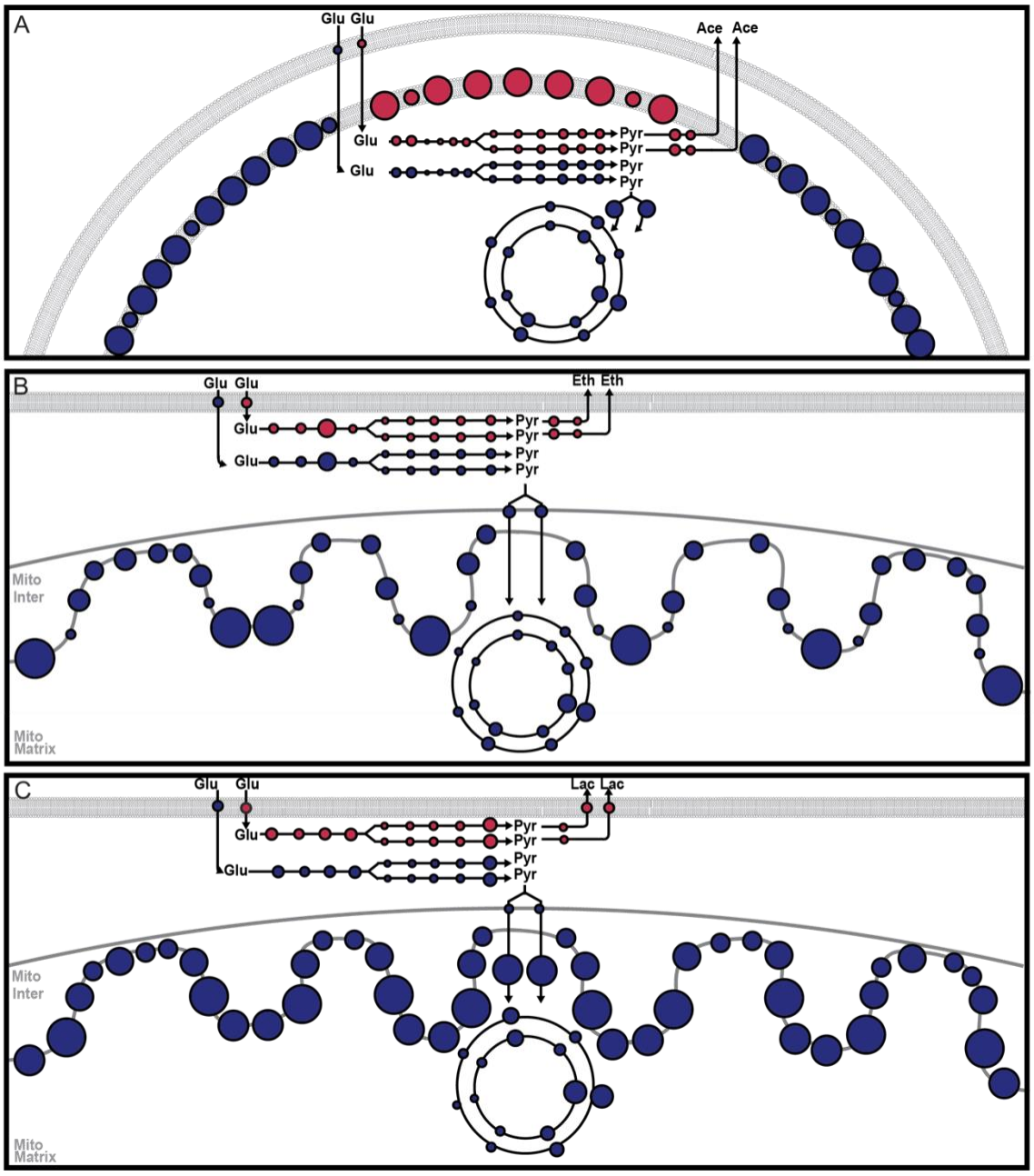


Fig. S3. Glycolysis and respiration pathway sizes in *E. coli*, *S. cerevisiae* and mammals. (*A*-*C*), Glycolysis (red) and respiration (blue) pathway outline for (*A*) *E. coli* (respiro-fermentative Pta-AckA pathway that uses both glycolysis and ETC is displayed), (*B*) *S. cerevisiae*, and (*C*) mammalian cells. Size of circle is proportional to the MW of each enzyme in the pathway. Furthermore, the pathway stoichiometry is represented under the assumption that each enzyme catalyzes its reaction at the same rate.

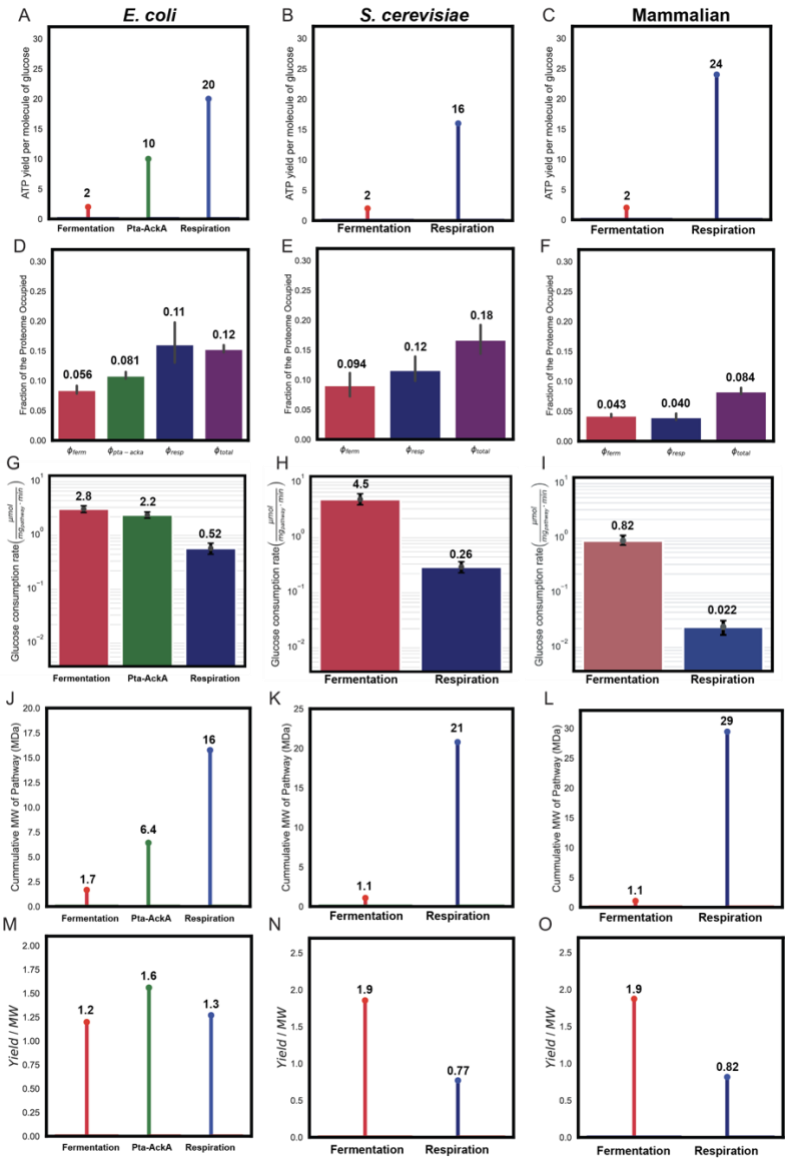


Fig. S4. Parameter estimates for *E. coli*, *S. cerevisiae*, and mammalian cells. (*A*-*C*) ATP yield per molecule of glucose for fermentation (red) and respiration (blue) for *E. coli*, *S. cerevisiae*, and mammalian cells, respectively. (*D*-*F*), The fraction of the proteome occupied by enzymes for fermentative glycolysis (red), Pta-AckA glycolysis (green), respiration (blue), and both pathways (purple) for *E. coli*, *S. cerevisiae*, and mammalian cells, respectively. For *E. coli* and *S. cerevisiae*, the glycolysis and respiration estimates represent proteome occupancies for cells grown in batch culture with non-limiting glucose or non-fermentative substrate, respectively. Error bars are 95 percent confidence interval. (*G*-*I*) Maximal observed glucose uptake rate (μmol per mg cellular protein per min) for fermentative glycolysis (red) and respiration (blue) for *E. coli*, *S. cerevisiae*, and mammalian cells, respectively. Error bars are 95 percent confidence interval calculated from 10000 bootstrap iterations. (*J*-*L*) Cumulative molecular weight (MDa) of each Pathway (*M*-*O*)**,** Ratio of the ATP yield per molecule of glucose to molecular weight (MDa) for each pathway.

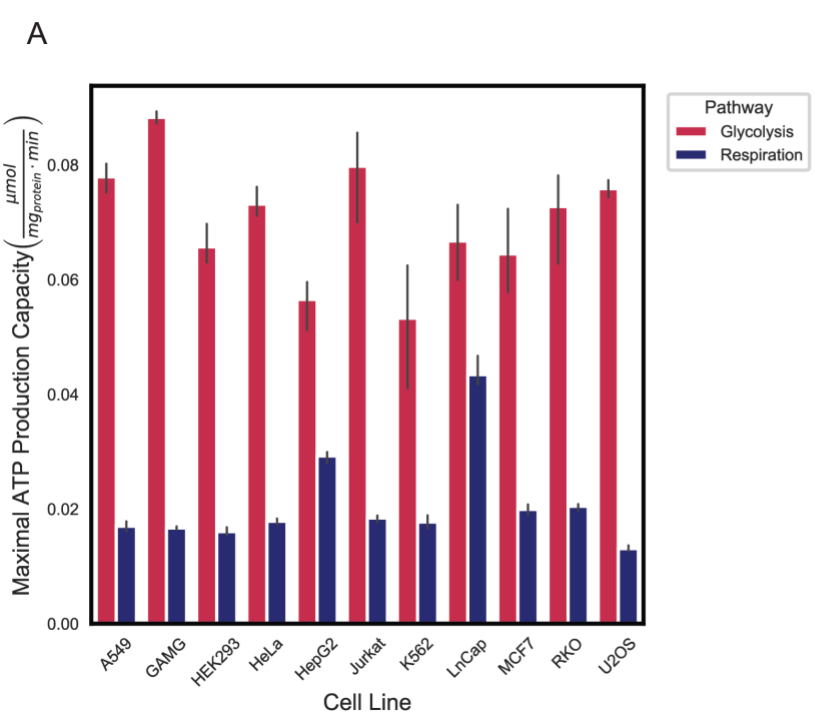


Fig. S5. Cell line-specific maximal ATP production rate capacities of glycolysis and respiration in mammalian cells. (*A*) Estimates of maximal ATP production rate (µmol $mg_{protein}^{-1}$ min^{-1}) for fermentative glycolysis (red) and respiration (blue) for 11 mammalian cells lines using proteomics data from Geiger et al. 2012.

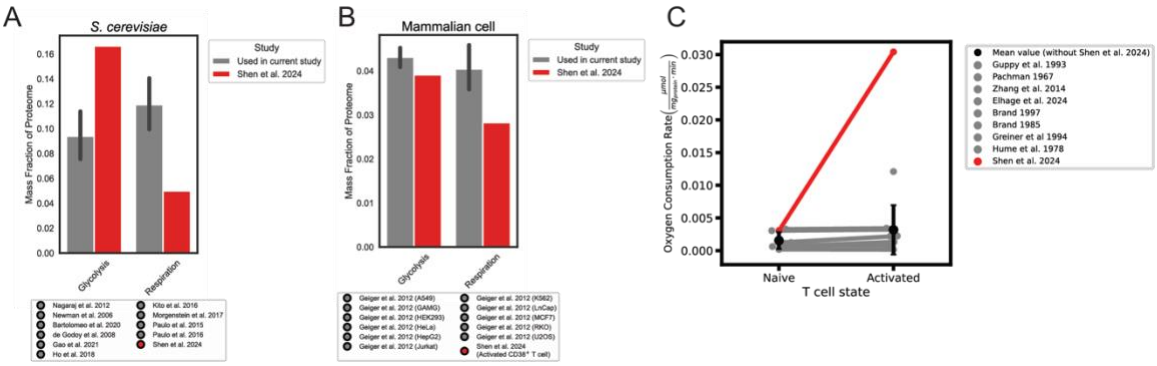


Fig. S6. Parameter differences in the current study and Shen et al. 2024. (*A*) Proteome occupancy for glycolysis and respiration in *S. cerevisiae* on ten previous reports that we used in our study (grey) and Shen et al. 2024 (red). The two-fold difference in both glycolysis and respiration occupancy is sufficient to account for the reported differences of proteome efficiency between our studies. (*B*) Proteome occupancy for glycolysis and respiration in mammalian cells in our study (grey) compared to Shen et al. 2024 (red). The differences in proteome occupancy are not sufficient to account for the reported differences of proteome efficiency. (*C*) Oxygen consumption in naïve and activated T-cells reported in Shen et al. 2024 (red) as compared to eight other studies (grey), which is likely the principal difference leading to our divergent conclusions for mammalian cells.

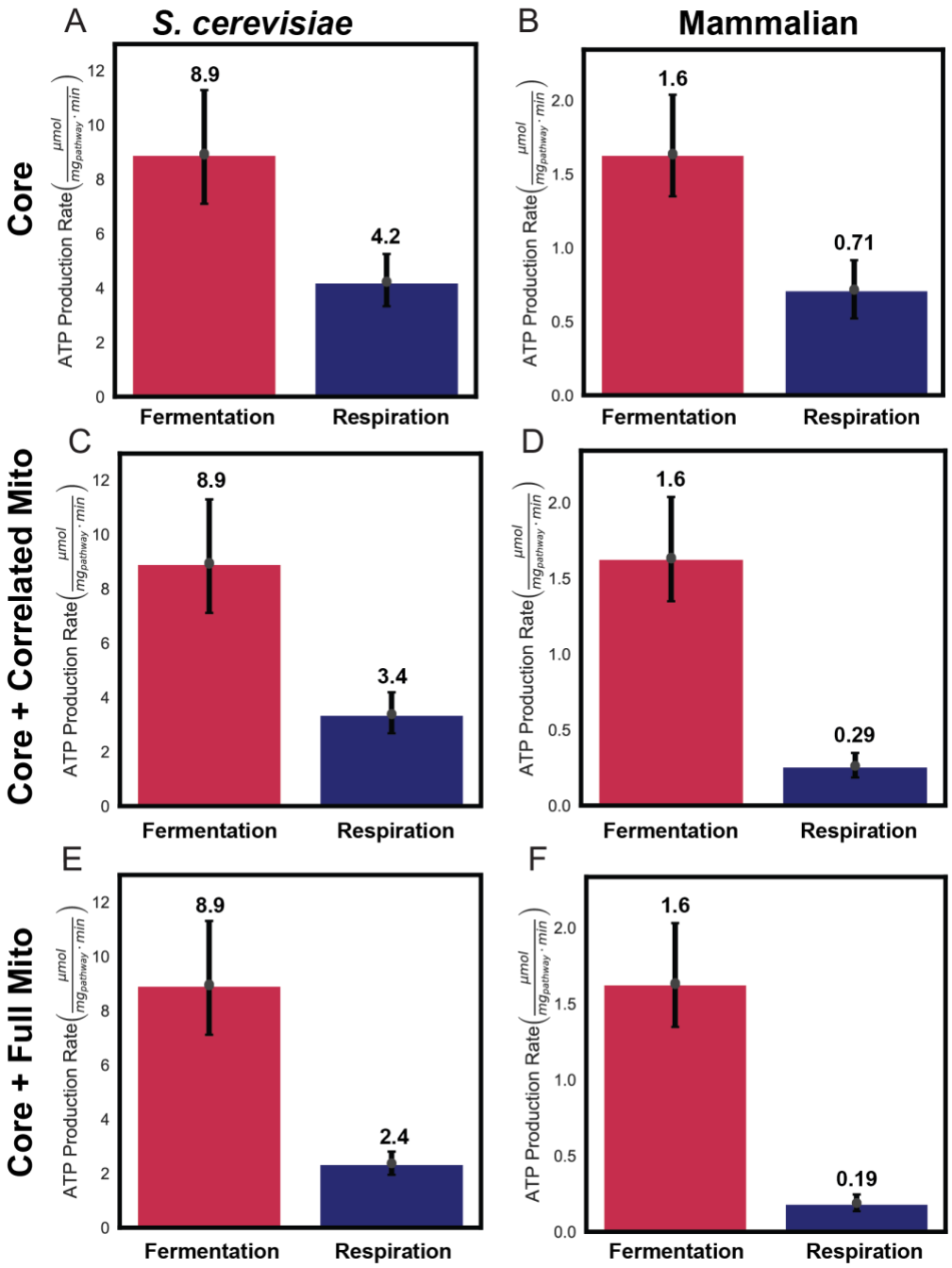


Fig. S7. Pathway-specific ATP production rates for *S. cerevisiae* and mammalian cells with additional mitochondrial proteins. (*A* and *F*) Maximal ATP production rate (μmol $mg_{pathway}^{-1}$ min^{-1}) for fermentative glycolysis (red) and respiration (blue) without any additional mitochondrial proteins (Fig. 2 *B* and *C* in the main text) (*A* and *B*) with inclusion of positively and significantly correlated mitochondrial proteins from (*C* and *D*) and all mitochondrial proteins (*E* and *F*) for *S. cerevisiae* (*A* and *C* and *E*) and mammalian cells (*B* and *D* and *F*). Error bars are the 95 percent confidence interval calculated from 10,000 bootstrap iterations.

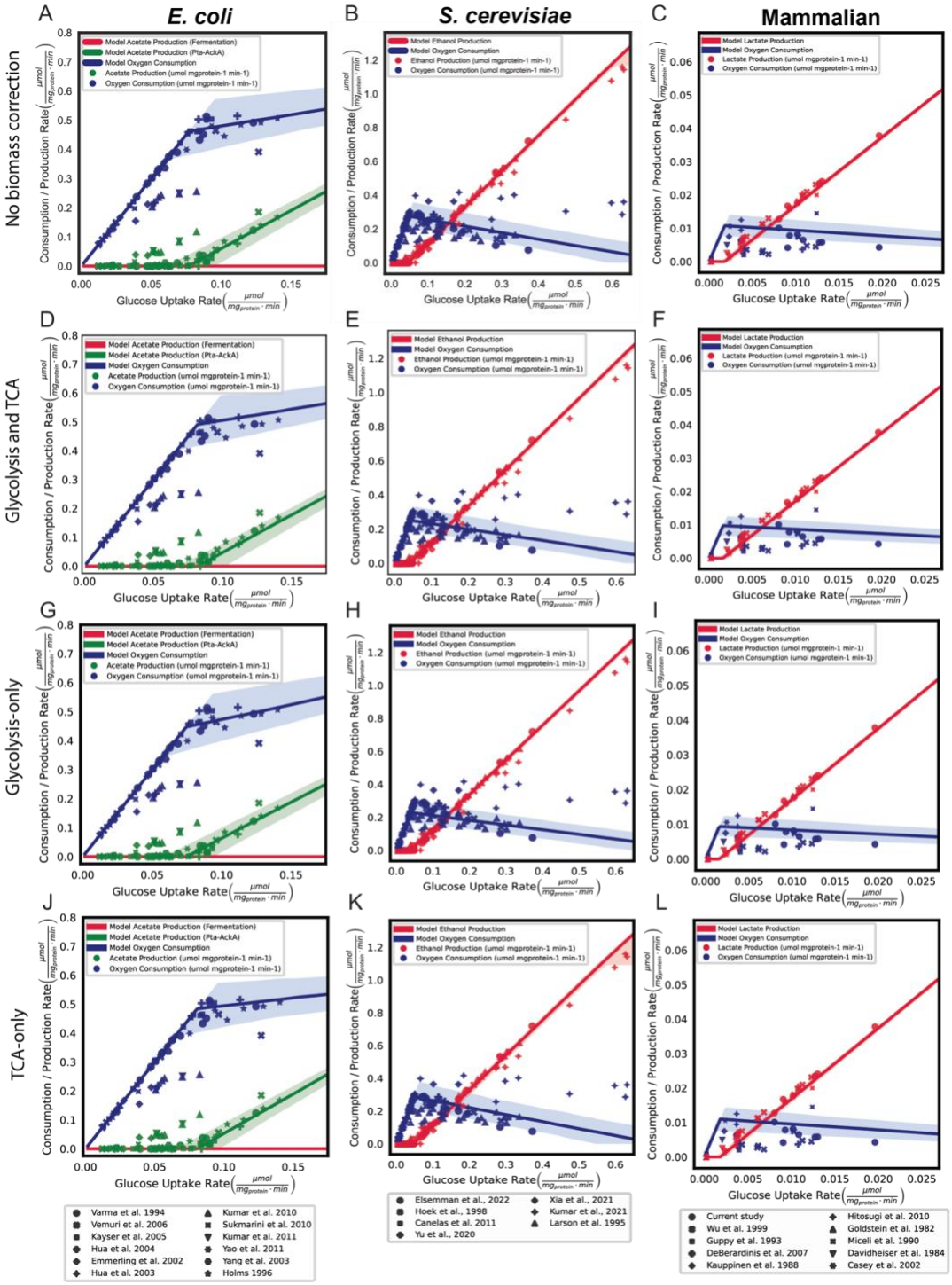


Fig. S8. Organism-specific model predictions of ATP production using different contributions towards biomass production. (*A-C*) Model prediction of fermentative glycolysis and respiration rates with no correction for contribution of glycolysis or TCA enzymes (Fig. 3 *A-C* in the main text), (*D-F*) a 30% correction for both glycolysis and the TCA cycle enzymes, (*G-I*) a 30% correction for only glycolysis enzymes, or (*J-L*) a 30% correction for only TCA cycle enzymes towards biomass production.

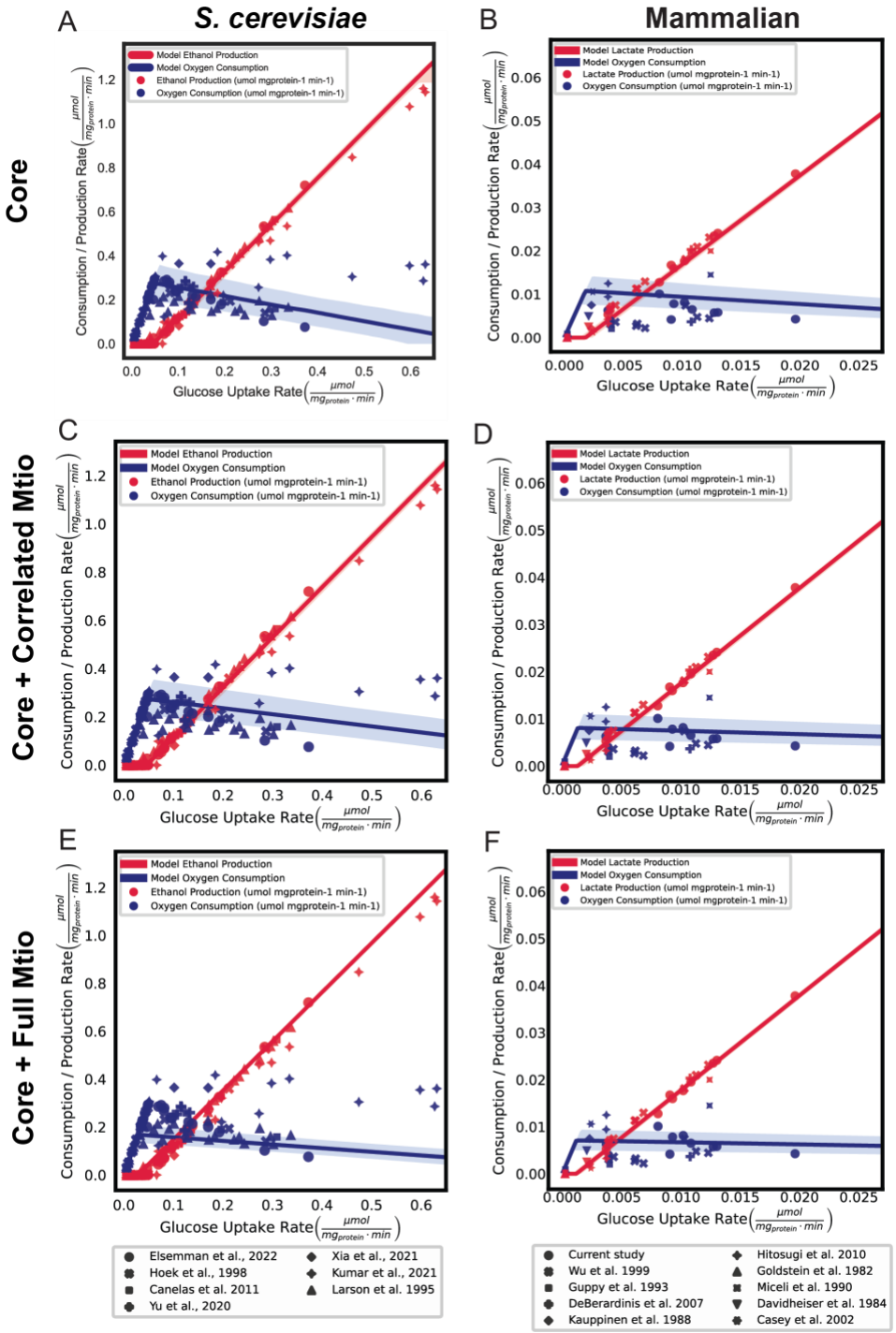


Fig. S9. Organism-specific model predictions of ATP production using different inclusion criteria for mitochondrial proteins. (A-F) Model prediction of fermentative glycolysis and respiration rates with only mitochondrial proteins that are directly involved in respiration (Fig. 3 *B* and *C* in the main text) (*A* and *B*) with inclusion of additional proteins that are positively and significantly correlated with mitochondrial proteins from (*C* and *D*) and all mitochondrial proteins (*E* and *F*) for *S. cerevisiae* (*A* and *C* and *E*) and mammalian cells (*B* and *D* and *F*).

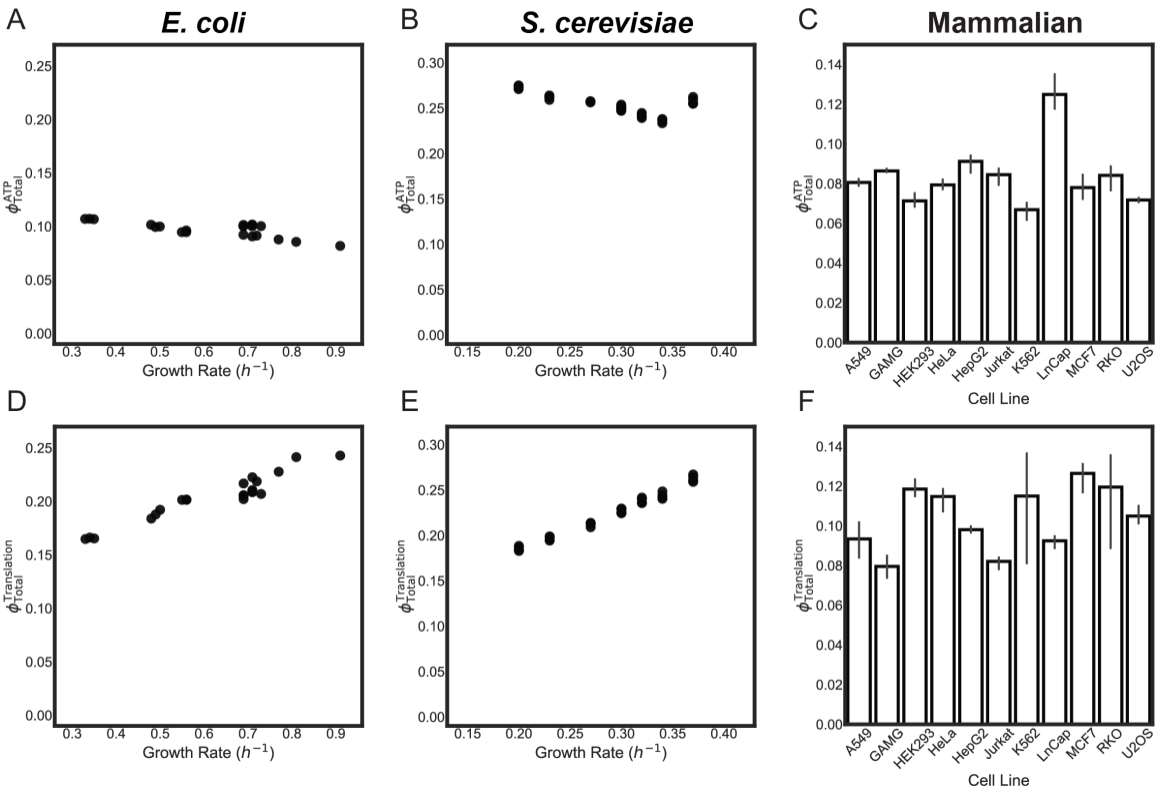


Fig. S10. Conservation of ATP-producing proteome allocation and variation in translational proteome allocation. (*A* and *B*) Fraction of ATP-producing enzymes across with increasing growth rates in *E. coli* and *S. cerevisiae*., respectively. (*C*) Fraction of ATP-producing enzymes for various mammalian cell lines. c, Fraction of ATP-producing enzymes across cell lines. (*D* and *E*) Fraction of translational enzymes across with increasing growth rates in *E. coli* and *S. cerevisiae*., respectively. (*F*) Fraction of translational enzymes for various mammalian cell lines. *E. coli*, *S. cerevisiae*, and mammalian cell data is from Mori et al. 2022, Elsemann et al. 2022, and Geiger et al. 2012, respectively.

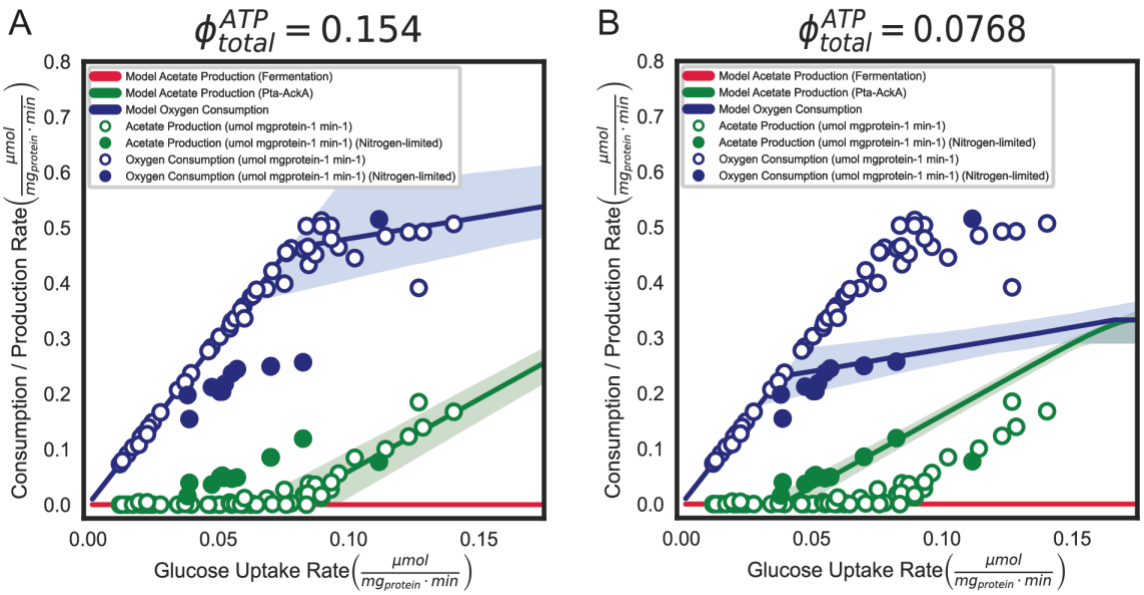


Fig. S11. Model predictions of ATP production under nitrogen limitation *(A)* Model predictions of acetate production and oxygen consumption with is ϕ_{total}^{ATP} = 0.154, which represents the mean value derived from our experimental proteomics data. *(B)* Model predictions of acetate production and oxygen consumption with is ϕ_{total}^{ATP} = 0.0768, reflecting a two-fold decrease in the allocation of proteome space to ATP-producing enzymes.

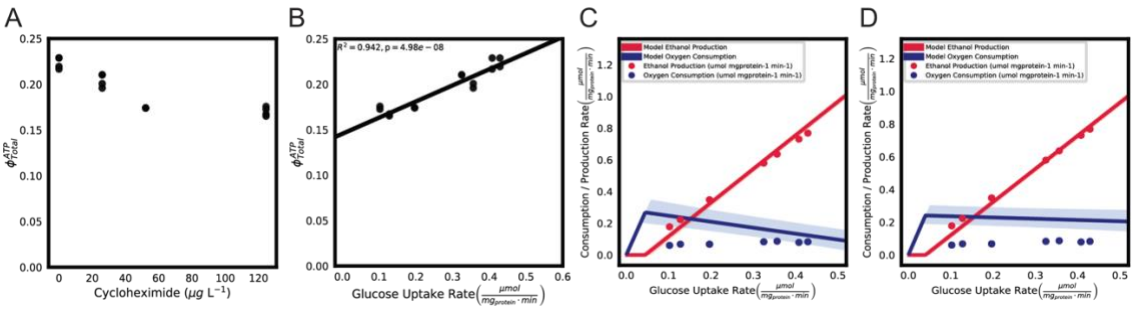


Fig. S12. Model predictions of ATP production with cycloheximide treatment. (*A*) Changes in ϕ_{total}^{ATP} with cycloheximide treatment in *S. cerevisiae*. (*B*) Linear regression of the glucose uptake rate (μmol per mg cellular protein per min) on ϕ_{total}^{ATP} with cycloheximide treatment. (*C*) Model prediction of glycolysis and respiration rates when ϕ_{total}^{ATP} is held constant with the glucose uptake rate. (*D*) Model prediction of glycolysis and respiration rates when ϕ_{total}^{ATP} increases with the glucose uptake rate. Data is from Elsemann et al. 2022.

Appendix Chapter 2

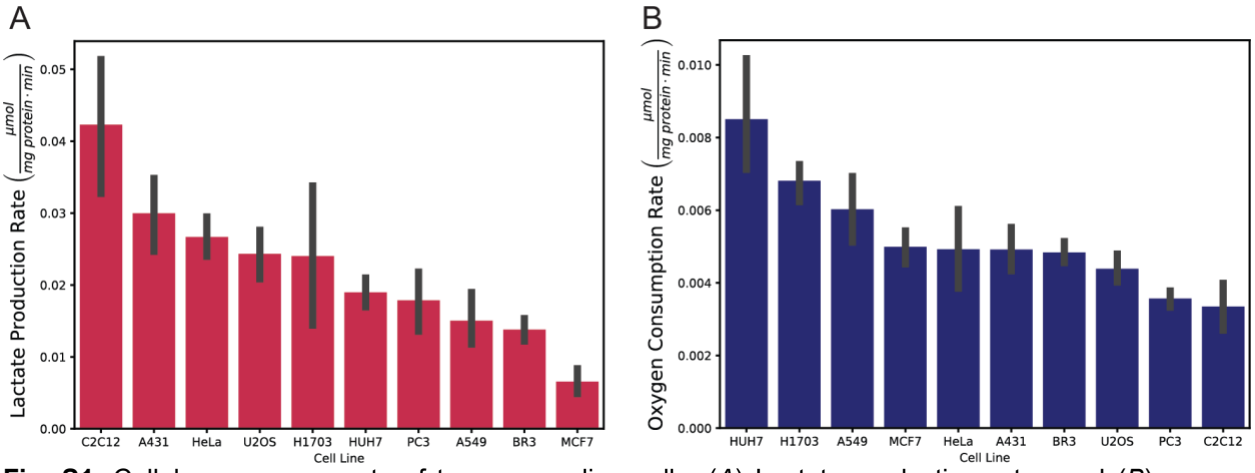


Fig. S1. Cellular measurements of ten mammalian cells. (*A*) Lactate production rates and (*B*) oxygen consumption rates of ten mammalian cell lines. The error bars in represent the **95% confidence interval.**

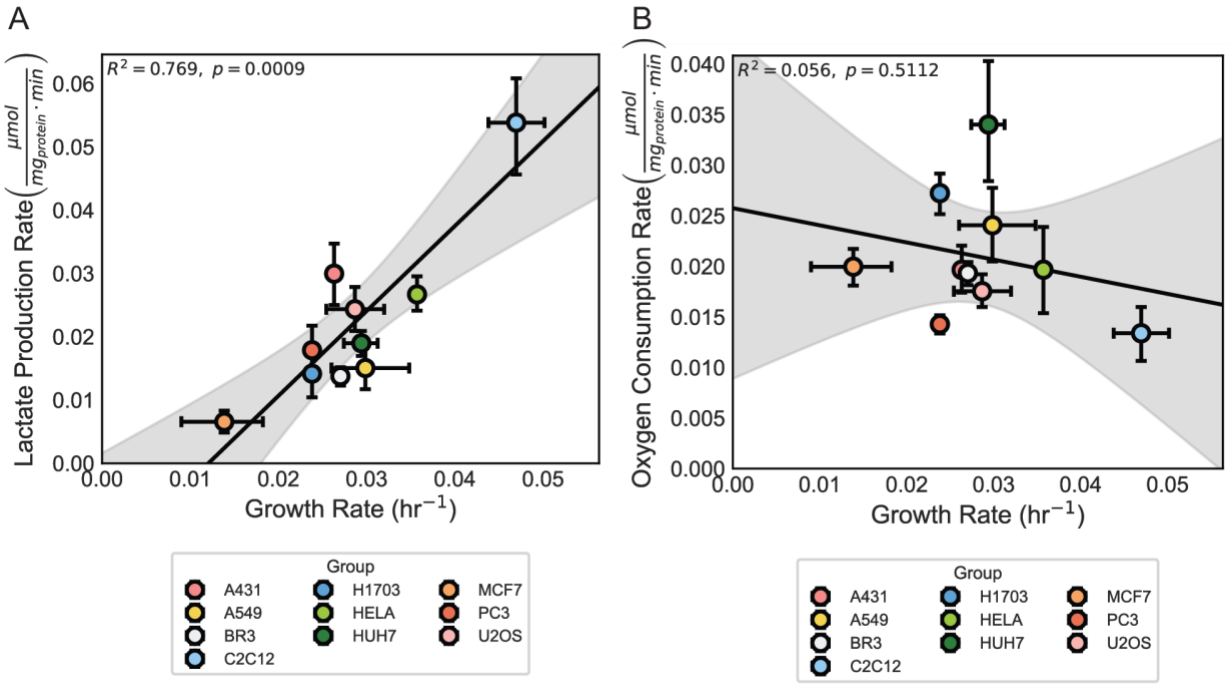


Fig. S2. Lactate production rate and oxygen consumption rate correlation with growth organisms. (*A*) Lactate production rate and (*B*) oxygen consumption rate correlations with cellular growth for ten mammalian cell lines. The grey shading in the plot represents the **95% confidence interval** of the regression line. The error bars in represent the **95% confidence interval** calculated from 10,000 bootstrap iterations**.**

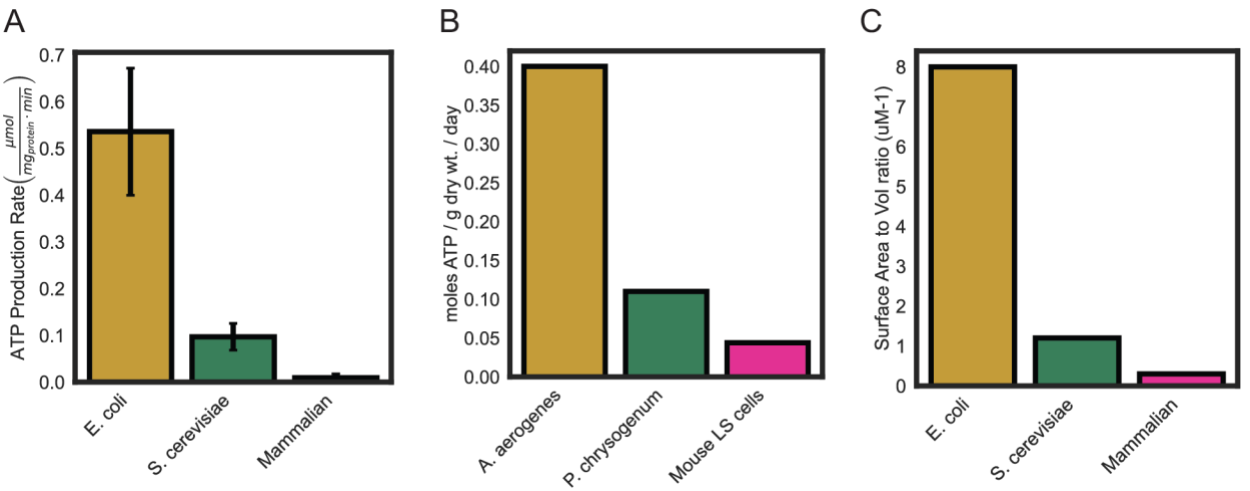


Fig. S3. Maintenance ATP production rates compared to surface area to volume ratio. (*A*) ATP production rates of non-growing cells. Error bar is the SEM of the regression line intercept from Figure 1. (*B*) Calculated ATP production rates of a non-growing bacterium, fungus, and mouse LS cells from Kiburn et al. 1969. (*C*) Surface area-to-volume ratio for *E. coli*, *S. cerevisiae*, and mammalian cells.

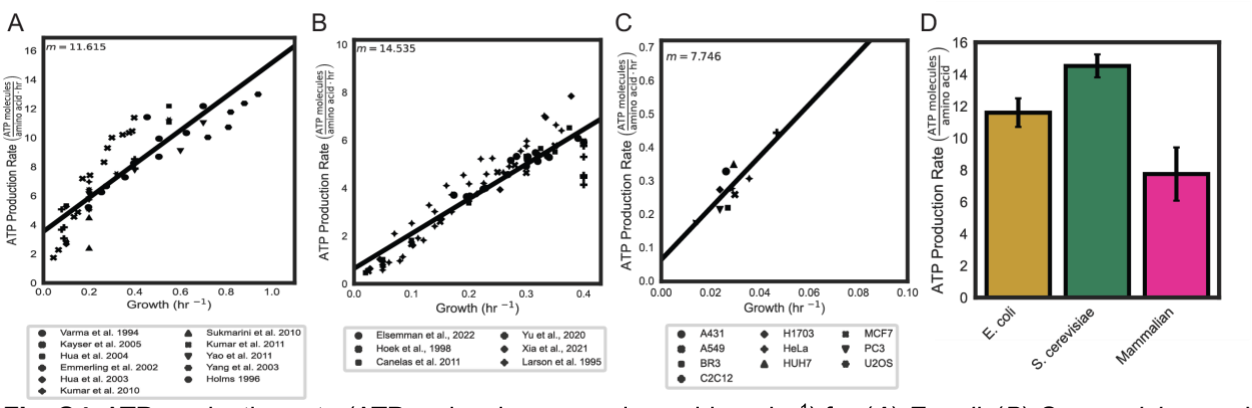


Fig. S4. ATP production rate (ATP molecules per amino acid per hr^{-1}) for (*A*) *E. coli*, (*B*) *S. cerevisiae*, and (*C*) mammalian cells. (*D*) The ATP production rate per amino acid represents the slope of the (*A*-*C*) for each organism. The error bars represent the standard error of the slope for each organism.

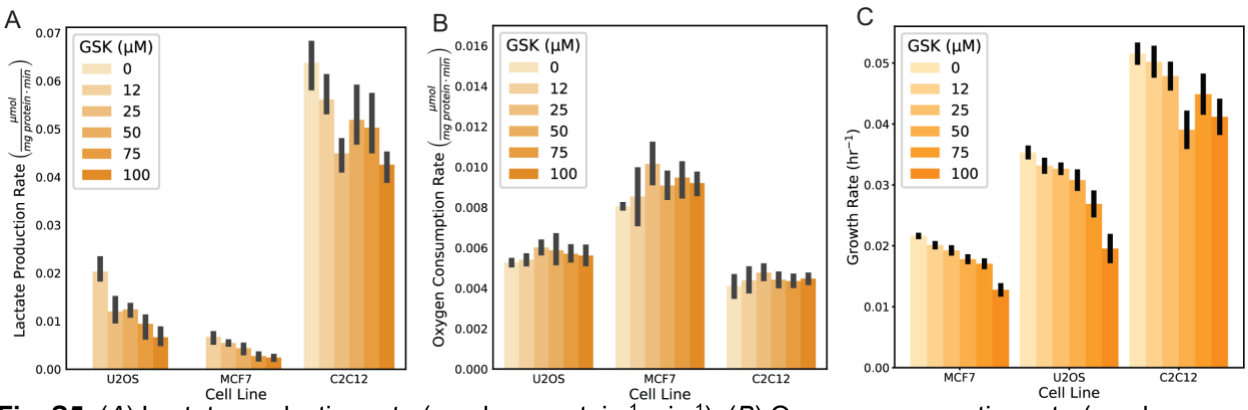


Fig. S5. (*A*) Lactate production rate (µmol mg protein^{-1} min^{-1}), (*B*) Oxygen consumption rate (µmol mg protein^{-1} min^{-1}), and (*C*) growth rate (hr^{-1}) with increasing treatment with GSK-2837808A (GSK). The error bars in represent the **95% confidence interval**.

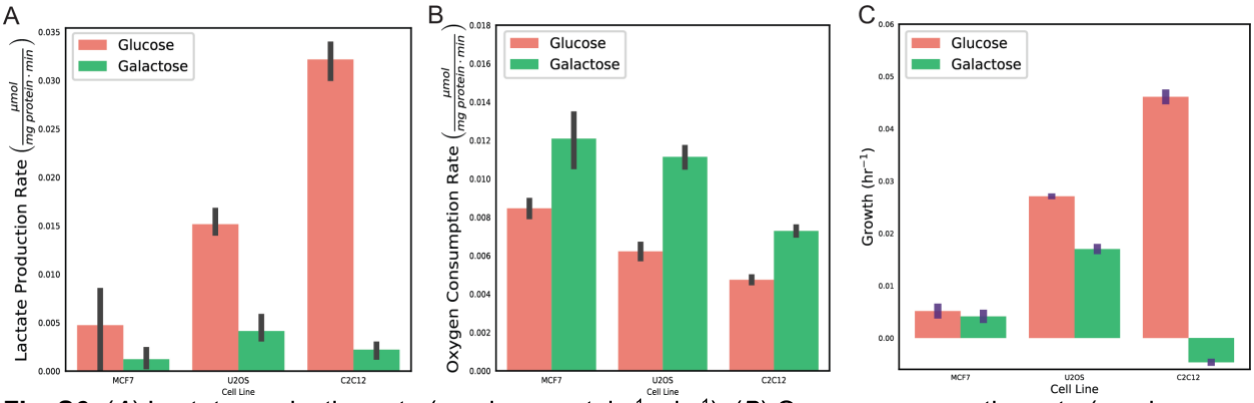


Fig. S6. (*A*) Lactate production rate (μmol mg protein^{-1} min^{-1}), (*B*) Oxygen consumption rate (μmol mg protein^{-1} min^{-1}), and (*C*) growth rate (hr^{-1}) with 10 mM glucose or 10 mM galactose. The error bars in represent the **95% confidence interval**.

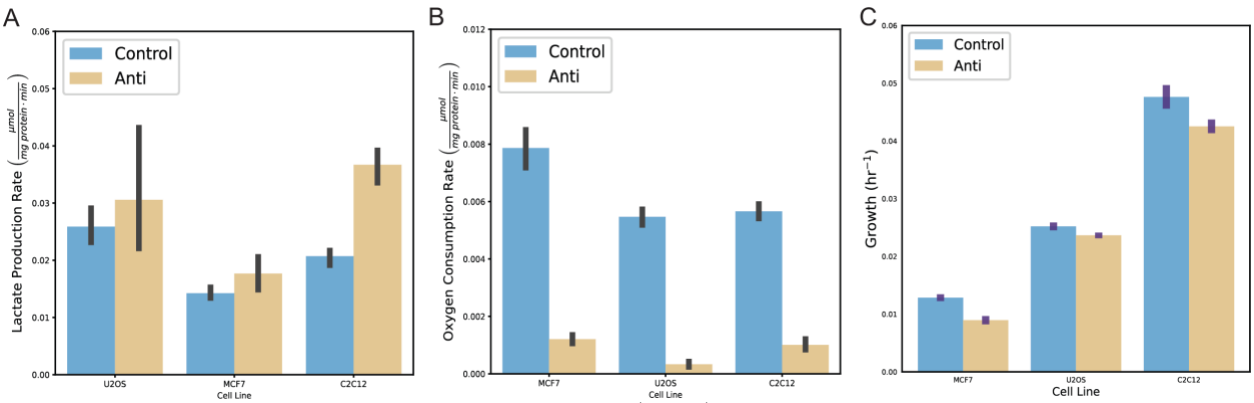


Fig. S7. (*A*) Lactate production rate (μmol mg protein^{-1} min^{-1}), (*B*) Oxygen consumption rate (μmol mg protein^{-1} min^{-1}), and (*C*) growth rate (hr^{-1}) with 1 uM antimycin treatment (Anti). The error bars in represent the **95% confidence interval**.